377.5
K-11
1-197

Kyushu Institute of Technology
Sensui 1-1, Tobata, Kitakyushu, Japan 804-8550

Kinetic Study of H-Induced Abstraction and Desorption of Hydrogen on Si Surfaces

by

Fouzia Khanom

A thesis prepared in fulfillment of the requirements for the
Doctoral Degree
in
Electrical, Electronic, and Computer Engineering
under supervision of
Prof. Akira Namiki

九州工業大学附属図書館

0010516169

March 2003, Kitakyushu, Japan

ABSTRACT

This Ph. D thesis is concerned to the H-induced HD as well as D_2 desorptions on the reaction system of H + D/Si surfaces. The former reaction is denoted as abstraction (ABS) and the later is as adsorption-induced-desorption (AID),

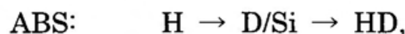

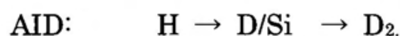

The kinetics study of the above mentioned reactions on Si(100) and Si(111) surfaces have been mainly focused in this work. So far, the kinetic mechanisms reported for these reactions on Si surfaces were unclear and controversial. The kinetics mechanisms for these reactions have been revealed in the present study. The experiments are performed in a system which is composed of an ultra-high vacuum reaction chamber ($<1\times10^{-10}$ Torr) and a beam chamber. Atomic beams are produced by a radio frequency plasma generator. The desorbing species are detected simultaneously by a quadrupole-mass-spectrometer.

For both Si(100) and Si(111) surfaces, HD ABS is found to follow a 1st order desorption kinetics for low initial D coverages θ_D^0 ($\leq$ 0.5 ML) and a 2nd order desorption kinetics for high θ_D^0. The evaluated reaction order for D_2 AID is about four on the Si(100) surface and three for the Si(111) surface. These results clearly rules out the hot atom (HA) mechanism for both the processes since the HA scenario claims a first- and a second-order kinetics with respect to D adatom coverages for ABS and AID, respectively. The rate spectrum of D_2 AID as a function of T_s for both the Si(100) and Si(111) surfaces looks similar in line shape to the β_2 temperature-programmed-desorption (TPD) spectrum arising from a di-deuteride phase. Rate equations are proposed for ABS and AID, based on the observed kinetics. A new mechanism is proposed for D_2 AID which is associated to the β_2 TPD arising from the second order desorption of adjacent dideuterides transiently formed during H irradiation. However, the evaluated activation energy for D_2 AID (about 0.16 eV) on Si(111) surface is considerably smaller than the activation energy of 1.5 eV for β_2 TPD. By taking steady state adsorption and desorption into consideration for Si(111) surface,

the origin of the third order rate law as well as the low activation energy for AID is considered to reflect the sticking process rather the desorption process. A hot-complex-mediated reaction model is proposed for ABS. The incident H atoms first make a hot complex with mono-deuterides. ABS and di-deuterides are considered to occur competitively in the energy relaxation process. This hot complex can explain the second-order kinetics for ABS.

CONTENTS

CHAPTER 1

General Introduction 1
1.1 Introduction 1
1.2 Si surfaces: structure and properties 2
1.2.1 Si(100) 2
1.2.1.1 Clean Si(100) 2
1.2.1.2 H/Si(100)- 2×1 4
1.2.2 Si(111)-7×7 6
1.2.3 H/Si (111)-1×1 9
1.3 H_2 desorption from H/Si(100) and H/Si(111) surfaces 10
1.4 Basic reaction mechanisms 13
1.4.1 Langmuir-Hinshelwood mechanism 13
1.4.2 Eley-Rideal mechanism 13
1.4.3 Hot-atom mechanism 14
1.5 Reactions of H with D/Si surfaces 15
1.6 This thesis 17
References 17

CHAPTER 2

Experimental Details 20
2.1 Introduction 20
2.2 Quality of RF plasma beam 22
2.3 Detection of desorbing species by QMS 23
2.4 Sample preparation and thermal treatment 23
2.5 Control and calibration of sample temperature 26
References 27

CHAPTER 3

Rate Equations in Si(100) at 573 K 28
3.1 Introduction 28
3.2 Kinetic model 30
3.3 Experiment 35
3.4 Calculating rates 36

3.4.1 Hydrogen coverages 36
3.4.2 η 42
3.4.3 D_2 and HD rates 43
3.5 Discussion 49
3.6 Summary 52
References 53

CHAPTER 4

Hot-Complex Model 55
4.1 Introduction 55
4.2 Experiment 56
4.3 Results and discussion 57
4.4 Summary 65
References 65

CHAPTER 5

D Abstraction by H on Si(111) 67
5.1 Introduction 67
5.2 Experiment 70
5.3 Results 71
5.3.1 β_2 TPD 71
5.3.2 AID and ABS 74
5.3.2.1 T_s dependence 74
5.3.2.2 θ_D^0 dependence 78
5.4 Discussion 81
5.4.1 Rate equation at T_s=620 K 81
5.4.2 AID in steady state 87
5.4.3 Hot-complex-mediated reaction model 88
5.5 Summary 92
References 93

CHAPTER 6

Summary 95
6.1 Common features 95
6.2 Different features 96
6.3 Future plan 97
References 97

Acknowledgement 98
Appendix 99
A. Symbols 99
B. Abbreviations 102

CHAPTER 1

General Introduction

1.1 INTRODUCTION

Where would we be without silicon? It is the second most abundant element that comprises almost 27 percent of the Earth's crust weight. Even then, elemental silicon does not naturally exist; it exists as compounds. Silicon is a group-IV semiconductor and has the diamond like structure in its crystalline form, where each Si atom is bonded by four Si atoms. The bonds run along [111] crystallographic directions. The bond length is 2.35 Å, and the bond angle is 109.28^{o}. Si is the fundamental material for the fabrication of most of the microelectronic devices that are indispensable in manufacturing modern electrical machines and equipments from televisions to artificial satellites, which have changed our life style. Continuing innovations in making smaller and faster electronic circuitry are driving us towards a new era. However, is silicon only responsible for bringing all the advancement in the microelectronic technology? Of course, no, it is not. For example, without the role of hydrogen in surface processing, the Si technology is groundless like a monarch without a crown. That is why there exists an immense interest in the research of hydrogen-silicon interaction at the silicon surfaces.

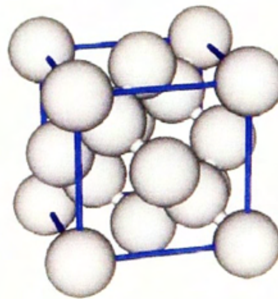

Fig.1.1: Diamond structure of crystalline Si

Interaction of hydrogen atom with Si surfaces is very important. Hydrogen atoms are the most promising agent for Si device processing such as passivation of dangling bonds at surfaces or Si-SiO_2 interfaces, abstraction of surface adatoms to create new

reaction sites for further crystal growth in chemical vapor deposition (CVD) process, formation of higher hydrides to etch Si atoms etc. Understanding these reaction mechanisms is important not only for technological relevance but also for fundamental surface science because of the simplicity of the reaction system.

In the plasma enhanced Si CVD process silanes mixed with H_2 are generally used. Hydrogen atoms generated in plasma play a critical role to the quality of deposited thin films. It is known that when the gaseous hydrogen atoms collide with adsorbed hydrogen atoms (adatoms), the hydrogen adatoms can be abstracted from the surface [1, 2]. The dangling bonds created by these abstraction processes offer new sites for CVD growth [3, 4]. Thus, the abstraction reactions of the hydrogen play an important role particularly in plasma CVD process. Yet, the reaction mechanisms proposed for these abstraction reactions are unclear and controversial. The objective of this thesis is to clarify the mechanisms of these reactions on Si surfaces.

1.2 Si SURFACES: STRUCTURE AND PROPERTIES

1.2.1 Si(100)

1.2.1.1 Clean Si(100)

The Si(100) surface is the simplest and the most technologically relevant surface.

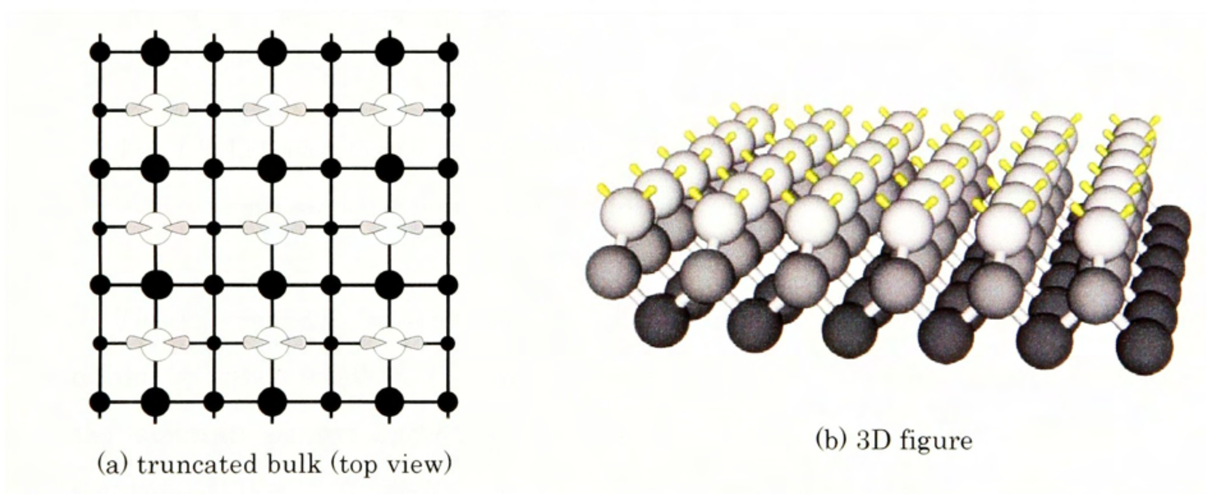

Fig. 1.2: {001} Truncated bulk (before reconstruction).

The ideal Si(100) - 1×1 surface is obtained by truncation of the bulk along a {001} plane.

The 2×1 reconstruction from 1×1 of Si(100) is caused by the fundamental geometric property of the {001} planes in the diamond structure [Fig. 1.1]. The most characteristic feature of the Si (100) - 2×1 reconstruction is the presence of Si dimers in the topmost layer [5]. In order to reduce the dangling bond density, the surface atoms dimerize and hence minimize surface free energy. The dimer bond length is about 2.3Å and is arranged in parallel row. Each surface dimer is bound by a strong σ -bond derived from the two dangling bonds of the dimerized surface atoms as well as by a weaker π -bond derived from the two dangling bonds pointing towards the vacuum.

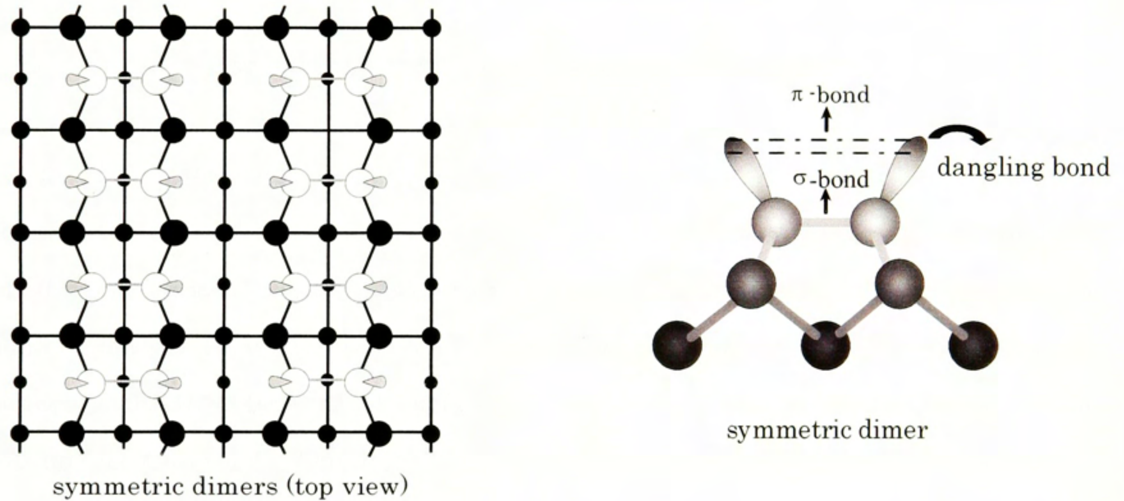

Fig. 1.3: Left panel represents symmetric 2×1 dimers from top view and right view represents a symmetric dimer [6].

The associated π^* antibonding orbital is empty but separated from the bonding orbital by only a small energy gap of around 0.5 eV [7]. Each dimer atom is bonded to the substrate by two backbonds. Only one backbond per atom is visible from this perspective (Fig. 1.3 (right panel)). The dimerized surface is metallic in eletronic nature, but the real Si(100) surface is semiconducting because the Si dimers are buckled [8, 9]. The reported buckling angle is about 20°. These buckled dimers can be arranged in a c(4×2) pattern with the lowest-energy structure [Fig. 1.4].

The asymmetric or buckled dimers were observed in low temperature STM

measurement [9]. The buckled dimers lower the surface energy. This effect has been well established experimentally as well as theoretically. Therefore, dimerization is a key factor in surface chemical activity. For example, atoms and molecules diffusing on the surface use dimers rows as convenient 'rails'.

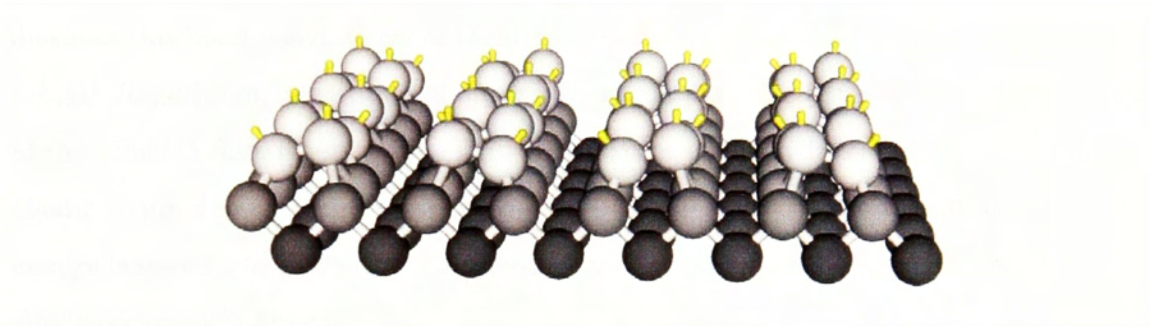

Fig. 1.4: Buckled dimers arranged in c(4×2) pattern.

1.2. 1.2 H/Si(100) - 2×1

Due to the technological importance, the system H/Si(100) - 2×1 is one of the best studied semiconductor system. Structures of the Si surface with adsorbed hydrogen depend on surface temperature T_s as well as hydrogen coverage θ_H. The most famous structure is the H/Si(100) - 2×1 surface. In this surface, the π-bond between two Si atoms on one dimer is broken, but the σ-bond remains unbroken, preserving the 2×1 reconstruction.

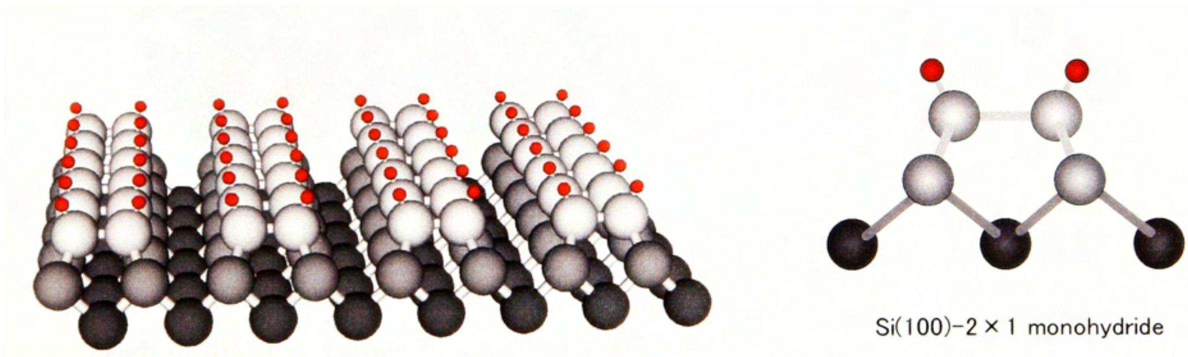

Fig. 1.5: 1 ML H/Si(100) - 2×1 surface (left panel). The right panel shows a mono-hydride.

This structure is called mono-hydride, which is symmetric in geometry. For the monohydride surface the Si dimer bond length is 2.4 Å, and that of the Si-H bond is

1.51 Å. The angle between Si-H and Si-Si bond is 112.3° [10].

Two H atoms passivate dangling bonds of a single dimer to form doubly occupied dimer rather than single bonds of separate dimers to form singly occupied Si dimer. H atoms have good reasons to form doubly occupied dimer. First, the two electrons in the dangling bonds of a clean dimer form a π-bond. A single H atom adsorbed on a dimer disrupts this bond, leaving one of the dimer Si atom with a truly unsaturated dangling orbital. In addition, adsorption of one H atom on a dangling bond reduces the buckling of the affected dimer noticeably. The consequence of the reduced buckling is that the elastic strain due to dimerization is less sufficiently relaxed. The net effect is that the energy is lowed when two H atoms occupy the same dimer rather than formation of two singly occupied Si dimers.

When the Si(100) surface is saturated with H at 623 K, essentially perfect monohydride dimer rows are observed in STM topographs [11] and sharp 2×1 LEED patterns [12, 13] are obtained. If the surface is further exposed to H for long time, the Si-Si σ-bonds are broken and di-hydride species are formed. When all the dimer bonds are broken to give di-hydrides, the surface would be transformed to 2 ML H/Si(100) - 1×1 surface. Any ideal 2 ML H/Si(100) - 1×1 surface has not been observed.

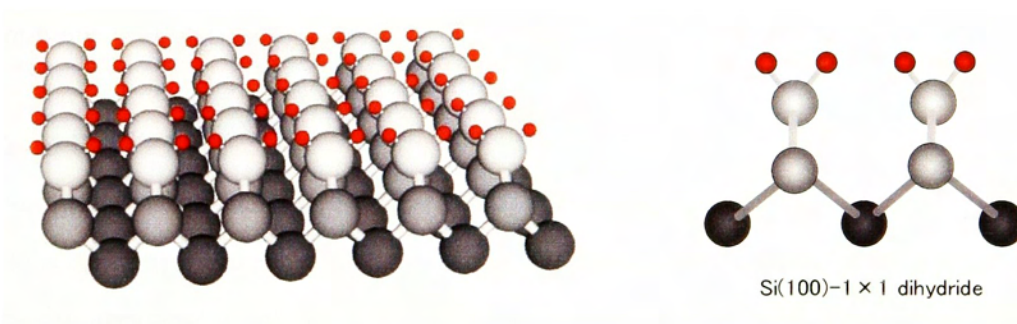

Fig. 1.6: H/Si(100) - 1×1 surface (left panel). The right panel shows dihydrides.

High-resolution infrared spectra and low-energy-electron-diffraction (LEED) patterns [14, 15] indicate that the Si (100) surface saturated with H at room temperature exhibits a 1×1 pattern which is a disordered phase where about half of the H atoms are in mono-hydride (H-Si-Si-H) and another half are in di-hydride (SiH_2) configuration. In contrast, the surface saturated at 380 K exhibits an ordered 3×1

LEED pattern. Based on the infrared spectra [14], the 3×1 hydrogen-saturated structure is attributed to the repeated alternating mono-hydride and di-hydride units. Later STM images [11] conclusively verified that the H/Si(100) - 3×1 surface consists of alternating rows of mono-hydride dimer units and di-hydride units.

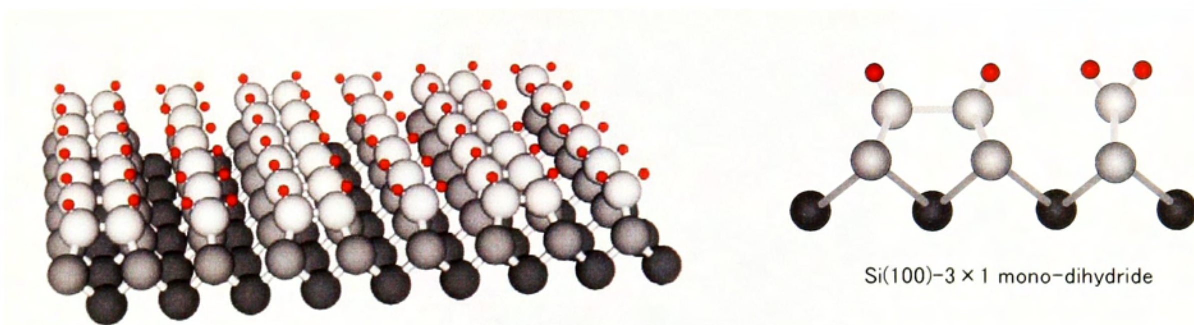

Fig. 1.7: H/Si(100) - 3×1 surface forming 1.33 ML (alternative rows of mono- and dihydride).

H-passivated Si(100) surface is not oxidized immediately in air [16]. This is a highly desirable property because conventional CMOS manufacturing involves temporary storage of wafers after HF cleaning. In any case, the hydrogen-saturated surface is hydrophobic (not wetted by water).

1.2. 2 Si(111) - 7×7

The 7×7 reconstruction corresponds to the thermodynamically ground state of a Si(111) surface at room temperature. In the bulk diamond structure [Fig. 1.1] the (111) planes are arranged in "double layer" or also known as "bilayers". Each double layer contains a set of atoms separated vertically by 0.78 Å.

The atomic arrangement of the 7×7 reconstruction is dramatically changed as compared to a truncated-bulk (Fig. 1.5) Si(111) surface. The DAS (dimer-adatom-stacking fault) model by Takayanagi [17] is now generally accepted to correctly describe this complex structure shown in Fig. 1.8 and more closely in Fig. 1.9. The reconstruction extends over at least three layers and can be characterized by the following features.

The third layer from the top (the dimer layer) contains nine Si dimers on the edges of the unit cell halves. Thirty-six dangling bonds of the second atomic layer (the rest

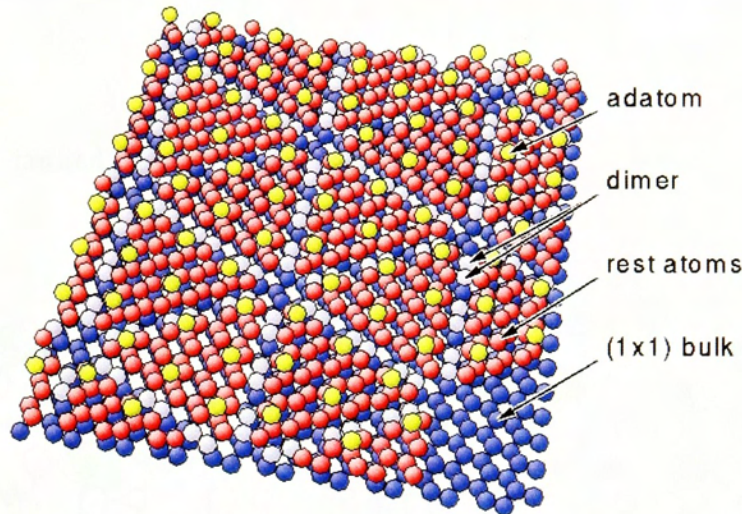

Fig. 1.8 Takayanagi's DAS model of Si(111) -7×7 structure (plotted by BALSAC).

atom layer) are saturated by 12 Si adatoms, each of which has one unsaturated (dangling) bonds. A stacking fault is present in one half of the 7×7 unit cell between the rest atom layer and the dimer layer. This part is called the faulted half, while the other is the unfaulted half. Six dangling bonds in the rest atom layer remain unsaturated. One more dangling bond remains at the 'corner hole atom' which is located in the fourth layer at the bottom of the corner holes. Therefore, each 7×7 unit cell contains 12 adatoms in the adatom layer, 42 atom in the rest atom layer and 48 atoms in the dimer layer. All layers below are complete bulk.

Thus, the 7×7 reconstruction replaces 49 dangling bonds of the truncated-bulk Si(111) by 19 dangling bonds among which 12 dangling bonds are on the adatoms, six on the second layer rest atoms and one in the corner hole. The 7×7 surface structure represents at least six chemically distinguishable types of atoms with a dangling bond. There are six adatoms in the faulted and six in the unfaulted half of the unit cell. The six rest atoms (three in the faulted and three in the unfaulted half) are topographically deeper than the adatoms. Finally, there is one more unsaturated atom in the corner hole (corner hole atom), which is located even deeper than the other rest atoms. These atoms are also chemically the most active ones and play a key role in the interaction of

H atoms or other molecules with the Si(111) - 7×7 surface. Adsorption energy of H atoms at the adatom site is 2.9 eV, at the rest atom site 3.2 eV, and at the corner hole

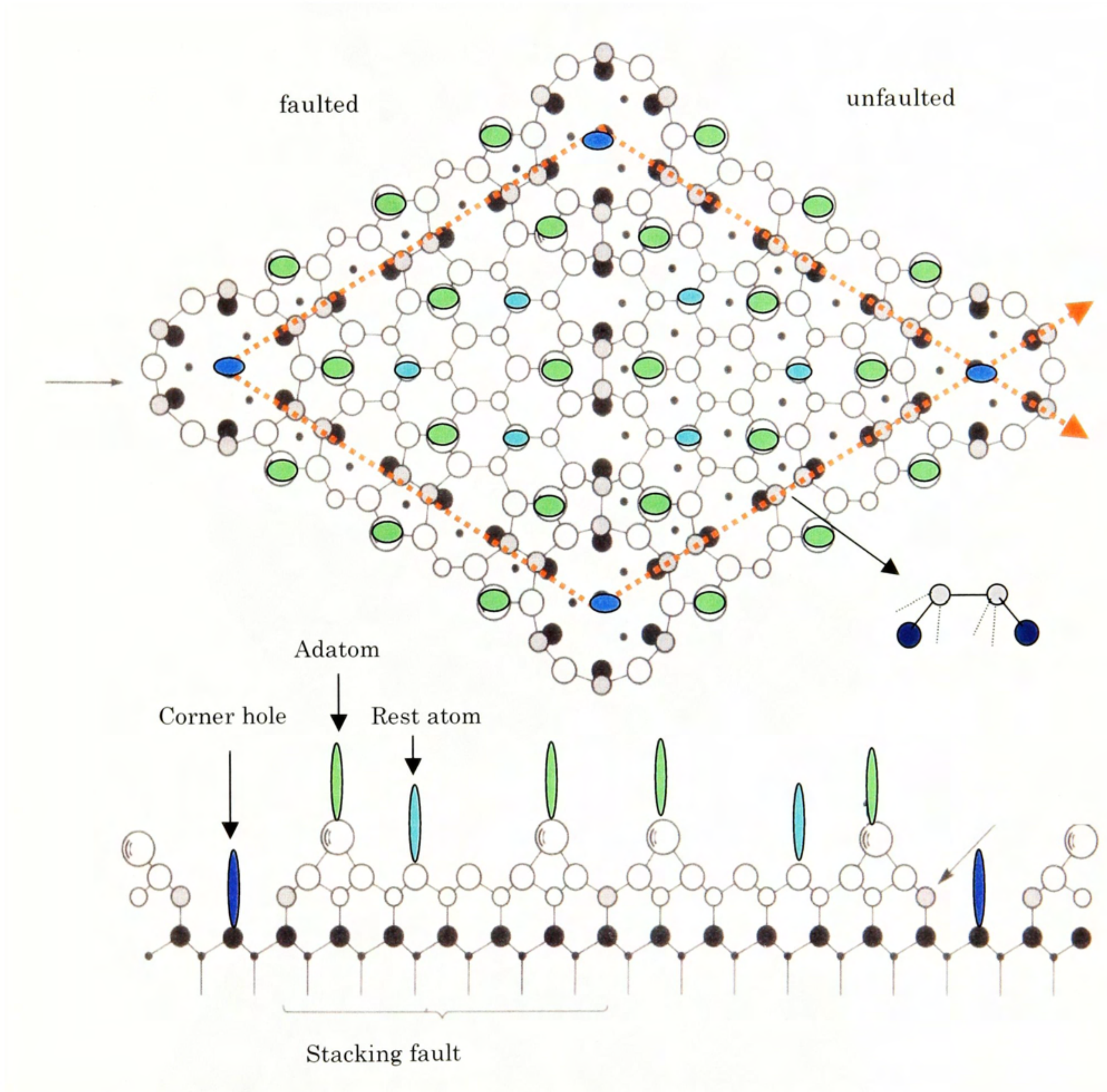

Fig. 1.9: Representative one unit cell of Si(111) -7×7 DAS-Model.

site 3.5 eV [18]. With high H exposure, the surface become a nearly bulk truncated 1× 1 structure at high T_s.

1.2. 3 H/Si (111) -1×1

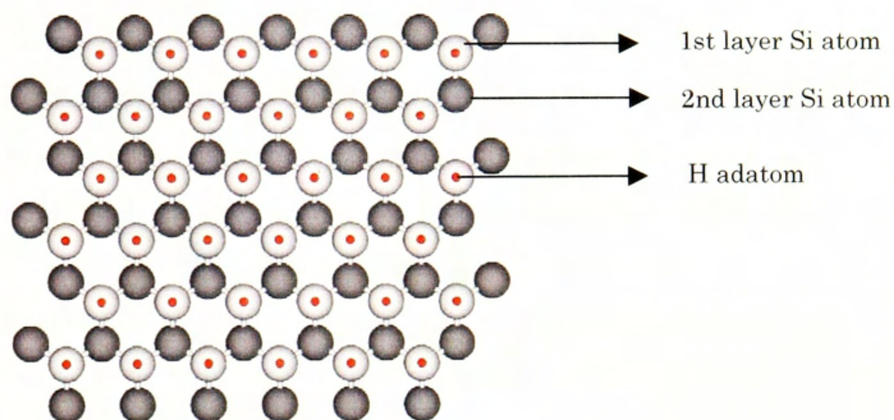

Fig. 1.10: Top view of H/Si(111) - 1×1.

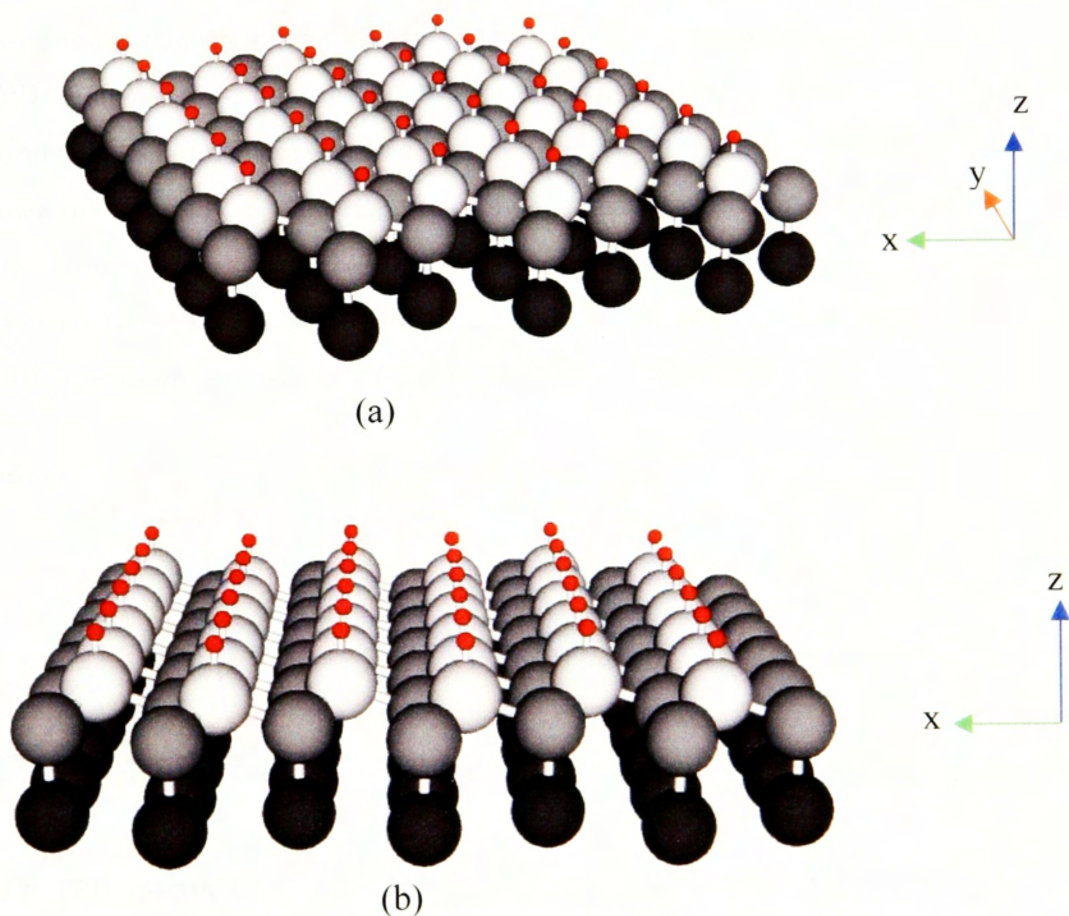

Fig. 1.11: (a) and (b) represents 1ML H/Si(111) -1×1 surface from different view points.

The ideal H/Si(111) - 1×1 surface is a truncated-bulk Si(111) structure where all dangling bonds, one for each Si atom, are terminated by a hydrogen atom. Hence, the hydrogen coverage on this surface is exactly one monolayer. This surface can be prepared in several ways. For instance, if the Si(111) - 7×7 surface is exposed to H atoms for long time at surface temperature $T_s \geq 620$ K, nearly a bulk truncated 1×1 structure can be obtained [19, 20]. The Fig. 1.10 shows the top view of the H/Si(111) - 1 ×1 surface and Fig. 1.11 represents that surface from different perspectives.

When the 1 ML H/Si(111) - 1×1 surface prepared along the above mentioned process is again exposed to H beams at T_s=400 ± 10 K, the surface can accumulate dihydrides, giving a saturation coverage of 1.25 ± 0.13 ML [21, 22]. Hydrogen desorption from this surface regenerates the 7×7 structure.

1.3 H_2 DESORPTION FROM H/Si(100) AND H/Si(111) SURFACES

To understand the mechanism and kinetics of thermal desorption process, various types of TPD (temperature-programmed-desorption) experiments have been provided. These desorption mechanisms are rather well established on the Si(100) surface. Two peaks known as β_1 and β_2 arising from monohydride and di-hydride species, respectively, are observed in the TPD spectra of hydrogen molecules from H/Si(100)-2×1 surfaces[23, 24, 25] prepared at ~400 K. The peak positions of the β_2 and β_1 TPD spectra are located at ~650 and ~790 K, respectively.

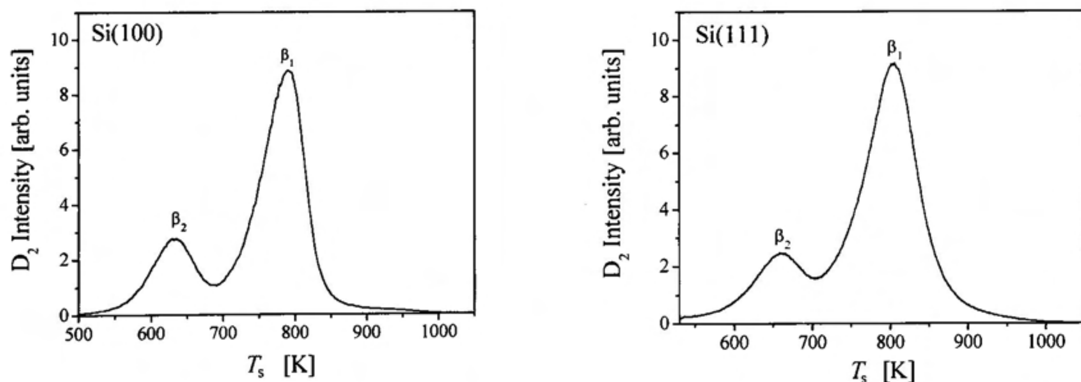

Fig. 1.12: TPD spectra from D/Si(100) surface (left), TPD spectra from D/Si(111) surface (right).

The measured activation energy for H_2 desorption from Si(100) surface varies from 2 to 2.5 eV [24, 25, 26] for β_1 and is about 2 eV for β_2 [27]. So far various desorption models have been proposed for the β_1 monohydride desorption. One is the intra-dimer or pre-paired mechanism where H_2 desorbs from the same dimer. Moreover, density functional (DF) calculations using slab models have obtained activation energies for the intradimer recombination, in good agreement with experiments. An early STM study [28] provides an influential hint that H_2 desorption from H/Si(100) - 2×1 surfaces appears to be accompanied by pairing of H on the same dimer. Numerous isolated clean dimes are seen in STM images acquired after partial desorption of H_2 from nearly saturated H/Si(100) - 2×1 surfaces.

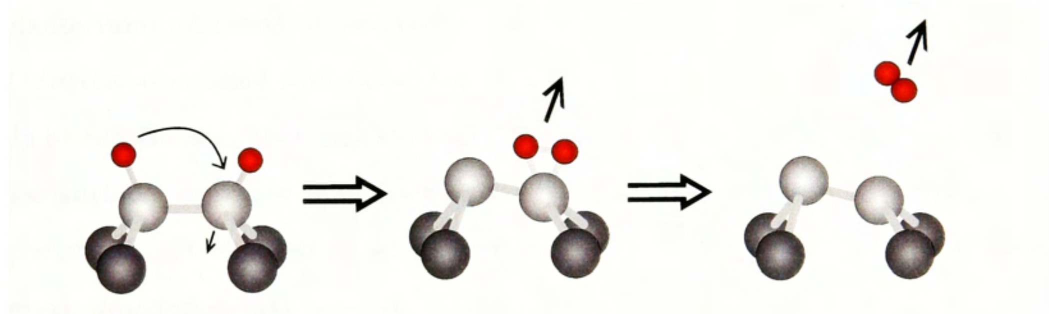

Fig. 1.13: Pre-paired desorption mechanism

Recently another mechanism is considered in case of the β_1 desorption, known as an interdimer mechanism where two H_{ads} combine to form a H_2 molecule from two neighboring dimers [29]. However, this mechanism is not well established.

The desorption of hydrogen molecules responsible for the β_2 peak from the H/Si(100) surface follow a second-order desorption kinetics with respect to the instantaneous coverages of the di-deuteride species (θ_{HSiH}) [23]. Two different mechanisms have been proposed for the desorption of H_2 from di-hydride species on the H/Si(100) surface.

One is the recombinative desorption [23, 30] of two hydrogen atoms from two adjacent di-hydride species (1,2-elimination) and the other is self-associated desorption of two H atoms on a single Si atom (1,1-elimination). The latter mechanism is well accepted [27] and is employed in the later discussion.

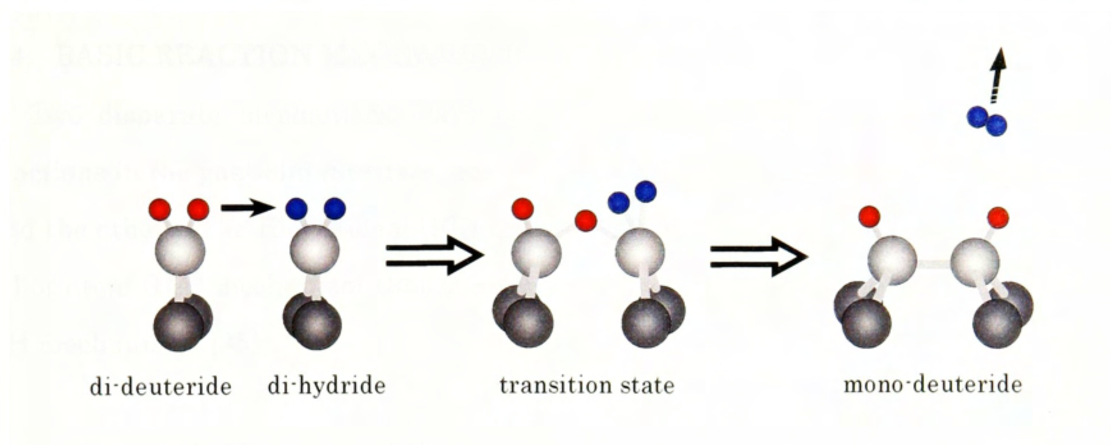

Fig. 1.14: 1,1-elimination of a H_2 molecule from H/Si(100) surface

Like H/Si(100) surface, two peaks are also observed in the TPD spectra of Hydrogen (or deuterium) adsorbed on Si(111) [31, 32], β_1 (~ 810 K) and β_2 peak (~660 K). The kinetics associated with these desorption processes is the subject of debate. A TPD study by Shulze *et al.* [31] indicated that the β_1 peak changed from a symmetric shape at low surface coverages indicative of second order kinetics, to an asymmetric curve characteristics of first-order behavior at high coverages. A series of laser induced thermal desorption experiments (LITD) found that the β_1 process showed a second-order behavior over the wide range of the atomic H or D saturation coverages from 0.2 to 0.8 ML [33,33]. On the basis of this result, a recombinative desorption mechanism in which randomly positioned hydrogen (or deuterium) atoms are moved to adjacent sites, was proposed. The second harmonic generation method method (SHG) by Reider *et al.* [26] for probing hydrogen coverages has been used in isothermal desorption experiments to show that at coverages <0.2 ML, the reaction order associated with the β_1 peak was nonintegral to be well within the range of 1.4-1.7. Reported activation energy for this β_1 desorption process is about 2.5 eV [26]. Spectral fitting was done by Flowers *et al.* [34] after considering second-order desorption kinetics for both β_1 and β_2 channel TPD. No quantitative experimental value has been reported for the β_2 TPD reaction order for Si(111) surface. In the present work, the β_2 channel desorption order is evaluated and is discussed in the CHAPTER 5.

1.4 BASIC REACTION MECHANISMS

Two disparate mechanisms have often been considered in evaluating chemical reactions in the gas/solid interface, one is the Langmuir-Hinshelwood (LH) mechanism and the other is the Eley-Rideal (ER) mechanism. Surface reactions can also occur via a hot atom (HA) mechanism that is an intermediate mechanism between the ER and LH mechanisms [35].

1.4.1 Langmuir-Hinshelwood Mechanism

In the Langmuir Hinshelwood (LH) mechanism [36], two reactants A and B are in the thermal equilibrium with the surface. For such a reaction on the surface, the two reactants approach each other in a critical distance to overcome the activation barrier. The product carries the energy produced by the reaction. The energy can be transferred either to the substrate or to the product molecule to desorb from the surface as the desorption barrier overcome.

The LH mechanism is strongly affected by T_s and the reaction rate depends on the coverage of the reactants. The reaction rate in the LH mechanism can be described as follows

$$dN_{AB} / dt = k_{LH}\theta_A\theta_B,$$

where θ_A is the coverage of reactant A, θ_B the coverage of reactant B, k_{LH} is the temperature-dependent rate constant with the form $\nu\exp(-E_A / kT_s)$, where E_A is the activation energy, and ν the pre-exponential factor.

1.4.2 Eley-Rideal Mechanism

In 1940 Eley and Rideal [37] suggested a mechanism known as an Eley-Rideal mechanism, which is a kind of direct impact process in which incident gas phase species, such as H atoms can directly abstract adsorbates such as D adatoms D_{ad}. The reactive gas phase species are not accommodated with the surface and the reaction rate typically shows a weak dependence on T_s. In order to proceed the abstraction reaction, the incident particle must collide with the adatom within a cross-section σ generally less than 1Å^2 [38]. This abstraction cross section is independent of the coverage and T_s.

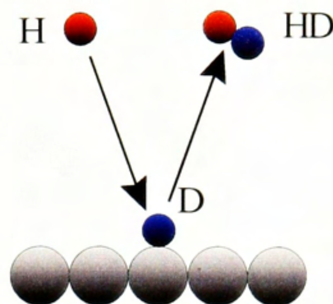

Fig. 1.15: ER mechanism

If θ_D is the coverage of D_{ad} and ϕ is the flux of incident H atoms, then the rate of rate of the product can be given as

$$dN_{HD} / dt = \sigma\phi\theta_D .$$

1.4.3 Hot-Atom Mechanism (HA)

Hot atom process (HA process) was characterized by Harris and Kasemo in 1981 [35] for the explanation of the reaction of hydrogen with adsorbed oxygen on a platinum surface. In this mechanism the incident H (or D) atoms are first trapped into the chemisorption potential of the surface, but laterally mobile as hot atoms H* (D*) since they still keep a considerable amount of reaction energy and can react with other adatoms. A hot atom process is therefore a generalization of the ER process, independent of T_s. In the above mentioned process the hot atoms H* are known as 'primary hot atoms'. This mobile H* atoms can abstract surface D adatoms to form HD molecules. This reaction follows a first-order kinetics.

Incident H atoms can also kick out D_{ad} to produce secondary hot atoms D* which can react with another D_{ad} to produce D_2 molecules. This process follows a second-order kinetics with respect to surface D coverage θ_D.

Pt (111) surface is a typical metal surface for H chemistry. This surface is atomically flat and hence the hydrogen chemisorption potential is weakly corrugated. This supports the HA mechanism because D* or H* can migrate over the surface to react with D adatoms to produce D_2 or HD molecule, respectively. Actually, the HA mechanism is rather well established on the metal surfaces. According to the recent

kinetics measurements, the HA mechanism plays an important in the abstraction process on various metal surfaces [39-43].

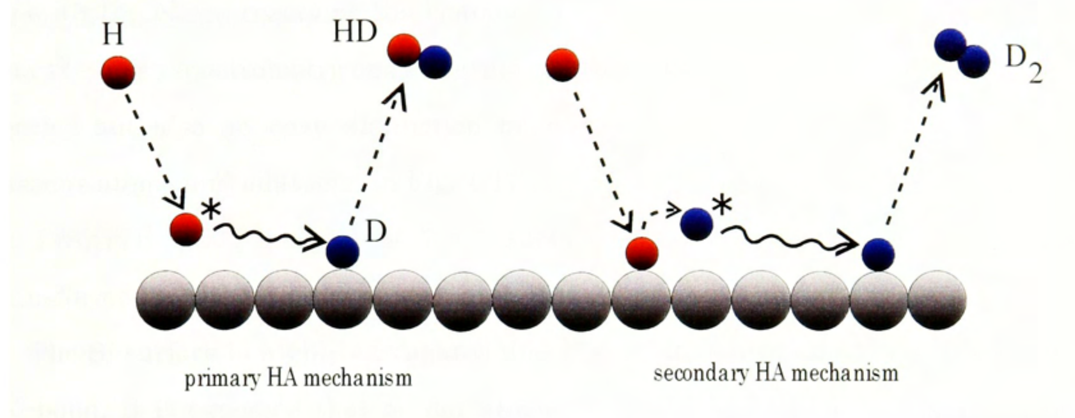

Fig. 1.16: Hot atom mechanism

1.5 REACTIONS OF H WITH D/Si SURFACES

It is known that when D-terminated Si surfaces (D/Si) are exposed to H beams HD molecules as well as D_2 molecules are generated simultaneously. The former reaction is called abstraction (ABS) and the latter is adsorption-induced-desorption (AID).

ABS: $H + D/Si \rightarrow HD$ (1-1)

AID: $H + D/Si \rightarrow D_2$ (1-2)

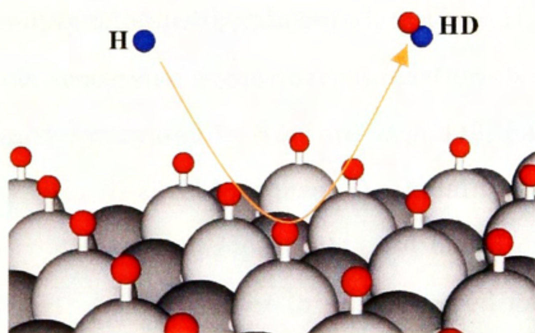

Fig. 1.17: Abstraction (ABS) reaction

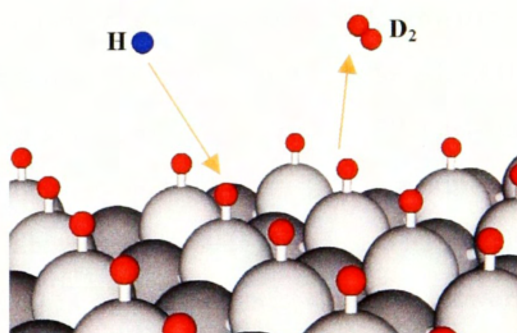

Fig. 1.18: Adsorption-induced-desorption (AID) reaction

Here the acronym AID is used rather than CID (collision-induced-desorption). The term CID was originally used to describe the so-called hot-atom (HA) mechanism based

on a kinematic model for the H-induced D_2 desorption. Previously we used the term CID [44-46] though the proposed mechanism was entirely of Langmuir-Hinshelwood type. In the above reactions the isotopic combination of H(g) and D_{ad} are chosen so that the mass spectrometry can allow not only a background free detection of desorbing species but also an easy distinction between ABS and AID processes by labeling gaseous atoms and adatoms. In Fig. 1.17 and Fig. 1.18, H induced reactions are shown on D/Si(111) -1×1 instead of 7×7 surface since the Si(111) -7×7 structure is transformed to the 1×1 phase with high H irradiation [19, 20].

The Si surface is highly corrugated due to the extremely high directionality of a Si sp^3 bond. It is expected that no hot atoms can be present on the surface due to the corrugation. Dinger *et al.* [47] reported that the H induced HD and D_2 desorptions on the Si(100) surface follow respectively a first- and a second-order desorption kinetics and explained with HA mechanism. On the other hand Shimokawa *et al.* [44] reported that the D_2 desorption follows nearly a 4th-order kinetics. The result rules out the HA mechanism on Si(100) surface. Again, Flowers *et al.* [48] recognized that the hydrogen uptake-curves do not fit with a Kisluik model [49] which is based on the HA mechanism. For hydrogen up-taking onto and losing from the surface, they proposed a new kinetics model which does not include any HA mediated channels. It includes efficient, although transient formation of dihydrides SiH_2 which not only terminate the empty dangling bonds but also induce H_2 desorption upon encounter of such dihydrides via successive isomerizarion reactions between dihydrides and monohydrides. The AID model proposed by Flowers *et al.* [48] follows, in principal, a β_2 channel TPD arising from a di-hydride phase. To explain such a high reaction order of 4, a new kinetics mechanism is proposed [44,45] based on the above mentioned β_2 TPD. The nearly fourth-order kinetics in θ_D observed for D_2 AID is not at variance with the Flowers model since the β_2 TPD obeys a second-order kinetics with respect to DSiD coverages involving four D_{ad} in the event. Thus, AID based on the β_2 TPD mechanism is categorized as a Langmuir-Hinshelwood (LH) reaction. HD AID is also expected to take place in the H and D co-adsorption system generated by substitution of D_{ad} with H during H admission.

Very recently Kubo *et al.* [50] reproduced the results on Si(100) already reported by

Shimokawa *et al.* using a quite different experimental condition. The H flux used in the Kubo's experiment is larger by a factor 10 than that of ours but almost the same with Dingers *et al.* [47].

Dinger *et al.* [51] carried out the same reactions on Si(111) surface and again they came to the same conclusion as on the case of Si(100) surface.

1.6 THIS THESIS

This thesis is concerned with the kinetic study of H-induced abstraction and desorption of deuterium on Si(100) and Si(111) surfaces. In CHAPTER 1 the background of H-induced reactions, Si surface structures and properties have been discussed as a general introduction.

Details about the ultra-high vacuum reaction system and the related techniques to carry out the H induced reactions are given in CHAPTER 2.

In CHAPTER 3 rate equations in Si(100) at 573 K are discussed.

In CHAPTER 4 hot-complex-mediated model is proposed on the basis of the observed kinetics on Si(100) surface.

In CHAPTER 5, a detail kinetic investigation about D abstraction by H on Si(111) is given.

In CHAPTER 6, a comparison is drawn for ABS and AID on the Si(100) and Si(111) surfaces as a summary.

REFERENCES

[1] C. -H. Chen and T. -R. Yew, J. Cryst. Growth 177 (1995) 305.

[2] G. Parsons, J. J. Boland, and J. C. Tsang, Jpn. J. Appl. Phys. 31 (1992) 1943.

[3] K. Sinniah *et al.*, J. Chem. Phys. 92 (1990) 5700.

[4] S. A. Buntin, J. Chem. Phys. 105 (1996) 2066.

[5] R. M. Tromp, R. J. Hammers, J. E. Demuth, Phys Rev. Lett. 55 (1985) 1303.

[6] H. E. Farnsworth, R. E. Schlier, T. H. George, R. M. Burger, J. Appl. Phys. 29, (1958) 1150.

[7] J. Ihm, M. L. Cohen, D. J. Chadi, Phys. Rev. B 21 (1980) 4592.

[8] D. J. Chadi, Phys. Rev. Lett. 43 (1979) 43.

[9] R. A. Wolkow, Phys. Rev. Lett. 68 (1992) 2636.

[10] Kratzer, J. Chem. Phys. 106 (1997) 6752.

[11] J. J. Boland, Surf. Sci. 261 (1992) 17.

[12] S. Maruno, H. Iwasaki, K. Horioka, S. –T. Li, and S. Nakamura, Phys. Rev. B 27 (1983) 4110.

[13] F. Stucki, J. A. Schaefer, J. R. Anderson, G. J. Lapeyre, and W. Gopel, Solid State Commun. 47 (1983) 795.

[14] Y. J. Chabal and K. Raghavachari, Phys. Rev. Lett. 53 (1984) 282.

[15] Y. J. Chabal and K. Raghavachari, Phys. Rev. Lett. 54 (1985) 1055.

[16] M. Niwano, J. –i. Kageyama, K. Kurita, K. Kinashi, I. Takahashi, N. Miyamoto, J. Appl. Phys. 76, (1994) 2157.

[17] K. Takayanagi, Y. Tanishiro, M. Takahashi, S. Takahashi, J. Vac. Sci. Technol. A 3 (1985) 1502.

[18] H. Kim, K. Cho, I. Park, J.D. Joannopoulos, and E. Kaxiras, Phys. Rev. B 52 (1995) 17231.

[19] F. Owman and P. Mårtensson, Surf. Sci. Lett. 303 (1994) L367.

[20] C. J. Karlsson, F. Owman, E. Landemark, Y. -C. Chao, P. Mårtensson, and R. I. G. Uhrberg, Phys. Rev. Lett. 72 (1994) 26.

[21] R. J. Culbertson, L. C. Feldman, P. J. Silverman, and R. Haight, J. Vac. Sci. Tech. 20 (1982) 868.

[22] M. C. Flowers, N. B. H. Jonathan, Y. Liu, and A. Morris, J. Chem. Phys. 102 (1995) 1034.

[23] P. Gupta, V. L. Colvin, and S. M. George, Phys. Rev. B 37 (1988) 8234.

[24] M. L. Wise, B. G. Koehler, P. Gupta, P. A. Coon, and S. M. George, Surf. Sci. 258 (1991) 166.

[25] K. Sinniah, M. G. Sherman, L. B. Lewis, W. H. Weinberg, J. T. Yates, Jr., and K. C. Janda, J. Chem. Phys. 92 (1990) 5700.

[26] G. A. Reider, U. Höfer, and T. F. Heinz, J. Chem. Phys. 94 (1991) 4080.

[27] M. C. Flowers, N. B. H. Jonathan, Y. Liu, and A. Morris, J. Chem. Phys. 99 (1993) 7038.

[28] J. J. Boland, Phys. Rev. Lett. 67 (1991) 1539.

[29] A. Vittadini and A. Selloni, Chem. Phys. Lett. 235 (1995) 334.

[30] S. Ciraci and I.P. Batra, Surf. Sci. 178 (1986) 80.

[31] G. Shulze and M. Henzler, Surf. Sci. 124 (1983) 336.

[32] B. G. Koehler, C. H. Mak, D. A. Arthur, P. A. Coon, and S. M. George, J. Chem. Phys. 89 (1988) 1709.

[33] B. G. Koehler and S. M. George, Surf. Sci. 248 (1991) 158.

[34] M. C. Flowers, N. B. H. Jonathan, Y. Liu, and A. Morris, J. Chem. Phys. 102 (1995) 1034.

[35] J. Harris and B. Kasemo, Surf. Sci. 105 (1981) L281.

[36] G. Ertl, Nachr. Chem. Tech. Lab. 31 (1983).

[37] D. D. Eley, E. K. Rideal, Nature 146 (1940) 401.

[38] B. Jackson and D. Lemoine, J. Chem. Phys. 114 (2001) 474.

[39] G. Eilmsteiner, W. Walker, and A. Winkler, Surf. Sci. 352 (1996) 263.

[40] Boh, G. Eilmsteiner, K. D. Rendulic, and A. Winkler, Surf. Sci. 395 (1998) 98.

[41] S. Wehner and J. Küppers, J. Chem. Phys. 108 (1998) 3353.

[42] Th. Kammler, S. Wehner, and J. Küppers, J. Chem. Phys. 109 (1998) 4071.

[43] J. -Y. Kim and J. Lee, Phys. Rev. Lett. 82 (1999) 1325.

[44] S. Shimokawa, A. Namiki, T. Ando, Y. Sato, and J. Lee, J. Chem. Phys. 112 (2000) 356.

[45] F. Khanom, S. Shimokawa, S. Inanaga, A. Namiki, M. N. -Gamo, and T. Ando, J. Chem. Phys. 113 (2000) 3792.

[46] E. Hayakawa, F. Khanom, T. Yoshifuku, S. Shimokawa, A. Namiki, and T. Ando, Phys. Rev. B 65 (2001) 033405.

[47] A. Dinger, C. Lutterloh, and J. Küppers, Chem. Phys. Lett. 311 (1999) 202.

[48] M. C. Flowers, N. B. H. Jonathan, A. Morris, and S. Wright, Surf. Sci. 396 (1998) 227.

[49] P. Kisliuk, J. Phys. Chem. Solids 3 (1957) 95.

[50] A. Kubo, Y. Ishii, and M. Kitajima, J. Chem. Phys. 117 (2002) 11336.

[51] A. Dinger, C. Lutterloh, and J. Küppers, J. Chem. Phys. 114 (2001) 5338.

CHAPTER 2

Experimental Details

2.1 INTRODUCTION

All the gas-solid phase reactions for this thesis are carried out in an ultra high vacuum reaction system, which is composed of a beam chamber and a reaction chamber. The beam chamber consists of three differentially evacuated chambers, where each of them is connected by a aperture of 2 mm diameter. The first differential chamber of the beam chamber is equipped with a radio-frequency (RF) plasma generator. The reaction chamber is equipped with a quadrupole mass spectrometer (QMS), an Ar+ ion gun, an Auger electron spectrometer (AES) and a sample manipulator. The beam chamber is connected to the ultrahigh vacuum chamber through 4 mm slit and can be opened or closed by using a gate valve during operation. Precise control of the time profile of the beam was achieved by a shutter at the exit of the RF plasma source, getting a sharp rise and fall of the beam within a second. A photograph (left hand side) and a schematic illustration (right hand side) of the experimental set-up are given below.

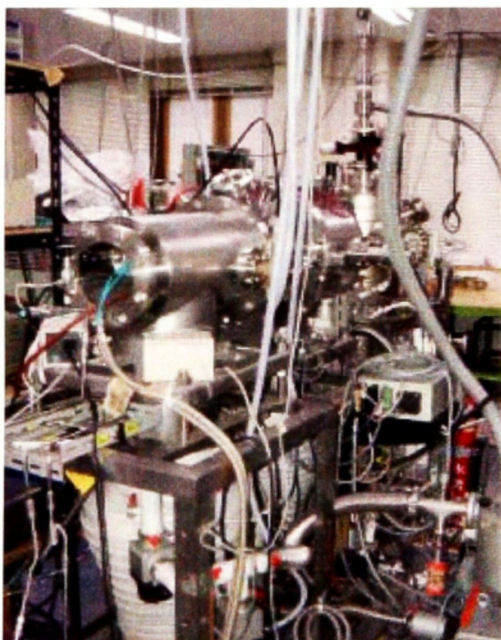

Fig. 2.1: Photograph of the experimental set-up from the direction of the beam chamber to the reaction chamber [1].

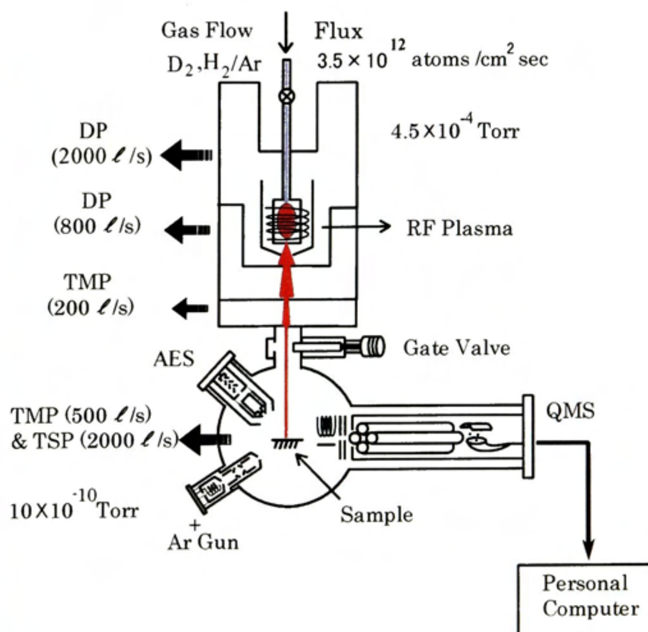

Fig. 2.2: Schematic diagram of the experimental set-up.

In the schematic diagram, the beam line is denoted by a red line from the RF generator to the sample. From the first chamber to the reaction chamber, the vacuum pressure increase gradually (1st chamber: 1×10^{-6} Torr; 2nd chamber: 1×10^{-7} Torr; 3rd chamber 5×10^{-9} and ultra-high vacuum chamber: 1×10^{-10} Torr) and hence the H plasma produced by the RF generator directed smoothly towards the sample. The beam size is controlled by the consecutive four slits of fixed sizes (2 mm) starting from the RF gun chamber to the gate valve of the reaction chamber. To achieve a high vacuum pressure as good as 1×10^{-10} Torr, the reaction chamber is baked out.

Flow sheet presentation for baking procedure can be presented as below:

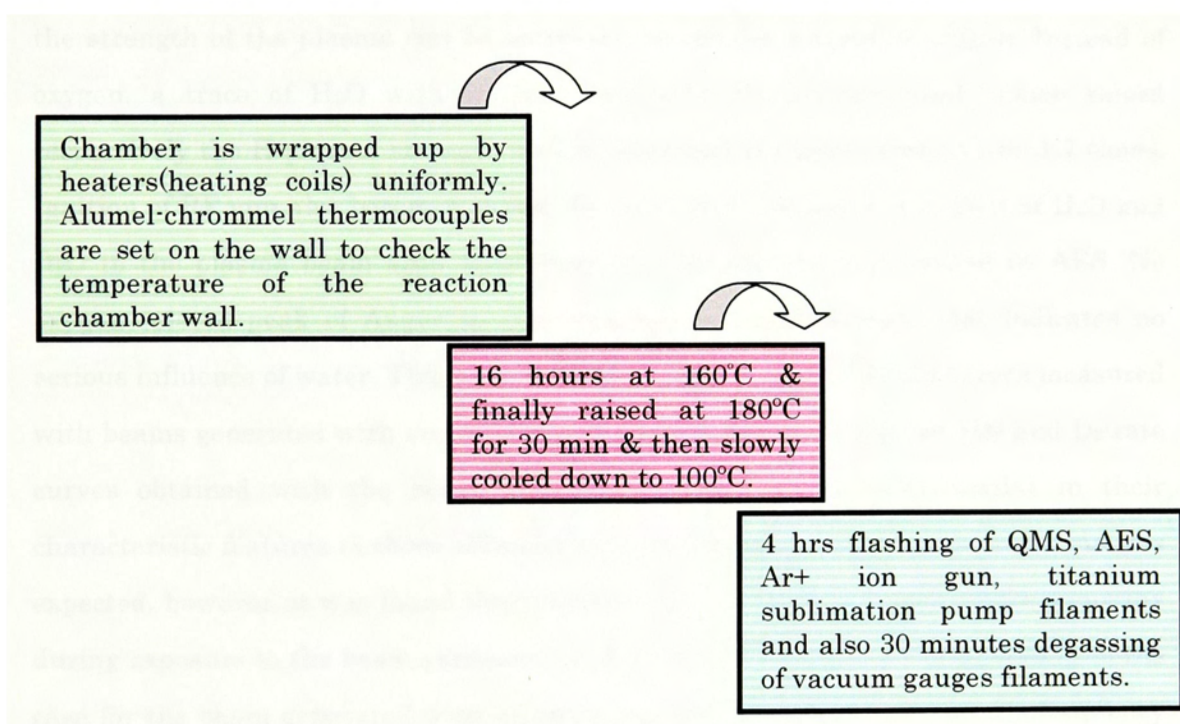

Good vacuum of the reaction chamber is the prime necessity for the gas-solid reactions, particularly in the order of 10^{-10} Torr region. High background of hydrogen always remains as an annoying factor. Practically it is not possible to make the hydrogen background nearly zero in the reaction chamber even at 10^{-11} Torr region vacuum. Best way to overcome this situation is by using deuterium (D) instead of hydrogen (H). Evacuation speed of the turbo molecular pump (TMP) and the titanium sublimation pump (TSP) in the reaction chamber are rapid enough to chase the desorbing species from the surface.

In CHAPTER 3, 4, and 5 experimental conditions and techniques are described briefly for each case. Here, a general description of the operations of the equipments and their performances has been discussed.

2.2 QUALITY OF THE RF PLASMA BEAM

The radio frequency plasma generator (RF generator) can produce plasma from the pure or diluted gas directly. The efficiency of making plasma or triggering the ignition varies with the molecular weight of the inlet gas. 99.9% pure hydrogen or deuterium gas mixed with 99.999% Ar (50:50) is used for the better plasma. It is reported that the strength of the plasma can be increased by mixing a trace of oxygen. Instead of oxygen, a trace of H_2O with H_2 and D_2O with D_2 gas are used, which raised respectively the H plasma strength by 2.6 times and D plasma strength by 1.7 times. Ignition of RF gun also becomes easier. To check the contamination effect of H_2O and D_2O in the plasma beam after long exposure, the sample was checked by AES. No oxygen related peak of Auger spectra was found on the sample that indicates no serious influence of water. This was checked in some D_2 and HD rate curves measured with beams generated with and without water. It was found that the HD and D_2 rate curves obtained with the beam generated without water were similar in their characteristic features to those obtained with the beam generated with water. As was expected, however, it was found that the time scale of the desorption events occurring during exposure to the beam generated without water became slower compared to the case for the beam generated with water. For 200 Watt power and 13.6 Hz frequency the RF plasma generator efficiently produces beam from H_2/Ar or D_2/Ar gas with high stability. The performance of the RF plasma generator and the stability of RF-beam are very sensitive to the vacuum condition of the beam chambers. Vacuum of the beam chambers are quite stable during the RF-plasma generation. A manual shutter is installed just in front of the RF gun along the beam line by which plasma irradiation to the surface can be controlled even for a few seconds.

H flux determined for Si(100) was $6.7 \times 10^{12}\,cm^{-2}\,s^{-1}$ and that for Si(111) was $3.5\ (\pm 1.5) \times 10^{12}\,cm^{-2}\,s^{-1}$. Flowing gas to the over heated tungsten filament (about 2000K) can also produce H beam but with a very low yield comparing with that from

the RF-plasma. The kinetic energy of hydrogen atoms produced by heated tungsten filament at 2000 K is about 0.3 eV. This is sometimes problematical because the surface is heated up to some extent. On the other hand, RF-plasma has an average kinetic energy of 0.05eV and thus no significant heating of the sample surface is expected during abstraction experiments. The beam size directed on the surface was nearly 4 mm in diameter. During exposure to the beam the reaction chamber pressure was 6~7 $\times 10^{-10}$ Torr.

2.3 DETECTION OF DESORBING SPECIES BY QMS

Desorbing molecules from the surface were detected by the QMS (Extrel Co.) with high resolution. It is possible to detect five different molecules simultaneously by using this QMS with good S/N ratio. Lowest possible detection time can be adjusted as low as 0.07 sec for a single molecule, but for better S/N ratio 0.65 sec detection time (retrace delay 0.05 sec + dwell time 0.2 sec $\times 3$) was used for three masses (H_2, HD & D_2). The QMS was attached directly to the reaction chamber with an angle of 90° with respect to the H beam line. So, the desorbing molecules do not come directly to the ionizer of the QMS, but it was rather integrated angular mode detection of the entire bulk molecules present in the reaction chamber. QMS sensitivity for H_2 (M/e = 2) and D_2 (M/e = 4) have been checked carefully and found no net difference in the sensitivity of both species. Mass calibrations for selected masses have been done over the mass range from 1 to 50 mass number. A good S/N ratio was adjusted by tuning the pre-amplifier sensitivity. Background for D_2 single mass detection was nearly zero at the tuned parameters of the QMS. During beam exposure, a QMS filament was intentionally set to "turn off" position for avoiding the extra atomic H production by the filament itself. If the clean surface is kept at room temperature for long time (overnight or 6-8 hours) there may be a background gas effect. For avoiding the background effect, minimum time delay was practiced before taking each data.

2.4 SAMPLE PREPARATION AND THERMAL TREATMENT

In this study two Si(100) and Si(111) surfaces were used. For both surfaces, the initial surface treatment was the same. Using a diamond cutter first the Si wafer is

cut into rectangular pieces of and then they are cleaned in pure grade acetone using an ultrasonic-vibrator. After three times repeated washing in acetone solution, the sample is dried in air and placed on the sample holder of the sample manipulator, where the sample wafer was supported with Mo plates on a ceramic disk. The electrical contact of the plates and sample surface is carefully monitored to assure the maximum contact between them, which is very important for homogeneous heating of the sample. Since the diameter of the beam is small (4 mm) it can avoid an influence of desorption from the Mo holders on the desorption events from the surface. Cleanliness of the sample is one of the prime conditions before starting any high vacuum experiment on the solid surface.

Table 2.1:

Sample	*Doping type*	*Resistance*	*Size (mm³)*	*Manufacturer*
Si(100)	B Doped, p-type	~10 Ωcm	13×21×0.5	Mitsubishi
Si(111)	P Doped, n-type	~10 Ωcm	13×22×0.5	Mitsubishi

A little contamination by carbon can affects the H induced reactions and the desorption yield would be reduced. Presence of impurity can change the resistance, which in turn causes the peak shift in TPD spectra. Less than 1% C-contamination for the Si surface is acceptable for avoiding such contamination effect; noise level signal for carbon Auger electron spectroscopy (AES) peak is desired or preferred. After achieving a good vacuum condition (~ 1×10^{-10} Torr) the sample was sputtered by Ar^+ ion gun with 60° angle to surface normal keeping the chamber pressure at $1.7\pm0.1\times10^{-7}$ Torr by flowing Ar^+ beam. If necessary, this Ar^+ cleaning process was repeated up to several times until a defined clean surface was obtained with less than 1% C AES intensity. Clean Si surfaces have affection towards oxygen also and upon exposure to air, oxygen always adsorbs on the surface. This adsorbed oxygen affects the surface property devastatingly. TPD peak shifting with a broadened peak, higher activation energy for desorbing species, low yield in the H-induced ABS and AID processes could be found if oxygen is present on the surface.

Table 2.2:

Sample	***Ar^+ Sputtering***				***Temperature Treatment***		
	T_s	Acceleration Voltage	Filament Current	Exposure Time	Annealing	Flashing	Cooling Rate
Si(100)	773K	1.5 KV	20 mA	15 min	1073 K (10 min)	1273 K (10 sec)	0.5 K/s
Si(111)	773K	1.5 KV	20 mA	15 min	1083 K (10 min)	1173 K (30 sec)	0.5 K/s

Particularly oxygen can change the structural geometry of the surface Si atom and ultimately results in a somewhat disordered surface. This oxygen can be removed by high temperature flashing of the sample for short time. For Si(100) the flashing was done at 1273 K for 10 sec and for Si(111) that was at 1173 K for 30 sec. For both surfaces at the mentioned temperatures, all adsorbed oxygen desorbs from the surface. For both surfaces, annealing was performed after brief flashing to get well ordered surface. The conditions for annealing and flashing are given in the table 2.2 for both Si(100) and Si(111) surfaces.

Cleanliness of the sample was checked by an AES method. Dirty samples show peaks attributed to C and O atoms. After sputtering and thermal treatments, those peaks were disappeared in AES spectra, which indicates the removal of C and O from the surface [Fig. 2.3]. Ar^+ ion sputtering, thermal treatment and AES check were done as a regular basis to confirm the quality of the Si sample.

Table 2.3: AES parameters details

T_s	***High Voltage source AC***	***DC Amplifier***	***Filament Current***	***Distance From Surface***	***Spectral Range***
RT	1.5 KV	1.3 KV	0.3 mA	0.8~1.0 cm	-50 ~ -550 eV

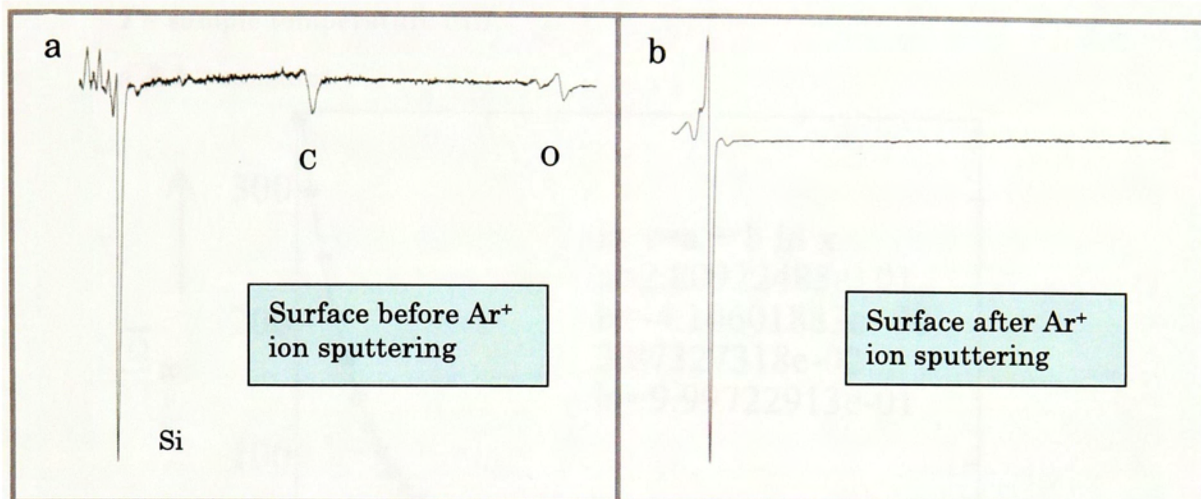

Fig. 2.3: AES spectra of Si(100) surface; a: dirty surface with C & O contamination, and b: clean surface without impurities.

2.5 CONTROL AND CALIBRATION OF SAMPLE T_s

During TPD experiment linear heating is important: Too rapid heating rate may yield error in chasing desorption (peak shift to higher temperature region) and too slow heating may results in isothermal decay loss. So an optimum heating rate is required to get an ideal TPD curve. For the Si(100) and Si(111) experiments, fixed heating rate was 3.4 K/s. The cooling rate of the sample is very important in obtaining well reproducible data. When the cooling rate was faster than 1.0K/s, uptake of H and abstraction reaction including AID were found to be non reproducible [2]. Therefore, the optimum-cooling rate for all the experiment was 0.5 K/s. Heating is done by direct resistive heating of the sample. DC electric current is supplied to the sample from a computer controlled setup. The computer program was written in C^{++} language. Particularly the home-made computer program can control the power supply unit through an AD converter. Using this device, T_s can be controlled over the range from 420 to 1273 K automatically or manually. A general relation of sample's resistance and sample temperature is used,

$$\ln R = a + b \ln T ,$$

(1.1)

Where, $\boldsymbol{R}$ = resistance (Ω)

T = sample temperature (°C)

a & b = constant

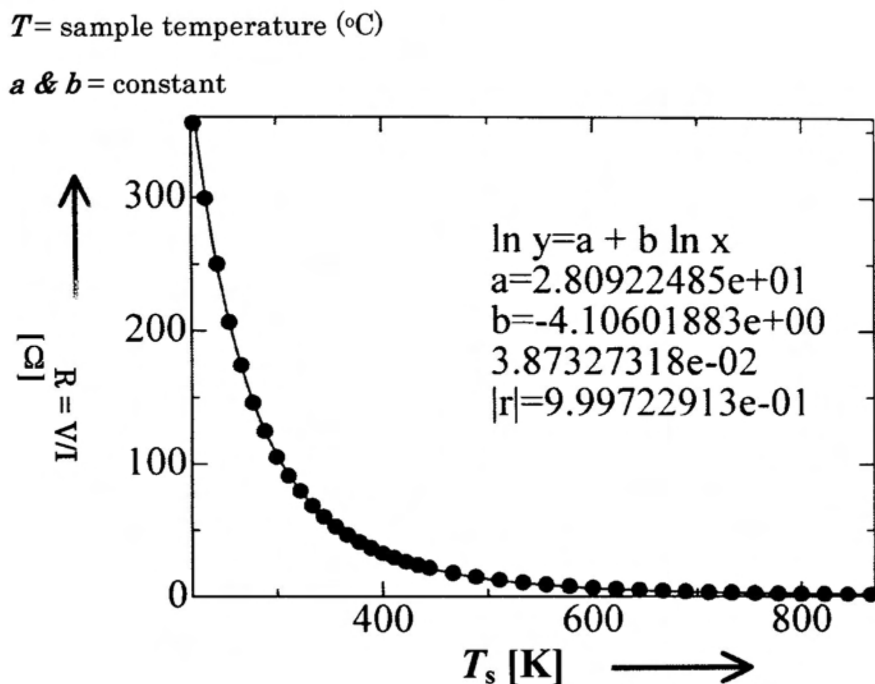

Fig. 2.4: Temperature calibration curve of the Si(100) sample: sample resistance vs. sample temperature .

For temperature calibration the sample was slowly heated up manually by supplying electrical power and the resistance R was read from the relation R = V/I while sample temperature was recoded by pyrometer (focusing to sample, situated at about 1 m apart), simultaneously.

After determining the constant values from the calibration curve, the executable C^{++} program was rebuilt to perform the updated heating system for the newly mounted sample. New heating system was rechecked for several fixed temperatures by the pyrometer again. Finally, pure D_2 TPD spectra clarify the correctness of T_s by referencing the established β_1 and β_2 TPD peak maxima.

REFERENCES

[1] Ph. D thesis of S. Shimokawa, March , 2001.

[2] S. Shimokawa, A. Namiki, M. N.-Gamo, and T. Ando, J. Chem. Phys. 113 (2000) 6916.

CHAPTER 3

Rate Equations in Si(100) at 573 K

This chapter is based on the paper J. Chem. Phys. 113 (2000) 3792.

Adsorption-induced desorption (AID) and Eley–Rideal (ER) type abstraction have been investigated in the reaction system, H(g)+ D_{ad}/Si(100) →D_2, HD, at surface temperature of 573 K where di-hydride phase is unstable. Rate equations for AID were obtained based on a second-order kinetics with respect to doubly occupied Si dimers which are considered as parent species of transiently formed di-hydrides. The coverages of the doubly occupied dimers were determined as a function of H exposure time by means of temperature -programmed-desorption (TPD), and then the rate equations were calculated. As a result, the experimental D_2 and HD rate curves were reasonably fit with the rate equations formulated. This fact indicates that AID is induced when two di-hydride species encounter during their propagation via di-hydride–mono-hydride isomerization reactions. It was found that HSi–SiH does not play a role in AID of both D_2 and HD. Possible origins of this isotope effect were discussed in terms of quantum effects on associative desorption and diffusion processes. The HD rate curve due to direct ER abstraction channel was fit with a first-order kinetics in D_{ad} coverage for a low coverage regime. However, for a high coverage regime the HD rate curve was fit with DSi–SiD coverages, suggesting that D_{ad} are paired up with H_{ad} in the same Si dimers are not abstracted.

3.1 INTRODUCTION

Hydrogen atom-induced abstraction and desorption from the D-terminated Si(100) surface

$$H(g)+D/Si(100) \rightarrow HD(g), D_2(g), \tag{3-1}$$

were studied by Shimokawa *et al.*[1] from a desorption point of view. The essence of their experimental results and the proposed model for AID are as follows: The features observed in both the HD and D_2 rate curves look quite similar to those observed in metal surfaces [2–9]. For low initial D_{ad} coverages θ_D^0 below 0.8 ML, there exists an induction time for AID. It might be considered that existence of such induction time is a result of preferential sticking of secondary HA to dangling bonds, until the surface is

saturated. However, the secondary HA mechanism for D_2 desorption was ruled out because the observed D_2 desorption at the surface temperature of 573 K does not follow second-order kinetics expected for the secondary HA abstraction, but rather manifests 3.5–4th order kinetics with respect to D_{ad} coverages θ_D. The unexpected fourth-order kinetics observed for AID may not be at variance with the Flowers' kinetics model [10], since AID proceeds along with a second-order kinetics with respect to the di-deuteride (DSiD) coverage, which is proportional to θ_D^2 as will be shown in Eq. (3-15). Furthermore, even the primary HA-induced abstraction of D_{ad} was also ruled out from the HD abstraction process because of no positive evidence for the HA mechanism. The observed HD rate curves for $\theta_D^0 \leq 0.5$ ML showed up a bimodal structure characterized with a steep rate jump followed by a monotonous decrease for $\theta_D^0 < 0.3$ ML, but with a small peaking for $\theta_D^0 > 0.3$ ML until the second peak sets in a high coverage regime, characterized with a highly efficient decay of the HD rate. The position of the second peak of the HD rate curves was approximately the same as that of the corresponding D_2 rate curves. Similarly to the D_2 rate curves, the second peak of the HD rate curves shifted to a shorter time region as θ_D^0 was increased. Therefore, the second peak was attributed to AID due to association of D_{ad} with H_{ad} rather than to generalized ER abstraction of D_{ad} by hot H atoms.

In this way, the features of abstraction and AID on Si(100) vary depending on the total surface coverages of D_{ad} and H_{ad} of which fractional ratio continuously changes with exposure time due to substitution of D_{ad} by H(*g*) during exposure. In this chapter the term AID is used instead of CID. The H-induced processes on Si(100) are categorized as a low and a high coverage regimes: For the low coverage regime that corresponds to the induction period for AID in the time domain, the incident H atoms have to cap Si dangling bonds which were not terminated in the pre-deposition process, competing abstraction and desorption. For the high coverage regime the surface gets saturated with D_{ad} and H_{ad}, and uptake and loss of hydrogen atoms are balanced under the equilibrium situation.

In the previous paper [1], kinetic equations to describe HD and D_2 rates were proposed to make a qualitative understanding of the mechanism of AID easier. Expected isotope effects on the rate constants for AID were neglected in that paper for

the simplicity of the kinetics model. For further rationalization of the mechanism proposed for the unusual fourth-order desorption in θ_D, it is desirable to reformulate HD and D_2 rates equations by taking the isotope effects into consideration. Then, the rate equations should be fit the experimental rate curves to extract physics and chemistry underlying in the H-induced processes on the D/Si(100) surfaces. In this work, we reformulate kinetics equations for the H-induced D abstraction and desorption of D_2 under the quasi-equilibrium condition first invoked by Flowers *et al.*[10] to explain the uptake process. Silicon di-hydride species formed during exposure are considered as key species for AID. However, their coverages are presently unable to be determined with our experimental system. Therefore, the rate equations are formulated not with momentary di-hydride coverages retained during exposure but with coverages of their parent species, i.e., doubly occupied Si dimers DSi–SiD (coverage: θ_{DD}), DSi–SiH(θ_{HD}), and HSi–SiH(θ_{HH}). Based on the pre-pairing mechanism [11, 12], the coverages of the doubly occupied species during exposure are determined by means of TPD. In this work, we do not intend to treat whole elementary reactions for H-induced process from sticking to desorption, but we calculate the rate equations for the abstraction and desorption during exposure by employing surface coverages determined experimentally as a function of exposure time.

3.2 KINETICS MODEL

Abstraction and AID in the reaction system of Eq. (3-1) at 573 K are described by the following reaction kinetics:

—Direct ER abstraction:

$$H(g) + D_{ad} \xrightarrow{k_{ER}} HD(g), \tag{3-2}$$

where, k_{ER} is the rate constant for the direct ER abstraction. Since substitutional reaction between H(*g*) and D_{ad} results in accumulation of H_{ad} during exposure, incident H(*g*) can also proceed such a direct ER abstraction reaction of H_{ad}. However, we do not treat this process because detection of H_2 produced during exposure is

difficult due to background H_2 gas.

—Sticking:

$$2H(g) + .Si\text{-}Si. \rightarrow HSi\text{-}SiH, \quad (3\text{-}3)$$

where .Si–Si. stands for unoccupied Si dimers. We, here, tacitly assume that all D_{ad} and H_{ad} are paired up to form doubly occupied dimers, and therefore, singly occupied dimers are not allowed to exist. This assumption may be valid for θ_D^0 > 0.2 ML [13].

—Adatom propagation and termination of dangling bonds:

$$HSiD + DSi\text{–}SiD \rightarrow HSi\text{–}SiD + DSiD, \quad (3\text{-}4)$$

$$2DSiD + .Si\text{-}Si. \rightarrow DSi\text{-}SiD. \quad (3\text{-}5)$$

—Adsorption-induced D_2 and HD desorptions:

$$DSiD + DSiD \xrightarrow{k_{DD}^{DD}} D_2(g) + DSi\text{–}SiD, \quad (3\text{-}6a)$$

$$DSiD + HSiD \xrightarrow{k_{DD}^{HD}} D_2(g) + HSi\text{–}SiD, \quad (3\text{-}6b)$$

$$DSiD + HSiH \xrightarrow{k_{DD}^{HH}} D_2(g) + HSi\text{–}SiH, \quad (3\text{-}6c)$$

$$HSiD + DSiD \xrightarrow{k_{HD}^{DD}} HD(g) + DSi\text{–}SiD, \quad (3\text{-}7a)$$

$$HSiD + HSiD \xrightarrow{k_{HD}^{HD}} HD(g) + HSi\text{–}SiD, \quad (3\text{-}7b)$$

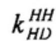

k_{HD}^{HH}

$$HSiD + HSiH \rightarrow HD\,(g) + HSi\text{–}SiH, \tag{3-7c}$$

where, k_i^j (i = DD, HD, and j= DD, HD, HH) are the rate constants for AID including propagation process such as Eq. (3-4). Regarding the hydrogen association, one should note that two adatoms in one Si dimer preferentially associate as two di-hydrides meet at a reaction site to induce desorption. This is the hydrogen desorption mechanism proposed by Flowers *et al.* [14] for the β_2 channel in TPD from a di-hydride phase. Figure 3.1 describes the model proposed above for the D_2 AID process over the D–Si(100) surface. In view of TPD, AID on Si(100) can be categorized as an isothermal desorption occurring via the β_2 channel TPD for H_2.

The quasi-equilibrium condition claims that uptake and loss of adatoms during exposure are balanced so that the total surface coverage of H_{ad} and D_{ad} including excessive di-hydride species is kept constant on the saturated surface. For nonsaturated surfaces, a fraction of surface Si atoms are not still bonded by H atoms in the early period of H exposure. In this case, the di-hydride species formed during exposure are consumed to cap the dangling bonds. In the quasi-equilibrium state achieved during exposure, we consider that AID is induced by the excess di-hydrides after Eqs. (3-6a) – (3-7c). This tacitly assumes that sticking probability of H (*g*) is high, and di-hydride species terminate dangling bonds immediately when they are introduced by the ER type abstraction. Thus, the model includes a mass balance between the incident flux J_{in} and number of abstracting (N_{abst}), sticking (N_{stick}), and reflecting particles (N_{ref}) in cm²/s,

$$J_{in} = N_{abst} + N_{stic} + N_{ref}. \tag{3-8}$$

A fraction of sticked hydrogen atoms terminate dangling bonds either directly by Eq. (3-3) or indirectly by Eq. (3-5), and the others remain on the surface as excessive di-hydride species which contribute to AID. Then, we get a balance for the sticking atoms

$$N_{stic} = N_{abst} + N_{dihyd}. \tag{3-9}$$

H (*g*) sticking probability, *s*, can be evaluated by Eqs. (3-8) and (3-9) as

$$s = \frac{N_{stic}}{J}.$$

or, $$s = \frac{N_{abst} + N_{dihyd}}{2N_{abst} + N_{dihyd} + N_{ref}}. \tag{3-10}$$

If N_{ref} is smaller than $2N_{abst}$ so that it can be neglected, it will be possible to evaluate s for $t \simeq 0$ when no HD AID takes place; s is expressed with D_2 and HD desorption rates, $I(D_2)$ and $I(HD)$, respectively, as

$$s \simeq \frac{I(HD) + 2I(D_2)}{2I(HD) + 2I(D_2)}. \tag{3-11}$$

In this way, the key surface species for adsorption-induced desorption are di-hydrides; DSiD, DSiH, and HSiH. They reside on the surface excessively beyond the saturation coverage retained after beam off. However, we cannot determine such excessive coverages during exposure, but can know only the surface coverages of H_{ad} and D_{ad} after turning off the H(*g*) beam when the di-hydride species have already been extinguished.

In Fig. 3.1, AID process which occurs as two surface di-hydride species encounter during exposure is illustrated. The di-hydride– mono-hydride isomerization reaction induces propagation of di-hydride species in such a way that only the configuration is exchanged between mono-hydride and di-hydride without nascent adatom transfer beyond the two sites. This implies that the kind of desorbing molecules is determined by the kind of adatoms on the adjacent two Si dimers on which two di-hydride species will meet to induce AID. Take Eq. (3-6b), for example. Two D atoms of a DSiD are handed down from its parent Si dimer which was doubly occupied with the same D atoms as denoted in Eq. (3-4) or schematically illustrated in Fig. 3.1. This is also the same for the counter di-hydride HSiD of which parent was HSi–SiD. Therefore, the D_2 desorption rate denoted in Eq. (3-6b) is essentially proportional to both θ_{DD} and θ_{HD}.

Therefore, including direct ER abstraction of Eq. (3-2), HD rate for the reaction denoted as Eq. (3-1) is formulated as follows:

$$\frac{dN_{HD}(t)}{dt} = K_{ER}N_0\theta_D + \eta N_0^2\{k_{HD}^{DD}\theta_{HD}\theta_{DD}$$

$$+2k_{HD}^{HD}\theta_{HD}\theta_{HD} + k_{HD}^{HH}\theta_{HD}\theta_{HH}\}. \qquad (3\text{-}12)$$

Here, N_0 is the Si density per unit area on the surface, and η is the probability of escaping from sticking to dangling bonds.

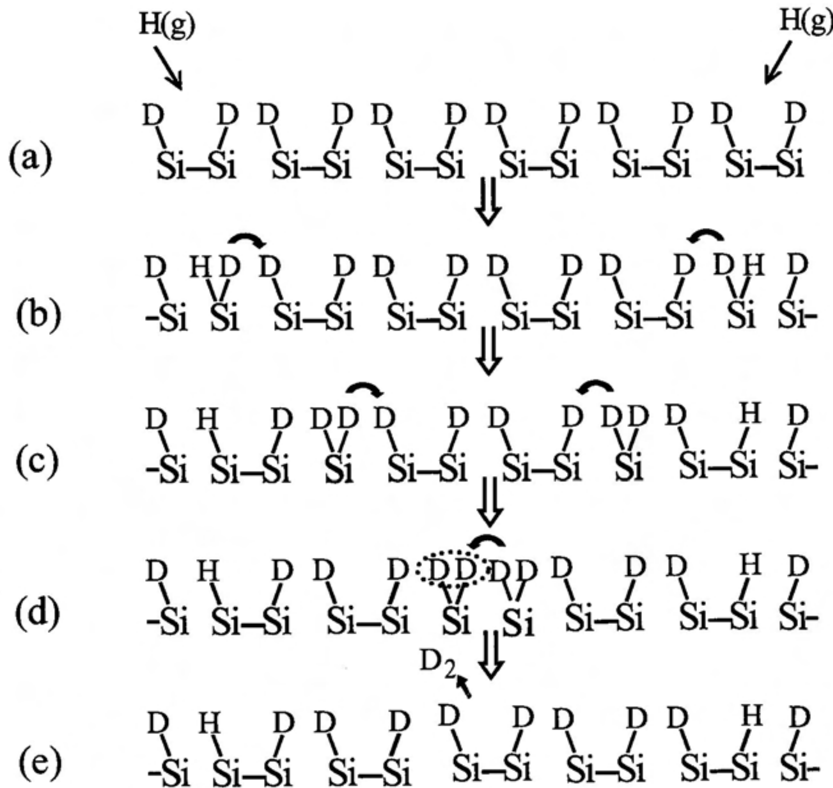

Fig. 3.1: Schematic view of the adsorption-induced desorption process for the reaction system H(g) + D(1ML)/Si(100). (a): Hydrogen atoms attack the D-terminated Si(100). (b): Incident H atoms are sticked to D-terminated Si dimers to form HSiD species which then proceed a di-hydride-mono-hydride isomerization reaction to form DSiD species. (c): DSiD species further proceed the isomerization and encounter with each other at the site where desorption of D_2 is then induced at (d) stage. (e): A D_2 molecule desorbs the surface leaving a doubly occupied Si dimer DSi–SiD. All the reactions are assumed to occur in the thermodynamically equilibrium condition.

On the other hand, adsorption-induced D_2 rate is formulated as

$$\frac{dN_{D_2}(t)}{dt}=\eta N_0^2\{2k_{DD}^{DD}\theta_{DD}\theta_{DD}$$
$$k_{DD}^{HD}\theta_{DD}\theta_{HD}+k_{HD}^{HH}\theta_{HD}\theta_{HH}\}. \quad (3\text{-}13)$$

If complete mingling takes place between D_{ad} and H(*g*) during exposure, θ_{DD} , θ_{HD}, and θ_{HH} are proportional to θ_D^2, $\theta_H\theta_D$, and θ_H^2, respectively. Hence, Eqs. (3-12) and (3-13) can be recast as

$$\frac{dN_{HD}(t)}{dt}=K_{ER}N_0\theta_D+\eta N_0^4$$
$$\times\{k_{DD}^{HD}\theta_H\theta_D^3+2k_{HD}^{HD}\theta_H^2\theta_D^2+k_{HD}^{HH}\theta_H^3\theta_D\}, \quad (3\text{-}14)$$

and for D_2 desorption

$$\frac{dN_{D_2}(t)}{dt}=\eta N_0^4\{k_{DD}^{DD}\theta_D^4+2k_{DD}^{HD}\theta_D^3\theta_H+k_{DD}^{HH}\theta_D^2\theta_H^2\} \quad (3\text{-}15)$$

In order to avoid cluttering the rate constants in the equations the same notation as defined in Eqs. (3-6a) –(3-7c) is used for the rate constants in the above equations. Equations (3-14) and (3-15) are fundamentally the same to the equations employed in the previous paper [1] except for the isotopic dependence on the rate constants. Equation (3-15) indicates that the adsorption-induced desorption of D_2 proceeds along a fourth-order kinetics with respect to surface coverages θ_D and θ_H. In particular, for the early period of exposure where θ_H is negligible, the D_2 rate is described essentially as a fourth-order kinetics in θ_D.

3.3 EXPERIMENT

The detail of the experiments is discussed in chapter 2 and the HD and D_2 rate curves were described previously [1].

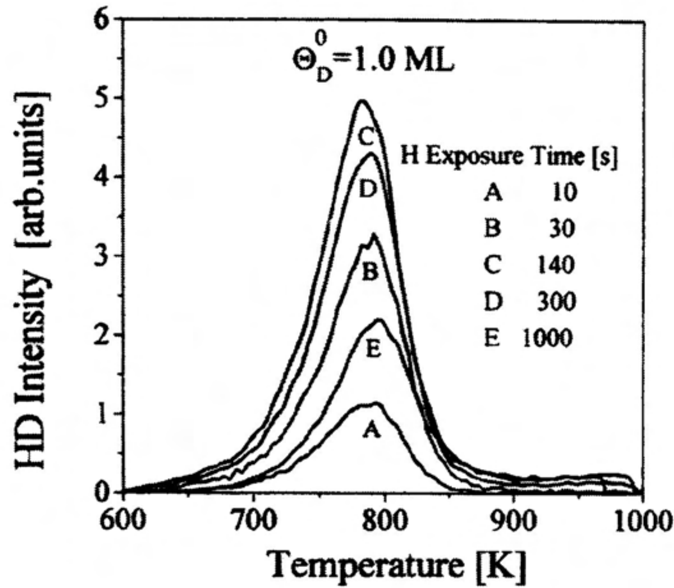

Fig. 3.2: HD TPD spectra measured for various H exposure times on the D/Si(100) surfaces for θ_D^0 = 1.0 ML. The surface temperature for both the D pre-deposition and H exposure is 573 K.

The clean Si(100) surface was first exposed to D beams to prepare D-covered Si(100) surfaces with $\theta_D^0 = 1$ ML or 0.45 ML. Then, the surface was exposed to H beams, and then D_2, HD, and H_2 TPD spectra were measured with a QMS for various exposure times in an angle integration mode. Figure 3.2 shows HD TPD spectra measured for various H exposure times on D(1 ML)/Si(100) surface at $T_s = 573$ K. It is observed that the HD TPD spectra first increase and then decrease.

3.4 CALCULATING RATES

3.4.1 Hydrogen Coverages

Coverages of DSi–SiD (θ_{DD}), DSi–SiH (θ_{HD}), and HSi–SiH (θ_{HH}) were evaluated from the D_2, HD, and H_2 TPD spectra as a function of time t. This method may be rationalized by the widely accepted hydrogen desorption mechanism [15–17] for the β_1 channel desorption from a mono-hydride phase, i.e., hydrogen desorption is induced

in a concerted fashion by the preferential association of two hydrogen atoms which have been paired up in a Si dimer [11, 12]. Hence, θ_{DD}, θ_{HD}, and θ_{HH} are evaluated as

$$\theta_{DD} = c.2I(D_2), \tag{3-16a}$$

$$\theta_{HD} = c.I(HD), \tag{3-16b}$$

$$\theta_{HH} = c.2I(H_2), \tag{3-16c}$$

where c is the calibration constant, and $I(i\,j)$ is TPD intensity for $i\,j$= D_2, HD, and H_2. The factor of 2 for θ_{DD} and θ_{HH} is introduced because the QMS data for D_2 or H_2 contain two same isotopes. Therefore, one should remark that the unit of θ_{ij} defined above is the number of i atom per surface Si atom. The calibration was done with the saturated D_2 TPD intensity at T_s=600 K where no di-hydride is formed. However, a very small β_2 TPD peak was recognized at T_s = 573 K for the prolonged exposures on the D–Si(100) system [1], and hence, the total saturation coverage can become a little bit larger than 1 ML by about 3%. Figures 3.3 and 3.4 show the plots of θ_{DD}, θ_{HD}, and θ_{HH} for θ_D^0= 0.45, and 1.0 ML, respectively, for various exposure times t. θ_{DD} and θ_{HH} are found to be, respectively decreasing and increasing functions with t, while θ_{HD} is found to exhibit a peak.

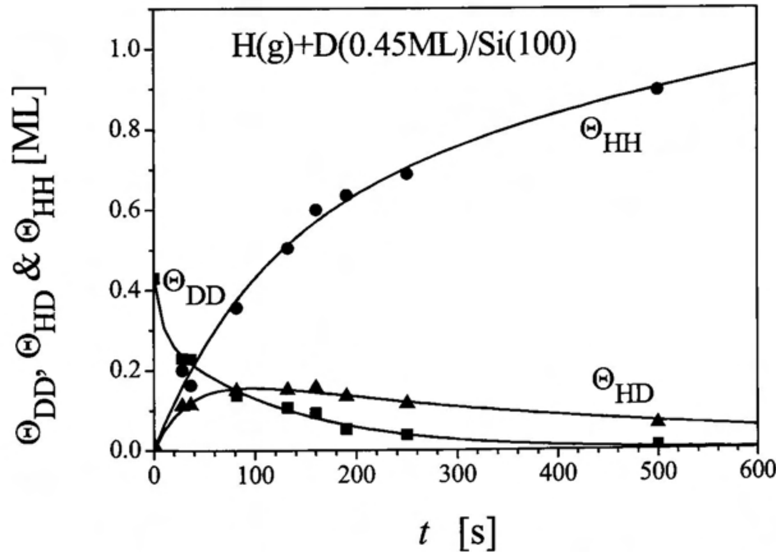

Fig. 3.3: Plots of θ_{DD}, θ_{HD}, and θ_{HH} vs H exposure time t for θ_D^0 = 0.45 ML. Solid lines are the best fit curves with: Eq. (3-18a) for θ_{DD} (c=0.14, c= 0.29, k_1=0.0009 s^{-1}, k_2= 0.0097 s^{-1}), Eq. (3-18b) for θ_{HH} (c=1.5, c_1= 0.94, c_2= 0.56, k_1= 0.12 s^{-1}, k_2= 0.0079 s^{-1}), and Eq.(3-18c) for θ_{HD} (c= 0.21, k_1= 0.0021 s^{-1}, k_2= 0.029 s^{-1}).

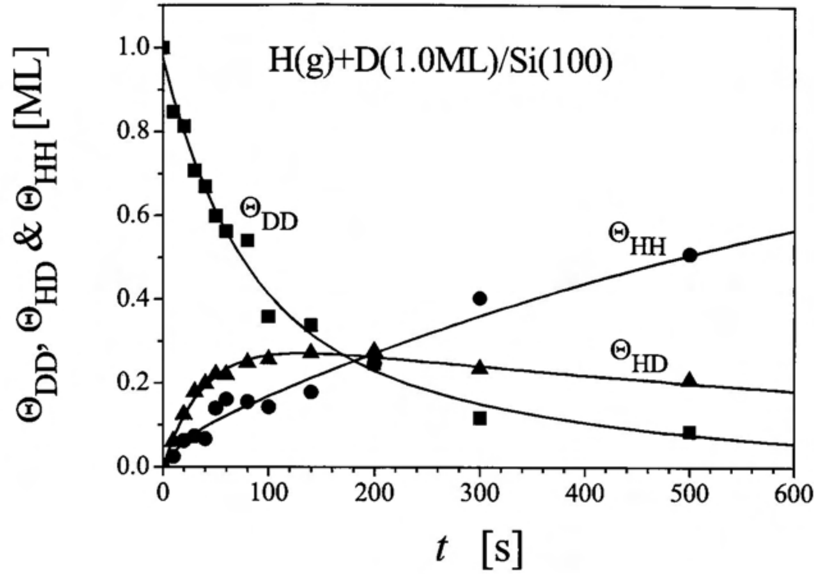

Fig. 3.4: Plots of θ_{DD}, θ_{HD}, and θ_{HH} vs H exposure time t for θ_D^0= 1.0 ML. Solid lines are the best fit curves with: Eq. (3-18a) for θ_{DD} (c_1= 0.36, c_2 = 0.61, k_1= 0.0031 s^{-1}, k_2=0.014 s^{-1}), Eq. (3-18b) for θ_{HH} (c=1.0, c_1= 0.057, c_2= 0.95, k_1= 0.057 s^{-1}, k_2= 0.0013 s^{-1}), and Eq. (3-18c) for θ_{HD} (c=0.32, k_1= 0.000 92 s^{-1}, k_2= 0.026 s^{-1}).

The coverages θ_D and θ_H (number of adatoms per surface Si atom) during H exposure at 573 K were also evaluated from the same H_2, D_2, and HD TPD spectra for various exposure times as,

$$\theta_D = c(2I(D_2) + I(HD)), \tag{3-17a}$$

$$\theta_H = c(2I(H_2) + I(HD)), \tag{3-17b}$$

where, c is the calibration constant. One should notice the relation θ_D (θ_H) = θ_{DD} (θ_{HH}) + θ_{HD}. In Figs. 3.5 and 3.6 θ_D and θ_H are plotted for θ_D^0 = 0.45 and 1.0 ML, respectively, for various t. θ_D shows monotonous decrease due to the D replacement by the incident H atoms. Nevertheless, during exposures no β_2 peak was recognized in the HD and H_2 TPD spectra, while θ_H increases first rapidly and later on slowly, but does not show a clear saturation even for 1000 s exposure.

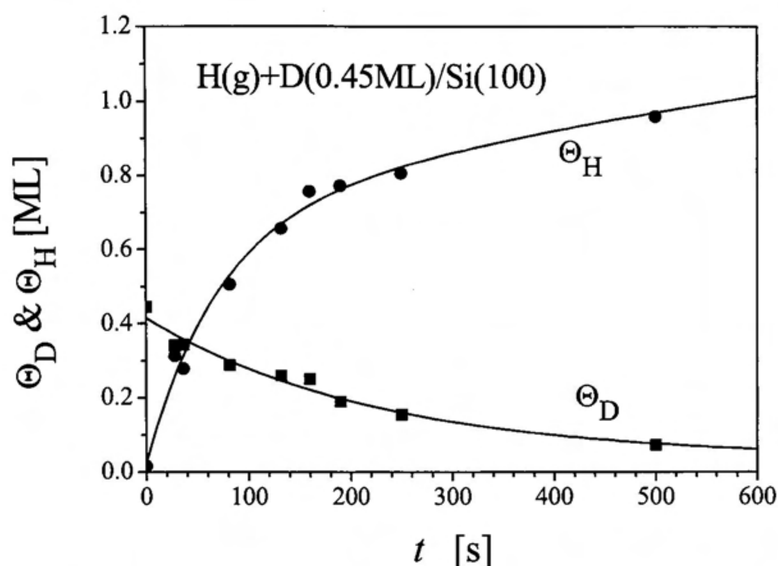

Fig. 3.5: Plots of θ_D and θ_H vs H exposure time t for $\theta_D^0 = 0.45$ ML. Solid lines are the best fit curves with: Eq. (3-18a) for θ_D ($c_1 = 0.36$, $c_2 = 0.052$, $k_1 = 0.0047$ s^{-1}, $k_2 = 0.00046$ s^{-1}), and Eq. (3-18b) for θ_H ($c = 1.5$, $c_1 = 0.65$, $c_2 = 0.82$, $k_1 = 0.014$ s^{-1}, $k_2 = 0.00087$ s^{-1}).

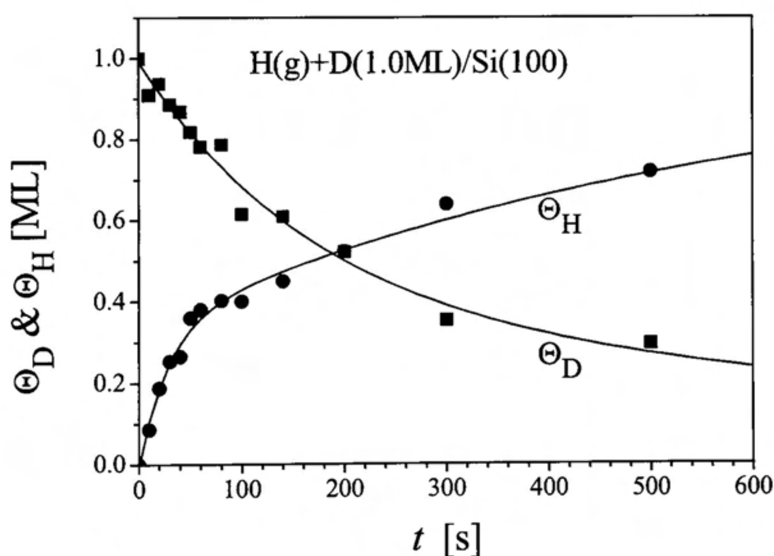

Fig. 3.6: Plots of θ_D and θ_H vs H exposure time t for $\theta_D^0 = 1.0$ ML. Solid lines are the best fit curves with: Eq. (3-18a) for θ_D ($c_1 = 0.36$, $c_2 = 0.63$, $k_1 = 0.00086$ s^{-1}, $k_2 = 0.0059$ s^{-1}), and Eq. (3-18b) for θ_H ($c = 1.0$, $c_1 = 0.34$, $c_2 = 0.66$, $k_1 = 0.035$ s^{-1}, $k_2 = 0.0017$ s^{-1}).

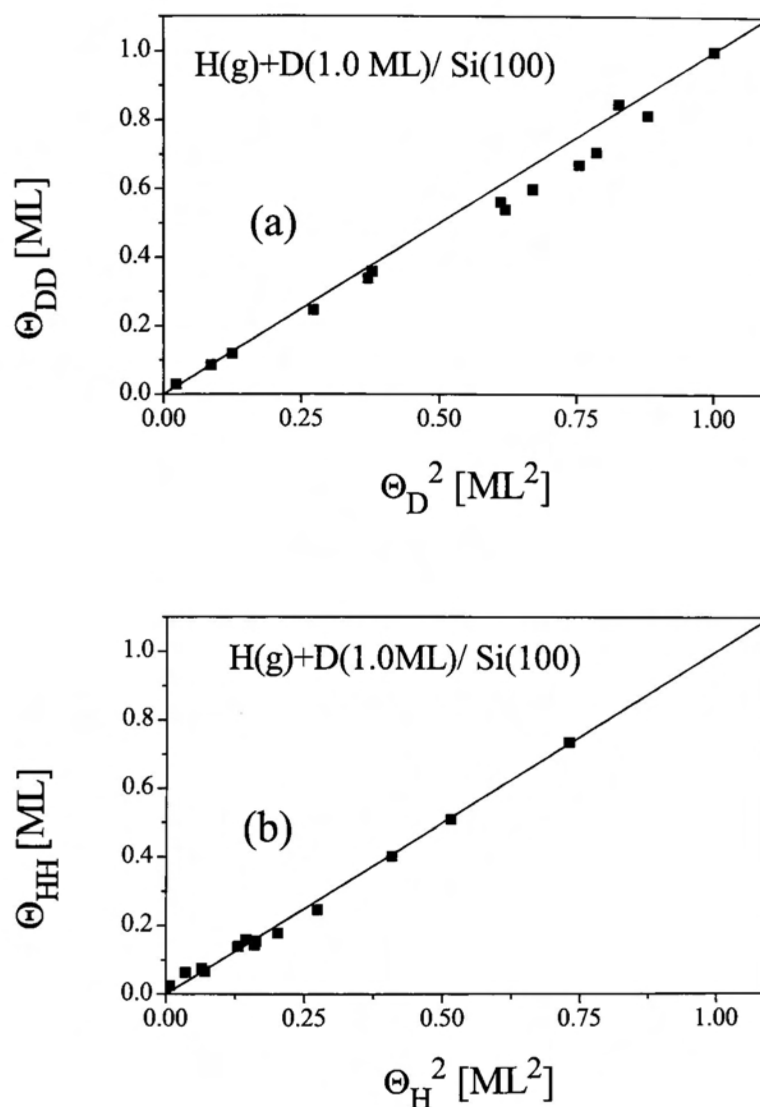

Fig. 3.7: Plots of θ_{DD} vs θ_D^2 (a), and θ_{HH} vs θ_H^2 (b) for θ_D^0 = 1.0 ML. Solid lines show the case of $\theta_{ii} = \theta_i^2$.

Figure 3.7(a) shows the plots of θ_{DD} versus θ_D^2, and Fig. 3.7(b) θ_{HH} versus θ_H^2 for θ_D^2 = 1.0 ML. The solid lines exhibit θ_{DD} (θ_{HH}) = θ_D^2 (θ_H^2). As can be seen clearly in both plots, the experimental data points are nearly on the straight lines. This indicates that $\theta_{DD} \simeq \theta_D^2$ and $\theta_{HH} \simeq \theta_H^2$. Therefore, this linear relationship between θ_{DD} and θ_D^2 or θ_{HH} and θ_H^2 might rationalize the hydrogen preparing mechanism employed

for the coverage determinations and H/D mingling assumed for Eqs. (3-14) and (3-15).

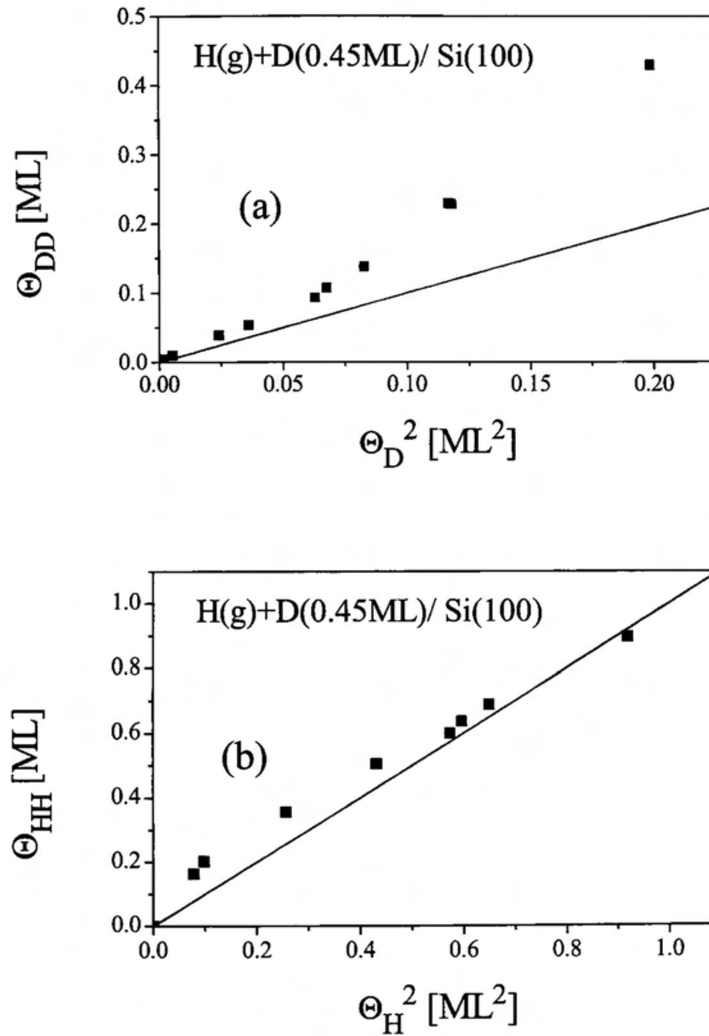

Fig. 3.8: Plots of θ_{DD} vs θ_D^2 (a), and θ_{HH} vs θ_H^2 (b) for $\theta_D^0 = 0.45$ ML. Solid lines show the case of $\theta_{ii} = \theta_i^2$.

For $\theta_D^0 = 0.45$ ML, however, the θ_{DD} versus θ_D^2 and θ_{HH} versus θ_H^2 plots show a deviation from such straight lines expected for the relationship θ_{DD} $(\theta_{HH}) = \theta_D^2$ (θ_H^2) particularly in the early stages of exposure as shown in Fig. 3.8. This deviation comes apparently from the relation that for $t = 0$, $\theta_{DD} = \theta_D$ (<1.0), thence $\theta_{DD} > \theta_D^2$.

Preferential pairing of H atoms supplied to the empty dangling bonds does not allow complete mingling of H and D. Therefore, it is not allowed to assume that θ_{DD} (θ_{HH}) = θ_D^2 (θ_H^2) for low θ_D^0.

In order to calculate desorption rate equations for any exposure time *t*, following functions of *t* are defined to represent θ_{DD} (θ_D) and θ_{HH} (θ_H), respectively

$$\theta_{DD/D}(t) = c_1.\exp(-k_1 t) + c_2.\exp(-k_2 t), \tag{3-18a}$$

$$\theta_{HH/H}(t) = c - c_1.\exp(-k_1 t) - c_2.\exp(-k_2 t), \tag{3-18b}$$

where, c_j and k_j are the fitting parameters. On the other hand, θ_{HD} which has a peak is fit with the following function:

$$\theta_{HD}(t) = c(\exp(-k_1 t) - \exp(-k_2 t), \tag{3-18c}$$

where, c and k_j are the fitting parameters again. One should note that above three functions have not been derived theoretically, but have chosen empirically without giving any physical meaning. The solid lines in Figs. 3.3–3.6 show the fitting results obtained using a least mean squares method for θ_D^0=0.45 and 1.0 ML, respectively.

3.4.2 η

For the quasi-equilibrium condition, already existing dangling bonds for low θ_D^0 act as a sink of H. di-hydride species formed during exposure will be consumed by the dangling bonds before AID. The probability of escaping from sticking to dangling bonds, η, is expected to be a function of adatom coverage. It must be zero when the surface is clean, and steps up to unity at about saturation with an *S*-shaped structure. Such an *S*-shaped function can be well represented by the following function:

$$\eta(t) = \frac{1}{2}\{1 + erf(x)\}, \tag{3-19}$$

for

$$x = (\theta_H(t) + \theta_D(t) - \theta_0)/w. \tag{3-20}$$

Here, erf(x) is the error function. η is characterized with two parameters, θ_0 and w. The former exhibits position of the maximum slope, and the latter exhibits width of the function changing from low to high values. Here, θ_0 = 0.65 ML and w= 0.1ML are chosen by taking into account the S-shape increase in the initial D_2 rate with θ_D^0; namely, D_2 rate around t =0 are characterized with the onset around θ_D^0 = 0.5ML with a maximum slope around θ_D^0 = 0.65 ML as observed in Fig. 5 of Ref [1]. The function η so determined really gives a reasonable fit for the D_2 rate as will be shown in the next section. Figure 3.9 shows the plot of η as a function of t for θ_D^0 =0.45 ML.

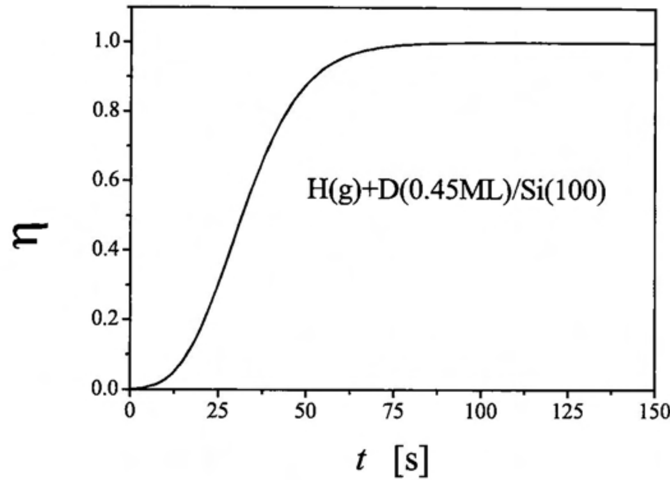

Fig. 3.9: η vs H exposure time for θ_D^0 = 0.45 ML. It is defined that $\eta(t)=\frac{1}{2}[1+erf((\theta_D+\theta_H-\theta_0)/w)]$, where θ_0 = 0.65 ML and w=0.1 ML.

3.4.3 D_2 and HD Rates

The HD and D_2 rate equations are formulated as Eqs. (3-12) and (3-13), or Eqs. (3-14) and (3-15). For AID Eqs. (3-12) and (3-13) employ θ_{DD} , θ_{HD}, and θ_{HH}, while Eqs. (3-14) and (3-15) employ θ_D and θ_H. HD and D_2 rates are calculated using both methods, Eqs. (3-12) and (3-13) and Eqs. (3-14) and (3-15). It turns out that the two results are more or less the same for θ_D^0 =1.0 ML, but are different for θ_D^0 = 0.45 ML. This is partly due to the break down of the prerequisite that θ_{DD} = θ_D^2 as noted before in the subec. 3.4.1 for θ_D^0 = 0.45 ML. Here, we give the results obtained with Eqs. (3-12) and (3-13), commenting the deviations appeared in the alternative method using Eqs. (3-14) and (3-15).

Since the D_2 desorption is solely due to AID, both the peak position and the decay rate of the D_2 rate equation may be good physical quantities to be compared with the experimental results without any influence by the ER abstraction term. The peak position of the rate curve is determined by balancing the increasing η function and the decreasing coverage functions with t. On the other hand, the slope of the rate curves in the high coverage regime is determined solely by the coverage functions since η =1. Firstly, we consider the D_2 rate curve for $\theta_D^0 = 0.45$ ML. Here, we intend to show their features analytically, however still qualitatively, by determining the coefficients with least mean-square methods: The D_2 rate curve for $\theta_D^0 = 0.45$ ML can be relatively fit to Eq. (3-13) with the best fit parameters $k_{DD}^{DD} : k_{DD}^{HD} : k_{DD}^{HH}$ =1.2:1.0:0, and the result is plotted in Fig. 3.10 [curve (a)].

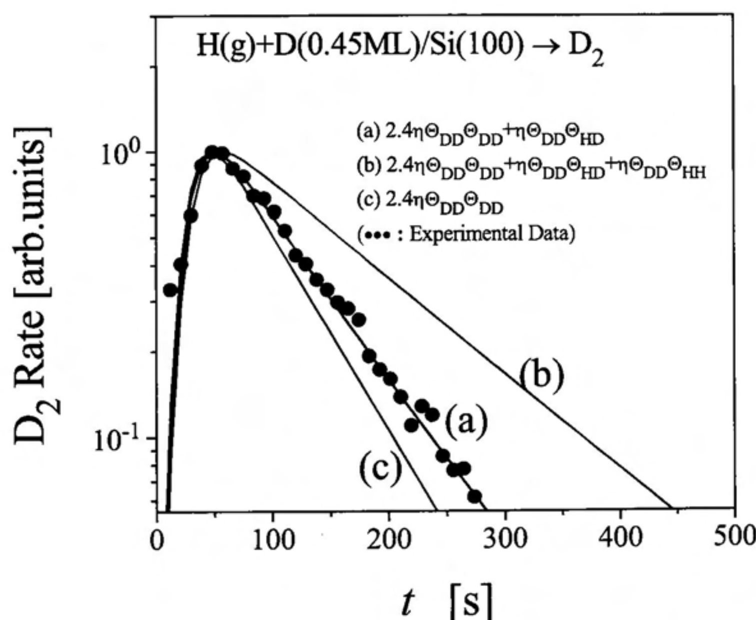

Fig. 3.10: Comparison of the calculated and experimental D_2 rate curves for $\theta_D^0 = 0.45$ ML in a logarithmic scale. Curve (a) is the best-fit result for Eq. (3-13) in the text. Curves (b) and (c) are calculated for checking the effect by the second and the third terms in Eq. (3-13). The coefficients in the rate equations are chosen as noted in the figure.

One can notice that the best-fit curve (a) reproduces the peak position and the slope after the peak fairly well. One interesting point about the rate constants obtained is

that there is an isotope effect on AID, i.e., $k_{DD}^{HH}=0$. It is interesting to know how the best-fit curve is modified after intentionally changing the contributions of each term. In Fig. 3.10 we plot two other cases, one includes the third term of Eq. (3-13) with a unity contribution of k_{DD}^{HH} [curve (b)] and the other [curve(c)] involves only the first term $k_{DD}^{DD}\,\theta_{DD}^{2}$ in Eq. (3-13), i.e., $k_{DD}^{HD} = k_{DD}^{HH} = 0$. Curve (b), which includes all the possible desorption channels, manifests its decay much slower than curve (a), thus deviating remarkably from the experimental result. This fact indicates that the $k_{DD}^{HH}\,\theta_{HD}\,\theta_{HH}$ term does not contribute to the D_2 AID. H_2 molecules could preferentially desorb when HSiH species encounter DSiD species. On the other hand, curve (c) shows a considerably reasonable peak position, but shows a much faster decay than the experimental one after the peak.

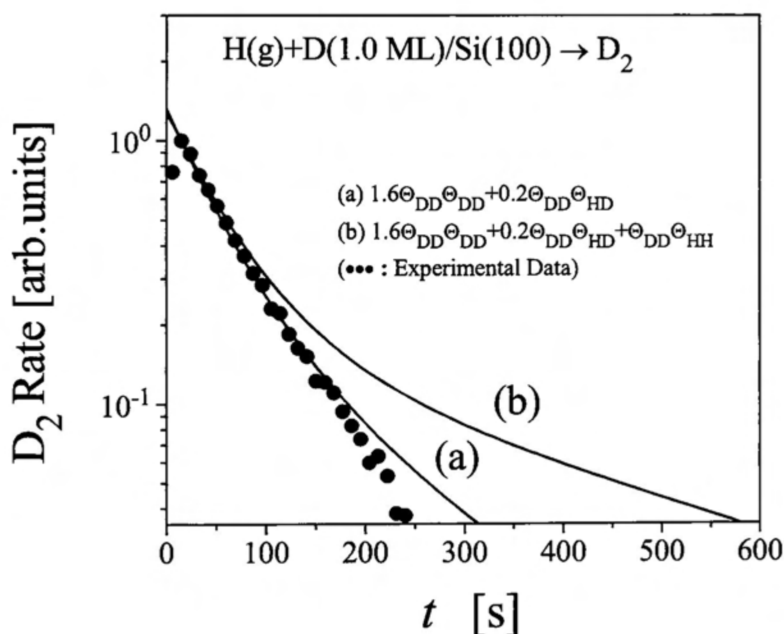

Fig. 3.11: Comparison of the calculated and experimental D_2 rate curves for $\theta_D^0 = 1.0$ ML in a logarithmic scale. Curve (a) is the best-fit result for Eq. (3-13) in the text. Curve (b) is calculated for checking the effect of the third term in Eq. (3-13).

Figure 3.11 shows the D_2 rate calculated with Eq. (3-13) for $\theta_D^0 = 1.0$ ML where $\eta = 1$. Curve (a) is drawn for the best-fit result with $k_{DD}^{DD} : k_{DD}^{HD} : k_{DD}^{HH} = 4{:}1.0{:}0$. There is an isotope effect again on the rate constants, and HSiH species do not contribute to AID

as in the case of $\theta_D^0 = 0.45$ ML. In order to check how the D_2 rate is affected by the third term of Eq. (3-13), we plot curve (b) after getting the contribution of $k_{DD}^{HH} : k_{DD}^{DD}$ = 1.0: 0.8. We find that the $k_{DD}^{HH}\,\theta_{HD}\,\theta_{HH}$ term leads to the much slower decay than the experimental result.

If Eq. (3-15) is used instead of Eq. (3-13) for $\theta_D^0 = 0.45$ ML, we find that the peak position of the D_2 rate curve is reproduced again fairly well, but the slope of the rate curve after the peak becomes slightly slower than the case of Eq. (3-13). This is due to the break down of the relation $\theta_{DD} = \theta_D^2$ and due to the slower decrease of θ_D^2 than θ_{DD}. For $\theta_D^0 = 1.0$ ML, on the other hand, it is found that the discrepancy between Eqs. (3-13) and (3-15) is small. This is natural because the relation $\theta_{ij} = \theta_i^2$ holds for $\theta_D^0 =$ 1.0 ML as shown in Fig. 3.7.

In case of the abstraction of HD, both the direct and the indirect abstractions due to AID are involved in the process. In order to calculate the HD rate equations, we need to deconvolute the HD rate curves into the two processes. However, we cannot experimentally deconvolute the rate curves. Therefore, for relative comparison between the calculated and experimental results in logarithmic plots, new fitting parameters C_1, C_2, and C_3 are introduced for the three AID terms after referencing the coefficient in the ER abstraction term. Hence, C_1, C_2, and C_3 include a ratio of the rate constant of the AID to that of the ER abstraction, k_{HD}^J / k_{ER} for
j=DD, HD, and HH. The HD rate equation [3-12] is recast as

$$\frac{dN_{HD}(t)}{dt} \propto \theta_D + \eta\{C_1\theta_{HD}\theta_{DD} + 2C_2\theta_{HD}\theta_{HD} + C_3\theta_{HD}\theta_{HH}\} \qquad (3\text{-}12')$$

By choosing values appropriate for C_j, Eq. (3-12′) can reproduce the peak position of the HD rate curve around t= 70 s for $\theta_D^0 = 0.45$ ML, but no reasonable fit after the peak is obtained for any C_j. The calculated curve is very slow in decay of HD rate after the peak compared to the experimental one. We find that this deviation arises from the ER abstraction term. This claims that the coverage function defined as target density for abstraction should decay more faster than θ_D for the high coverage regime where the surface gets saturated. Preserving the same functional dependence on θ_D as before for the low coverage regime but switching to θ_{DD} for the high coverage regime, we

tentatively employ $(1-\eta)\theta_D+\eta\,\theta_{DD}$ instead of θ_D for the ER abstraction term. This means that on going from the low to the high coverage regime during exposure, the D_{ad} coverage as the target density for abstraction is switched from $\theta_D\,(=\theta_{DD}+\theta_{HD})$ to θ_{DD}. Namely, Eq. (3-12′) is recast as

$$\frac{dN_{HD}(t)}{dt}\propto(1-\eta)\theta_D+\eta\theta_{DD}+\eta\{C_1\theta_{HD}\theta_{DD}+2C_2\theta_{HD}\theta_{HD}+C_3\theta_{HD}\theta_{HH}\}. \qquad (3\text{-}12'')$$

The rate curve calculated for the parameters $C_1=C_2=4$, and $C_3=0$ for Eq. (3-12″) is the best fit one for $\theta_D^0=0.45$ ML and plotted as curve (a) in Fig. 3.12. Curve (a) exhibits the moderate decrease in HD rate with a shallow dip in the low coverage regime, and gives the peak around 70s. Thus, the overall behavior of the calculated HD rate agrees with the experimental HD rate.

Figure 3.12 also includes curves (b) – (d) which are calculated for comparison with the best fit one to make the trend clear when different ER or AID parameters are chosen.

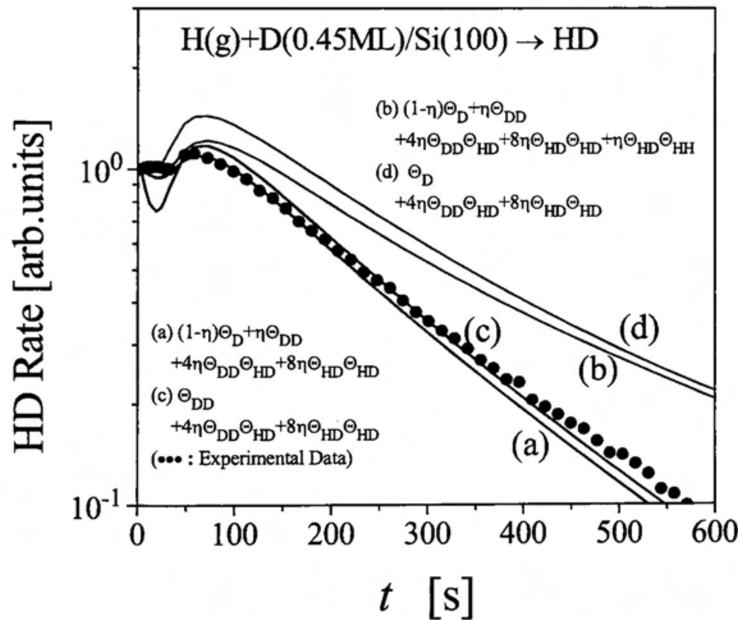

Fig. 3.12: Comparison of the calculated and experimental HD rate curves for $\theta_D^0=0.45$ ML. Curve (a) is the best-fit result for Eq. (3-12″) in the text. Curves (b)–(d) are calculated for checking the contribution of $\theta_{HD}\,\theta_{HH}$ for CID, θ_{DD} for the ER abstraction term, and θ_D for the ER abstraction term, respectively.

Curve (b) is obtained after adding $\theta_{HD}\ \theta_{HH}$ to curve (a). It shows a quite slow decay of the HD rate in the high coverage regime compared to the experimental result, suggesting no contribution of HSiH species to the HD AID process. This result seems to be consistent with the case of the D_2 AID as shown above.

Curves (c) and (d) are calculated by employing different coverage function for the ER abstraction term. For θ_{DD} instead of $(1-\eta)\theta_D + \eta\theta_{DD}$ for the ER abstraction term, the initial decay of the HD rate is quite high so that a deep minimum appears at around t= 30 s as shown in curve (c). On the other hand, curve (d) is obtained after choosing θ_D for the ER abstraction term. As can be seen in curve (d), the feature of the HD rate in the low coverage regime is more or less the same to curve (a), but reveals a quite large discrepancy in the high coverage regime because of its slow decay. This slow decay is never improved with any parameter values other than those chosen for curve (a).

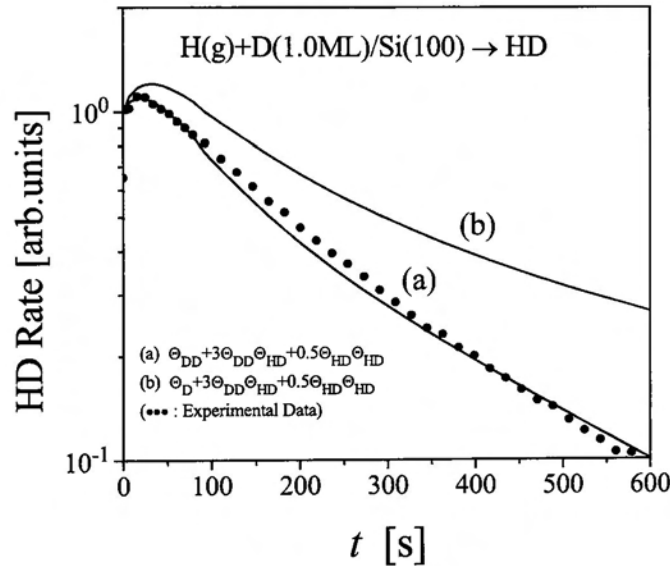

Fig. 3.13: Comparison of the calculated and experimental HD rate curves for θ_D^0 = 1.0 ML. Curve (a) is the best-fit result for Eq. (3-12′′) in the text. Curve (b) is calculated for checking the effect of θ_D instead of θ_{DD} for the ER abstraction term.

Figure 3.13 shows the calculated HD rate curves for θ_D^0 = 1.0 ML where η =1. Curve (a) is the best fit curve obtained for C_1 = 3, C_2 = 0.25, and C_3 = 0, while curve (b) is drawn for comparison to make the trend clear when θ_D is chosen for the ER

abstraction term. The interesting fact is that $C_3 = 0$ gives the best fit result, indicating that HSiH do not contribute to the HD AID again. Comparing curve (b) with curve (a) we find that θ_D gives a quite slow decay compared to the case of θ_{DD}. This slow decay is never been improved even if all the AID terms are eliminated. This is quite consistent with the case of $\theta_D^0 = 0.45$ ML where the HD rate in the high coverage regime is determined by θ_{DD} rather than θ_D as mentioned above.

If we literally understand the meaning of the switching function exerted to the ER term, we notice that for the low coverage regime the incident H atoms abstract D adatoms regardless whether they are paired up either with D or H. On the other hand, for the high coverage regime where the surface is saturated, the incident H atoms abstract D adatoms, which have paired up with D, but do not abstract D adatoms, which have paired up with H.

3.5 DISCUSSION

The quasi-equilibrium model for AID has its basis on the fact that the key surface species are Si di-hydrides DSiD, DSiH, and HSiH which are formed transiently by reaction of H(*g*) with D-terminated Si atoms during exposure. Such di-hydride species can propagate across the surface via successive isomerisation reactions between di-hydrides and mono-hydride s as described by Eq. (3-4) at surface temperatures high enough so that the β_2 TPD channel is active. One should note that the manner of hydrogen propagation in this picture is totally different from that of HA. If AID were induced by a HA-related mechanism, the D_2 rate curves could be fit with second-order kinetics with respect to θ_D. As we saw in the previous section, the D_2 rates as well as the HD rates except for the ER term are able to be fit well with the rate equations proposed as Eqs. (3-12$''$) and (3-13), which is based on the fourth-order kinetics in θ_D and θ_H. Therefore, we conclude that HA-mediated abstraction mechanism is not operative for AID, but the di-hydride -mediated associative desorption as described by Eqs. (3-6a) – (3-7c) is a possible mechanism operative for the indirect abstraction reactions. This is a unique and characteristic feature on Si(100), being compared to the case on metal surfaces. In case of metal surfaces, H-surface interaction potential is

determined not only by *d*-derived bands which are localized but also by *s*-derived bands which are delocalized. Hence, the H chemisorbed potential is not much corrugated due to the *s*-derived bands. On the other hand, bonding energy of H on Si is higher than on metal atoms by about 0.5 eV. The Si surface is less closely packed than metal surfaces, and besides Si *sp*3 bonds are highly directional in a Si–H configuration. Thus, It is expected that the hydrogen chemisorption potentials be highly corrugated. Bonding energy between Si and H does not change so much even for di-hydrides. This fact suggests that incident hydrogen atoms always see attractive potential everywhere impinged even out of the cross-sectional area for the ER abstraction [18]. As a result, this gives rise to a high sticking probability for H(*g*) incident to D-terminated Si atoms, which fulfills the conditions of Eqs. (3-8) and (3-9). As was obtained in the previous work [1], D_2 rate is about 20% of HD rate at t = 0 and θ_D^0 = 1.0 ML. Hence, for $I(D_2)/I(HD) = 0.2$ we evaluate from Eq. (3-11) that $s = 0.59$. After neglecting reflection, this result gives that an abstraction probability of 0.4, which is quite agreeable with the results obtained from the uptake experiments [19,20]. Recent simulation done by Hansen and Vogl [18] does not contradict this result because they recognize efficient sticking to the terminated surface (~56% of J_{in}), direct ER abstraction (~39%), small reflection (~5%) and no HA-mediated abstraction reaction.

Concerning the isotope effect on AID, the reasonable fit does not need any contributions of AID arising from HSiH, i.e., the terms of $k_{DD}^{HH}\,\theta_{DD}\,\theta_{HH}$ in Eq. (3-13) and of $k_{HD}^{HH}\,\theta_{HD}\,\theta_{HH}$ in Eq. (3-12) do not play any role in AID. In order to pursue possible origins of this isotope effect, we may need understanding the dynamics of AID including the desorbing process as well as propagation of adatoms via an isomerisation reaction between mono- and di-hydrides. When DSiD meets with HSiH, either D_2 or H_2 can desorb the surface [14, 21]. It might be conceivable that H_2 association precedes D_2 association because of superiority of lighter atom to heavier one for quantum effects on transition. Possible quantum effects include a zero-point vibrational energy effect on the activation energy to a transition state, a harmonic vibration attacking a transition state to molecular desorption which contributes to a pre-exponential factor of a rate constant, and tunneling from atomic chemisorption to an associative state of a hydrogen molecule. If such quantum effects are operative upon desorption, certain

isotope effects can be observed even in the conventional H_2/D_2 TPD spectra. Actually, on Ge(100)[22] and Cu(111) [23] clear isotope shifts in hydrogen TPD spectra have been observed. Kammler and Küppers consider that the observed isotope shift is due to the zero-point vibrational energy effect [23]. Even on Si(100) an isotope effect has been observed for the isothermal decay in the β_1-derived TPD process since the D_2 desorption rate constant is found to be smaller by a factor of 2 or 3 than that for H_2 while the activation energies are identical for both H_2 and D_2 [17]. On the other hand, no reports on isotope effect on the β_2 channel desorption have been done yet.

Alternatively, such quantum effects as described above can be also anticipated on the isomerization reaction between a mono-hydride and a di-hydride that promotes effective diffusion of hydrogen adatoms. If the diffusion length of adatoms is comparable to the H beam diameter (~4 mm), it may be probable for the adatoms to get out of the beam area to its periphery where dangling bonds exist. The termination of the dangling bonds at the periphery results in an increase in the H-terminated area. The enlargement in the H-terminated area leads to an overestimation in θ_{HH}, since a fraction of H_2 TPD come from the periphery. No occurrence of clear saturation in the θ_{HH} curve depicted in Figs. 3.3 or 3.4 could supports this picture. A fraction of D_{ad} may be also delivered to the periphery by DSiH which is lighter than DSiD. This allows apparently unabstractable D_{ad} to exist as DSi–SiH in the periphery. The θ_{HD} curves in Figs. 3.3 and 3.4 are found to show a quite long decay lifetime, suggesting the existence of such di-hydride species DSi–SiH in the periphery.

A horizontal diffusion of adatoms to the subsurface could be alternatively conceivable for the isotope effect on both the AID and the direct ER abstraction processes. Recently, it has been proposed that H atoms diffuse into the bulk Si, forming trapped hydrogen molecules [24]. Kang *et al.* [25] find a new H_2 TPD peak around T_s = 850 K for large H exposure on Si(100), ascribing it as due to the subsurface hydrogen molecules. If H atoms preferentially diffuse into the bulk we can expect a similar isotope effect on the abstraction processes. Unfortunately, in the present experiments such a subpeak was not clearly discernible in the TPD spectra around T_s = 850 K partly due to a poor S/N ratio in the H_2 TPD signals.

So far we have discussed the possible origin of the isotope effect on the AID.

Quantum effects were considered for the associative desorption and diffusion processes of the adatoms. At the present stage, because of the lack of direct evidences we cannot conclude which process, diffusion or desorption, is important for the isotope effect observed on the AID. Further experiments such as measuring H_2 rate curves, beam size effect, spatial distribution of adatoms, etc. may be particularly needed. As a part of future work, a background-free experiment on H_2 AID will be done by setting a differential pumping system for the QMS.

3.6 SUMMARY

Rate equations for adsorption-induced desorption (AID) of D_2 and Eley–Rideal (ER) type abstraction of HD in the reaction system, H(*g*) + D_{ad} /Si(100) →D_2, HD, were formulated and then analyzed qualitatively. Under a quasiequilibrium condition at 573 K where a di-hydride phase is thermally unstable, transiently formed di-hydride species such as DSiD, DSiH, and HSiH are considered to be key substances for AID. The basic idea in formulating the rate equations is that the coverages of those di-hydride species are proportional to their parent species, doubly occupied Si dimers such as DSi–SiD (coverage: θ_{DD}), DSi–SiH (θ_{HD}), and HSi–SiH (θ_{HH}). For calculation of the rate equations, θ_{DD}, θ_{HD}, and θ_{HH} were determined as a function of t by means of TPD. From the same TPD spectra D_{ad} (coverage: θ_D) and H_{ad} (θ_H) coverages were also determined. Following facts were revealed and discussed for D_{ad} precoverages $\theta_D^0 = 0.45$ and 1.0 ML:

(1) The D_2 rate curves are reasonably fit with the rate equations based on a second-order kinetics with respect to θ_{DD} and θ_{HD}. The reasonable fits verify that AID of D_2 obeys the second-order kinetics with respect to the coverage of the di-hydrides.

(2) The term including θ_{HH} has to be eliminated from the D_2 rate equations since it gives an unreasonably slow decay in the rate curves. This fact suggests that an isotope effect exists on the AID process.

(3) The second peak of the HD rate curves is well explained with a kinetics same to that for D_2 desorption, ruling out a hot atom-mediated abstraction mechanism.

(4) The HD rate due to the direct abstraction channel is fit with θ_D at the low coverage regime where dangling bonds still exist. However, for the saturated surfaces it is not fit with θ_D, but is fit with θ_{DD}. This fact suggests that only DSi–SiD species contribute to the direct abstraction process for the high coverage regime.

(5) Sticking probability of an H atom on the D(1 ML)/ Si(100) surface is evaluated to be about 60% and the abstraction probability about 40%, which is quite consistent with the recent simulation by Hansen and Vogl [18].

REFERENCES

[1] S. Shimokawa, A. Namiki, T. Ando, Y. Sato, and J. Lee, J. Chem. Phys. 112 (2000) 356.

[2] G. Eilmsteiner, W. Walker, and A. Winkler, Surf. Sci. 352 (1996) 263.

[3] J. Boh, G. Eilmsteiner, K. D. Rendulic, and A. Winkler, Surf. Sci. 395 (1998) 98.

[4] S. Wehner and J. Küppers, J. Chem. Phys. 108 (1998) 3353

[5] Th. Kammler, S. Wehner, and J. Ku¨ppers, J. Chem. Phys. 109 (1998) 4071.

[6] J.-Y. Kim and J. Lee, Phys. Rev. Lett. 82 (1999) 1325.

[7] H. Pölzl, G. Strohmeier, and A. Winkler, J. Chem. Phys. 110 (1999) 1154.

[8] C. T. Rettner, Phys. Rev. Lett. 69 (1992) 383.

[9] C. T. Rettner and D. J. Auerbach, Phys. Rev. Lett. 74 (1995) 4551.

[10] M. C. Flowers, N. B. H. Jonathan, A. Morris, and S. Wright, Surf. Sci. 396 (1998) 227.

[11] M. L. Wise, B. G. Koehler, P. Gupta, P. A. Coon, and S. M. George, Mater. Res. Soc. Symp. Proc. 204 (1991) 319.

[12] M. P. D'Evelyn, Y. L. Yang, and L. F. Sutcu, J. Chem. Phys. 96 (1992) 852.

[13] M. C. Flowers, N. B. H. Jonathan, A. Morris, and S. Wright, J. Chem. Phys. 108 (1998) 3342.

[14] M. C. Flowers, N. B. H. Jonathan, Y. Liu, and A. Morris, J. Chem. Phys. 99 (1993) 7038.

[15] E. Pehlke and M. Scheffler, Phys. Rev. Lett. 74 (1995) 952.

[16] P. Kratzer, B. Hammer, and J. K. Nørskov, Phys. Rev. B 51 (1995) 13432.

[17] P. Bratu, W. Brenig, A. Groß, M. Hartmann, U. Höfer, P. Kratzer, and R. Russ, Phys. Rev. B 54 (1996) 5978.

[18] U. Hansen and P. Vogl, Phys. Rev. B 57 (1998) 13295.

[19] D. D. Koleske, S. M. Gates, and B. Jackson, J. Chem. Phys. 101 (1994) 3301.

[20] S. A. Buntin, J. Chem. Phys. 105 (1996) 2066.

[21] T. Watanabe, T. Hoshino, and I. Ohdomari, Appl. Surf. Sci. 117/118 (1997) 67. See also the references cited therein. In Ref. 21, various desorption models for the β_2 TPD were considered by calculating the energy of transition state for desorption. It was suggested that the most possible desorption occurs also from two adjacent HSiH species. Contrary to the Flowers' model, however, it turned out that the recombination occurs for two H atoms each of which belongs to the different di-hydride (*1,2-* elimination). If this were the case, because of the prepairing mechanism a second-order D_2 desorption in θ_D would be observed.

[22] S. Shimokawa, A. Namiki, M. N. –Gamo and T. Ando, J. Chem. Phys. 113 (2000) 6916.

[23] Th. Kammler and J. Küppers, J. Chem. Phys. 111 (1999) 8115.

[24] K. Murakami, N. Fukata, S. Sasaki, K. Ishioka, M. Kitajima, S. Fujimura, J. Kikuchi, and H. Haneda, Phys. Rev. Lett. 77 (1996) 3161.

[25] J. H. Kang, S. K. Jo, J. Lee, B. Gong, D. Lim, J. M. White, and J. G. Ekerdt, Phys. Rev. B 59 (1999) 13170.

CHAPTER 4

Hot-Complex Model

This chapter is based on the paper Phys. Rev B 65 (2001) 033405-1.

The adsorption-induced associative desorption (AID) and abstraction (ABS) of D adatoms by H have been studied on the Si(100) surfaces. D_2 AID exhibits a feature common to that of a thermal desorption from a di-deuteride phase. HD ABS proceeds along an apparently second-order kinetics rather than a first-order kinetics with respect to surface D coverages. The ABS cross section is about 6 Å², extremely large compared to the theoretical values. Both of the direct Eley-Rideal mechanism and the hot-atom mechanism are ruled out. A hot-complex-mediated reaction model is proposed for ABS and AID.

4.1 INTRODUCTION

Dinger, Lutterloh, and Küppers proposed HA mechanism for both H induced abstraction (ABS) and adsorption-induced-desorption (AID) on D/Si surfaces [1,2]. On the other hand, Shimokawa *et al.* [3] observe that the reaction order of D_2 AID is approximately four with respect to surface D coverage θ_D, indicating that four adatoms take part in the D_2 desorption process. The fourth-order kinetics in θ_D is quite unexpected, which rules out the HA mechanism. This fourth-order kinetics in θ_D for D_2 AID is not at variance with the Flowers [4] model since the β_2 TPD obeys a second-order kinetics with respect to DSiD coverages [5,6] involving four D_{ad} in the event. Thus, AID based on the β_2 TPD mechanism is categorized as a Langmuir-Hinshelwood (LH) reaction. HD AID is also expected to take place in the H and D coadsorption system generated by substitution of D_{ad} with H_{ad} during H admission. Actually, the observed HD rate curves exhibit a bimodal structure particularly at small initial D coverages θ_D, suggesting the occurrence of two distinct channels, i.e., HD AID along the LH mechanism and ABS via the direct ER mechanism [3]. In the previous paper [7], HD rate equation is proposed to fit the experimental data obtained for θ_D^0=1.0ML, as follows

$$dN_{HD} / dt = k_{ABS}\theta_{DD} + C_1\theta_{HD}\theta_{DD} + 2C_2\theta_{HD}\theta_{HD} + C_3\theta_{HD}\theta_{HH}, \qquad (4\text{-}1)$$

where k_{ABS} is the rate constant for the ER type ABS, and C_n (n=1 ~ 3) stands for the rate constants related to the three possible combinations of di-deuterides upon their encounters for the LH type AID. For the AID terms in Eq. (4-1), the coverages of D_{ad} in the prepaired Si dimer, θ_{ij} (i, j = H, D), are employed instead of the unmeasured transient dideuteride coverages. Even for the ABS term θ_{DD} is taken instead of $\theta_D (=\theta_{DD}+\theta_{HD})$. This means that in the viewpoint of ER scenarios for ABS [3,4,8], H abstracts D_{ad} preferentially in the doubly occupied Si dimers DSi-SiD rather than D_{ad} in DSi-SiH [7]. Yet, the significance of this unexpected isotope effect on ABS has not been clarified.

In the two papers [1,3], however, the experiments were carried out at a fixed temperature around 600 K without systematic changes of surface temperature T_s. If ABS and AID proceed along the HA scenario [1,2], it can be anticipated that they commonly receive a little T_s effect [9]. It is thus a dilemma for Dinger *et al.* to see a somewhat strong T_s dependence on AID studied on Si(111) [2]. On the contrary, the AID model based on the LH mechanism [3,7] predicts a strong T_s dependence as was partly exemplified on Ge(100) [10]. In this chapter, by examining T_s effects, kinetic mechanisms of ABS and AID on Si(100) surface is revealed and a hot-complex-mediated reaction model is proposed thereby.

4.2 EXPERIMENT

The details of the experimental method have been discussed in chapter 2. Here, the essential points are described briefly. Clean Si(100) surface was exposed to D beam to prepare saturated 1 ML D covered surface at 600 K. Then the H beam was admitted to that saturated D/Si(100) surface to induce HD and D_2 desorption at various surface temperatures ranging from 300 to 700 K. The quick temperature rise from 600 K to desired temperatures for T_s > 600K were accomplished within a few seconds by means of a direct resistive heating. During H admission to the D/Si(100) surface, HD and D_2 molecules were detected simultaneously with a quadrupole mass spectrometer (QMS), while we failed to detect H_2 because of background H_2.

4.3 RESULTS AND DISCUSSION

Fig. 4.1 represents some examples of HD and D_2 rate curves measured as a function of H exposure time t for various T_s. Here, H was admitted to the D(1ML)/Si(111) surface at $t = 0$, after changing T_s from 600 K to the desired temperatures as shown in Fig. 4.1. It can be seen clearly from the Fig. 4.1 that HD rates do not depend much on T_s. The D_2 rates, on the other hand, depend strongly on T_s. At $T_s = 300$ K, the D_2 rate step at $t = 0$ is very small compared to that on 593 K. Beyond 593 K, D_2 rate increases before irradiating to H beams because of the spontaneous thermal desorption arises for increasing T_s from 600 K to higher desired temperatures. The rates again jump up after irradiating to H beams at $t = 0$.

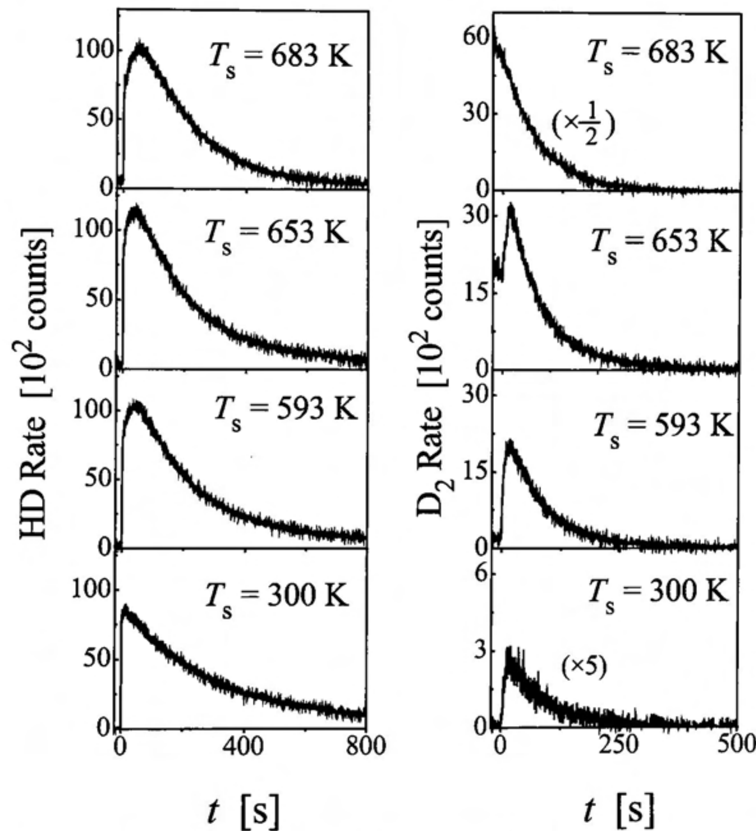

Fig. 4.1: Plots of HD and D_2 rate curves as a function of H exposure time t on the reaction system H + D(1 ML)/ Si(100) for various T_s.

However, at the highest $T_s = 683$ K, no rate step is observed at $t = 0$. From the D_2 rate curves of Fig. 4.1, it can be seen that the spontaneous thermal desorption of D_2 already

started before H admission above 600 K, and thus the D_2 rates at t = 0 can be decomposed into AID (solid rectangles) and spontaneous thermal desorption (STD) (solid circles) as shown in the inset of Fig. 4. 2.

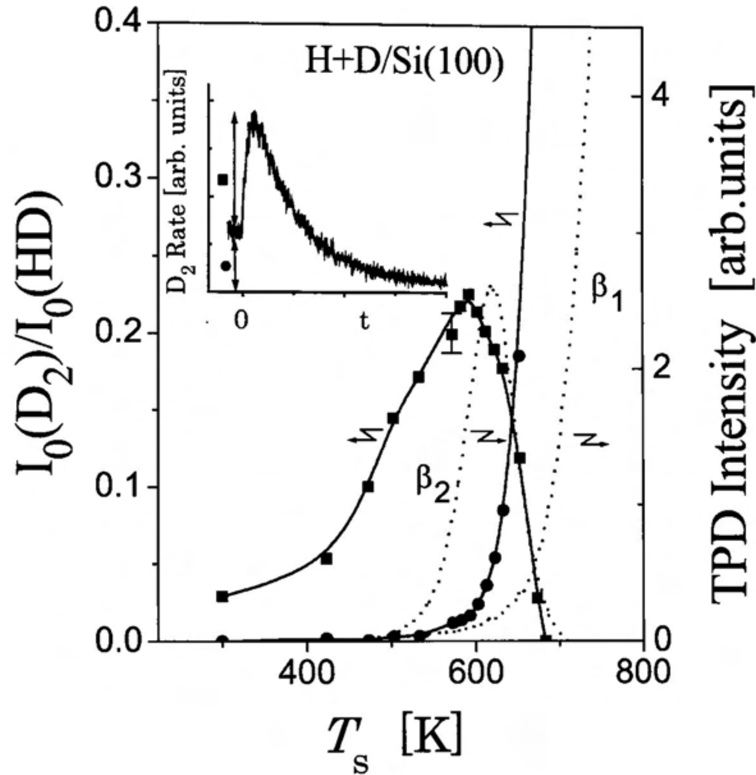

Fig. 4.2: Plots of D_2 rates $I_0(D_2)$ normalized with HD rates $I_0(HD)$ at the beginning of H admission as a function of T_s. The D_2 rates are decomposed into AID (solid rectangles) and STD (solid circles) as defined in the inset. For comparison, D_2 TPD spectra (rising speed of T_s: 3.3 K/s) decomposed into β_2 and β_1 TPD spectra arising from the di-deuteride and mono-deuteride phases are also plotted.

Plots of D_2 rates normalized with the initial HD rate $[I_0(D_2)/I_0(HD)]$ versus T_s are shown in Fig. 4.2. The D_2 AID curve exhibits a clear peak around 590 K above which the D_2 AID rates decrease quite rapidly in spite of the sizable amount of residual D_{ad} at the beginning of H admission (the loss of D_{ad} before H admission was at most 0.15 ML at T_s = 683K). On the other hand, STD begins to appear around 600 K and increases quite rapidly with T_s. For comparison, we plot decomposed β_2 and β_1

TPD spectra arising from the di-deuteride and mono-deuteride phase, respectively. The STD spectrum exhibits a close relation to the β_1 TPD spectrum, which was expected since it occurs from the mono-deuteride phase. On the other hand, the D_2 AID spectrum looks similar in line shape to the β_2 TPD spectrum. The peak of the D_2 AID spectrum shifts by about 30 K with respect to the β_2 TPD peak at 620 K, accompanied with tailing down to the lower-temperature region below 300 K. The feature of the AID and STD rate spectra manifests an anticorrelation for $T_s \geq$ 600 K, indicating the former succumbs to the latter at higher T_s. From $I_0(D_2)/I_0(HD) = 0.23$ at 590 K, we know that about one third of the desorbed D atoms were due to AID on the H_{ad} free D/Si(100) surface.

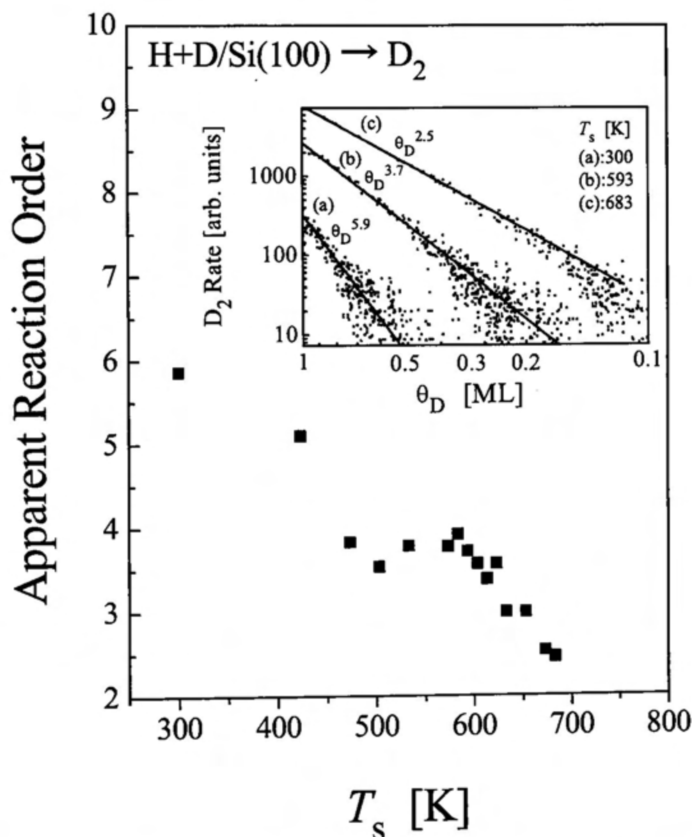

Fig. 4.3: Plots of apparent D_2 CID reaction order as a function of T_s. The inset shows the log-log plots of the D_2 rate curves fit to the rate equation, $dND_2/dt=k\ \theta_D^m$, where m is the apparent reaction order to be determined by a least-mean-squares method.

Reaction orders for the D_2 desorptions were evaluated by fitting the experimental

rate curves to a rate equation, $dN_{D_2}/dt = k\theta_D^m$, that consists of a single term characterized with the rate constant k and the reaction order m. However, the actual rates may include not only multi-terms of AID as in Eq. (4-1) but also a term of STD, and the evaluated reaction orders are thus apparent. Figure 4.3 shows a plot of the D_2 AID reaction orders so determined as a function of T_s. The inset shows the curve fittings based on a least mean-squares method for T_s= 300, 593, and 683 K. Here, the momentary D_{ad} coverages θ_D during H admission were obtained by integrating the HD and D_2 rate curves [3,10]. The reaction orders for D_2 AID were evaluated to be 3.7 ± 0.3 for the temperature range from 500 to 600 K where the AID rates are high but the STD rates are low, indicating that D_2 AID proceeds along a nearly fourth-order kinetics in θ_D as noted previously for T_s= 573 K [3]. The fourth-order kinetics rules out the HA mechanism for D_2 AID. It is also ruled out even at T_s = 300 K because the observed reaction order is about six.

From the facts shown in Figs. 4.2 and 4.3, we conclude that D_2 AID on Si(100) proceeds along the same mechanism as for the β_2 TPD arising from the di-deuteride phase. In other words, the DSiD species are formed by H exposure to the D/Si(100) surface, however, transiently since T_s is so high that they do not steadily survive. The second-order kinetics with respect of to di-deuterides DSiD implies that the surface di-deuterides do not make stable clusters, but they are rather repulsive to each other [6]. For such second-order D_2 desorptions, the di-deuterides have to migrate across the surface to make binary collisions among them. For higher T_s, where STD takes place efficiently, the migrating di-deuterides will terminate the dangling bonds created by STD before AID, which causes the reduction in D_2 AID at higher T_s. On the other hand, for T_s ≤ 400 K their migration across the surface is limited because of the insufficient thermal activation, and thus D_2 AID becomes inefficient as observed in Fig. 4.2.

Figure 4.4 shows the HD rate curve as a function of θ_D for T_s= 593 K where the D_2 rate becomes maximum. The curve has a clear maximum around θ_D= 0.85 ML, after which the HD rate superlinearly tends to the (0,0) point. For T_s= 300 K, on the other hand, the HD rate curve shows a tiny peak around $\theta_D \simeq 0$, and exhibits a roughly first-order decrease with decreasing θ_D as shown in the inset. However, the rate

curve does not tend to the (0,0) point again likely in Fig. 4.4. In order to get to the (0,0) point, the HD kinetics must be characterized with a reaction order higher than unity. This is evident as the HD rate curve is compared to the straight line along the first-order kinetics in θ_D [curve (a) in Fig. 4.4]. The HD rate is clearly lower than the line for $\theta_D \leq$ 0.5 ML. Therefore, we conclude that neither the HA mechanism nor the direct ER one is operative for the D_{ad} abstraction by H because the two mechanisms commonly claim a first-order kinetics in θ_D.

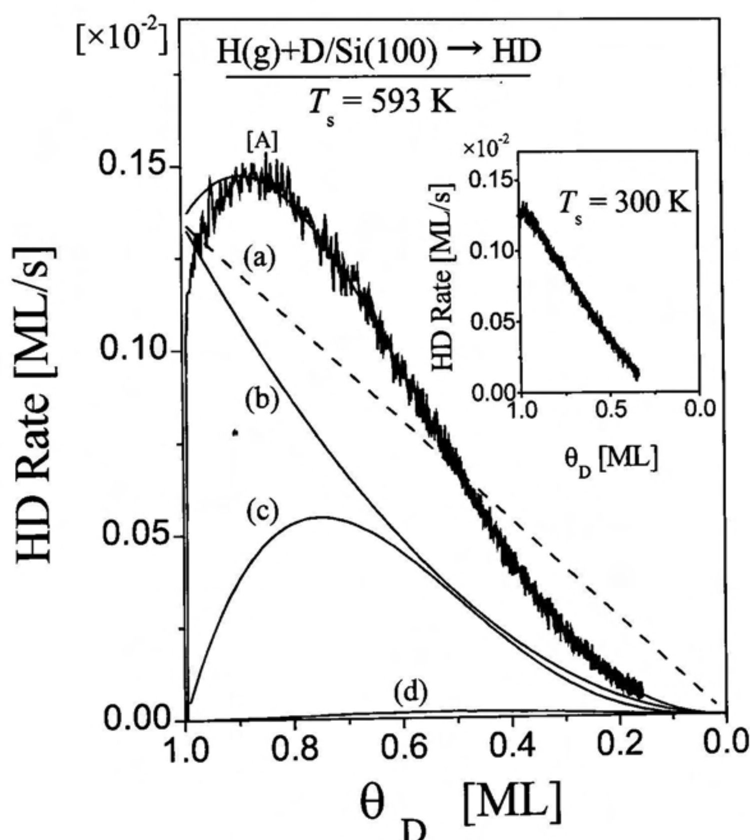

Fig. 4.4: Plots of HD rate curves measured at T_s = 593 K and 300 K (inset) as a function of θ_D. The dashed line (a) shows the first-order kinetics with respect to θ_D expected in the direct ER or HA scenario. The experimental rate curve is fit to the rate equation, $dN_{HD}/dt = k_{ABS}\theta_D^2 + C_1\theta_H\theta_D^3 + 2C_2\theta_H^2\theta_D^2 + C_3\theta_H^3\theta_D$. Curve [A] is the best-fit curve. The curve (b), (c) and (d) represents the decomposed curved after getting corresponding rate constants from the best fit result for ABS, first term for CID and second term for CID, respectively.

Besides, taking into account the feature that the ABS rate curve is a simply decreasing

function with decreasing θ_D on the saturated surface, the maximum in the HD rate around θ_D = 0.85 ML is attributed to HD AID overlapping ABS. With the light of the present results and the rate-curve analysis done at T_s = 573 K [7], we confirm that the equation (4-1) and the physics and chemistry behind it are valid. Since the relation that $\theta_{ij} = \theta_i \theta_j$ (i,j=D,H) is held on the surface saturated with randomly mixed H_{ad} and D_{ad} [7], the equation (4-2) can be derived from the Eq. (4-1)

$$dN_{HD}/dt = k_{ABS}\theta_D^2 + C_1\theta_H\theta_D^3 + 2C_2\theta_H^2\theta_D^2 + C_3\theta_H^3\theta_D \tag{4-2}$$

According to the Eq. (4-2), the ABS term in Eq.(4-1) is recast as $((dN_{HD}/dt)_{ABS} = k_{ABS}\theta_D^2$. Thus, the HD ABS reaction on the saturated Si(100) surface follows an apparently second-order kinetics in θ_D. Using the relation that $\theta_D+\theta_H$ = 1 during H admission, the experimental HD rate curve is fitted using the Eq. (4-2) by the least-mean squares method. The curve [A] represents the best fit result for the rate constants k_{ABS} =1.35× 10^{-3} s^{-1}, C_1=5.2×10^{-3} ML^{-1} s^{-1}, and C_2=0.27×10^{-3} ML^{-1} s^{-1}. The rate constant C_3 is so small that contribution from the third-order AID term becomes negligible. By using these rate constants the HD rate curve is further decomposed into ABS and AID terms. The curve (b) represents the contribution from the ABS term, curves (c) and (d) represents the contribution from the 1st and 2nd AID terms, respectively in Eq. (4-2). We notice that the rates for both ABS and AID are comparable after the middle stages of H admission.

Taking into account the balance between the uptake on and loss from the surface keeping the 1 ML saturation coverage, we can evaluate ABS efficiency ξ at t = 0 as $\xi = I_0(HD)/[2I_0(HD)+2I_0(D_2)+I_{ref}]$ for T_s ~600 K. Here, $I_0(HD)$ and $I_0(D_2)$ are the initial HD and D_2 rates, respectively, and I_{ref} is the reflected H flux. Taking the reflection probability of 0.05 as evaluated theoretically by Hansen and Vogl [11], and employing $I_0(D_2)/I_0(HD) = 0.23$ for T_s = 593 K as plotted in Fig. 4.1, we obtain ξ = 0.39. This value corresponds to a sticking probability s = 0.56, and yields an abstraction cross section $\sigma \simeq 6$ Å² as evaluated from the relation $\sigma = \xi . S$ (S: 1×1 unit cell area). This is extremely large compared to the size of a hydrogen molecule. According to the recent quantum-mechanical calculations based on a flat surface model avoiding sticking [12], cross sections of the direct ER abstraction, σ_{ER}, becomes small

with increasing H-substrate binding energy E_B. For E_B = 3 eV, close to the value E_B = 3.4 eV on Si [13], it has been estimated that $6 \times 10^{25} \leq \sigma_{ER} \leq 0.025$ Å^2 [12]. Thus, there exists a serious discrepancy between the theory and the experiment on the ABS cross sections.

Since it was observed in this work that the ABS reaction is neither of a direct ER type nor of a HA one, a new model for the ABS mechanism is needed to solve the ABS puzzle, i.e., the large cross section and the apparently second-order kinetics for ABS. We seek a hint in the high reactivity of H with the substrate, since the formation of di-deuterides are quite facile on Si(100) as confirmed by the β_2 TPD. In other words, the sticking probability of H to the D/Si(100) surface is much larger than that of the direct ER type ABS. The classical molecular-dynamics simulation [11] in the same system showed that in addition to the high ABS probability of about 0.4 the adsorption probability of H is as high as 0.6. Although the adsorption in the simulation does not necessarily mean di-hydrides, the simulated feature of the H reaction with D_{ad} is thus quite close to the present results. Such high reaction probability may be assured by three mechanisms [11]: (1) the potential felt by the incident H is attractive on almost the entire surface, (2) the corrugation of this potential prolongs the interaction time and confines the event locally, and (3) the efficient momentum and energy transfer take place to the Si lattice as well as to the adsorbates. If we look at this feature from a quantum-mechanical point of view, the chemisorbed hydrogen before full relaxation is in vibrationally excited states rather than in free conduction-band states. Here, such a vibrationally excited H-chemisorbed system is called a hot complex, and is invoked to explain a new mechanism for ABS other than an ER mechanism and a HA one. The following is proposed as a new mechanism of hot-complex-mediated ABS and AID on Si(100): Major fractions of incident H atoms first get trapped in the chemisorption potential not as a hot atom H* but as a hot complex (H+DSi-SiD)*, where based on the fact that $(dN_{HD}/dt)_{ABS} = k_{ABS}\theta_{DD}$ in Eq. (4-1), the doubly occupied Si dimers DSi-SiD (including DSi- SiH and HSi-SiH for t>0) is chosen as a skeleton of the complex. This hot complex does not allow us to release the H atom into the mobile states or H*. The generation of ABS and formation of HSiD take place from the hot complex competitively;

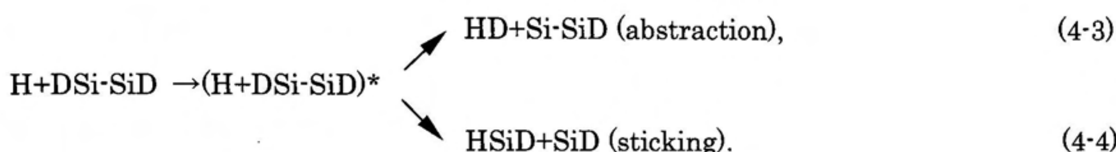

[A schematic description about hot-complex model is represented in CHAPTER 5 in the case of Si(111) surface.]

The exo-thermicities of the relevant reactions are evaluated to be -1.1 and -2.6 eV for Eqs. (4-3) and (4-4), respectively, for the bond energies of HD (4.5 eV), H-Si (3.4 eV), Ref. 13) and Si-Si dimer (1.9 eV, Ref. 14). Therefore, the HSiD formation is facile compared to ABS, which is not at variance with the experiment. The HSiD species formed along Eq.(4-4) are precursors for AID that subsequently proceeds along the same mechanism as for the β_2 TPD [6]. Hence, the HD desorptions consist of ABS via Eq. (4-3) and AID initiated by HSiD formed via Eq. (4-4). The HD desorption via Eq. (4-3) is a non-thermal process and thus expected to show a dynamic feature [8] similar to those theoretically predicted in the ER and HA scenarios [11,15]. The fate of the hot complex either to ABS or to di-hydride followed by AID may be determined by potential-energy surfaces at impact sites, phases of vibrations relevant to reaction coordinates, mass of the adatoms, etc. A hot complex (H+HSi-SiD)* arising from H sticking to HSi- SiD has a chance to generate either H_2 ABS or formation of HSiH, competing with HD ABS and formation of HSiD. This competition could cause the less efficient HD ABS at the late stages of H admission. In the ER scenario, the isotope effect on ABS is interpreted in terms of kinematics upon collision [4,16,17]. In the present hot-complex model, it is explicable in terms of quantum effects upon relaxation of the hot complex, including a zero-point vibrational energy effect, an attempting frequency factor to transition states, tunneling through barriers, etc. Generally speaking, lighter atoms are superior to heavier ones in such quantum-mechanical transitions. Therefore, the preferential D_{ad} abstraction from DSi-SiD rather than from DSi-SiH, i.e., the first term in Eq. (4-1), could be reconciled with such quantum effects on the reaction in the hot complex.

4.4 SUMMARY

H induced HD abstraction (ABS) and collision-induced desorption (AID) of D_2 from D/ Si(100) surface were studied at various T_s. HD rates were observed not to be affected much with T_s; D_2 rates, on the other hand, showed a strong T_s dependence. Reaction order for D_2 AID was evaluated to be about four with respect to θ_D for T_s = 450-600 K and exhibited a feature common to that of a thermal desorption from a di-deuteride phase. HD ABS reaction order follows apparently second-order kinetics rather than a first-order kinetics with respect to surface D coverages. The evaluated ABS cross section is about 6 Å^2 which is extremely large compared to the theoretical values. Both of the direct Eley-Rideal mechanism and the hot-atom mechanism were ruled out. To explain this unexpected second order kinetics for ABS and the large ABS cross-section, a hot-complex-mediated reaction model was proposed. Both ABS and AID phenomena were successfully explain by this hot-complex-mediated reaction model.

REFERENCES

[1] A. Dinger, C. Lutterloh, and J. Küppers, Chem. Phys. Lett. 311 (1999) 202.

[2] A. Dinger, C. Lutterloh, and J. Küppers, J. Chem. Phys. 114 (2001) 5338.

[3] S. Shimokawa, A. Namiki, T. Ando, Y. Sato, and J. Lee, J. Chem. Phys. 112 (2000) 356.

[4] M. C. Flowers, N. B. H. Jonathan, A. Morris, and S. Wright, Surf. Sci. 396 (1998) 227.

[5] P. Gupta, V. L. Colvin, and S. M. George, Phys. Rev. B 37 (1988) 8234.

[6] M. C. Flowers, N. B. H. Jonathan, Y. Liu, and A. Morris, J. Chem. Phys. 99 (1993) 7038.

[7] F. Khanom, S. Shimokawa, S. Inanaga, A. Namiki, M. N.-Gamo,and T. Ando, J. hem. Phys. 113 (2000) 3792.

[8] S. A. Buntin, J. Chem. Phys. 105 (1996) 2066; 108 (1998) 1601.

[9] J. Harris and B. Kasemo, Surf. Sci. 105 (1981) L281.

[10] S. Shimokawa, A. Namiki, M. N.-Gamo, and T. Ando, J. Chem. Phys. 113 (2000) 6916.

[11] U. Hansen and P. Vogl, Phys. Rev. B 57 (1998) 13 295.

[12] B. Jackson and D. Lemoine, J. Chem. Phys. 114 (2001) 474.

[13] M. P. D'Evelyn, Y. L. Yang, and S. M. Cohen, J. Chem. Phys. 101 (1994) 2463.

[14] P. Krüger and P. Pollmann, Phys. Rev. Lett. 74 (1995) 1155.

[15] P. Kratzer, J. Chem. Phys. 106 (1997) 6752.

[16] B. Jackson and M. Persson, J. Chem. Phys. 96 (1992) 2378.

[17] C. T. Rettner, Phys. Rev. Lett. 69 (1992) 383.

CHAPTER 5

D Abstraction by H on Si(111) Surface

This chapter is based on the paper submitted to Surface Science.

We studied H-induced abstraction (ABS) and adsorption-induced-desorption (AID) on the D/Si(111) surface for various initial D coverages θ_D^0 and surface temperatures T_s. As θ_D^0 was increased, the kinetics of HD ABS was found to switch from the first- to second -order rate law with respect to θ_D. D_2 AID appeared to obey a nearly third-order rate law in θ_D. The hot atom HA mechanism is ruled out for both ABS and AID. We found that AID is associated with β_2 TPD, i.e. D_2 AID proceeds as a spontaneous desorption of deuterium from a di-deuteride or di-hydride phase formed by H atoms. Rate equations for HD and D_2 desorptions at 620 K were proposed based of the observed rate laws. The apparent activation energy of D_2 AID is evaluated to be ~0.16 eV for $T_s \leq 650$ K. Taking steady state adsorption and desorption into consideration, the origin of the third order rate law as well as the low activation energy for AID was ascribed to the process of sticking by H atoms rather the process of D_2 desorption. An isotope effect was recognized in the rate curve analysis. The hot complex-mediated reaction model proposed on Si(100) was invoked to explain the complicated kinetic phenomena appeared in ABS and AID on the Si(111) surface.

5.1 INTRODUCTION

H induced the HD and D_2 rate curves on D/Si(100) surface measured by Küppers' group [1] and our group [2] show up complex features depending on the initial D coverage θ_D^0. Results obtained by the two groups are quite similar, but their analysis and thereby proposed kinetic mechanisms for ABS and AID are totally deferent and controversial. Dinger, Lutterloh, and Küppers (DLK) [1] propose the HA mechanism as they deduced first- and second-order desorption kinetics for ABS and AID, respectively as discussed in CHAPTER 1. On the contrary, our group find that the measured kinetic data for AID and ABS can be best fit with the rate equations characterized with unexpectedly high reaction orders, ~4 for D_2 AID [2] and ~2 for HD ABS [3, 4] at $\theta_D^0 = 1$ ML as discussed in CHAPTER 3 and CHAPTER 4. This unexpected result is quite incompatible with the HA mechanism. A new kinetic mechanism is proposed for the 4th-order D_2 AID reactions on the basis of the β_2 temperature-programmed desorption

(TPD) [CHAPTER 3] model originally proposed by Flowers *et al.* [5, 6] for the thermal desorption from a di-hydride phase. A key ingredient of this mechanism is that the incident H atoms efficiently stick to D-terminated Si atoms to form di-hydride HSiD. The di-hydrides then undergo an isomerisation reaction with their neighboring double occupied Si dimmers DSi-SiD to exchange their sites, i.e., DSiH + DSi-SiD $\rightarrow$ DSi-SiH+ DSiD. So formed di-deuterides DSID will further experience similar isomerisation reactions to nominally propagate D adatoms across the surface without access to any HA states. The di-deuterides either terminate dangling bonds created by ABS or generate D_2 desorption that obey a second-order rate law with respect to the DSiD coverage, i.e., 2DSiD $\rightarrow$ D_2+ DSi-SiD. In other words, four D adatoms take part in the D_2 desorption, which thus seems to be able to reconcile the observed fourth-order rate law. Kubo et al. [7] have recently reproduced the above results under the condition of the H flux nearly one order higher than ours, but similar to the condition employed by DLK. This suggests that the discrepancy between the Küppers' group and our group cannot be attributed to the difference in the experimental condition employed, but rather attributable to the different criterions applied for the best curve fitting procedure as will be shown below.

DLK revisits the same issue on the Si(111) surface focusing on temperature dependence of HD and D_2 rates [8]. As a consequence, they come to the same conclusion as derived by them on the Si(100) surface, i.e., the first order rate law for ABS and the second-order rate law for AID, again insisting on the HA mechanism. However, the conclusion may be blurred when certain deviations are admitted between the best-fit curves and the experimental HD and D_2 rate data as replotted in Fig. 5.1. In case of the HD rate curve, for instance, it is clear that the curve obtained on the basis of the first-order rate law does not tend to the (0,0) point. Besides, it tends to deviate downward from the experimental rate data for $\theta_D \geq$ 0.8 ML. This systematic deviation becomes more prominent if a straight line of HD rate $dN_{HD}/dt \propto \theta_D$ is drawn so as to get to the (0,0) point as shown in Fig. 5.1(a). The experimental data and the first-order rate curve cross over at around θ_D = 0.7 ML. Thus the HD rate data may not be simply interpreted in terms of such a first-order rate law in θ_D but a higher order rate law. Furthermore, in case of the D_2 rate curve in Fig. 5.1, the best fit

curve (B) plotted by DLK along the second-order rate law, a systematic deviation from the experimental data is again discernible: for $\theta_D \geq 0.8$ ML the curve becomes smaller, while for $\theta_D \leq 0.8$ ML, it becomes larger than the experimental data. Thus, the measured D_2 rate curves seem to be fit with a reaction order higher than two. Indeed the DLK's D_2 rate curve can be nicely fit with a nearly third-order rate law, e.g., $dN_{D_2}/dt \propto \theta_D^{2.8}$, as shown in Fig. 5.1(b). It is clear that the deviation of curve (b) from the experimental data is much smaller for the entire D coverage region examined except for the initial point.

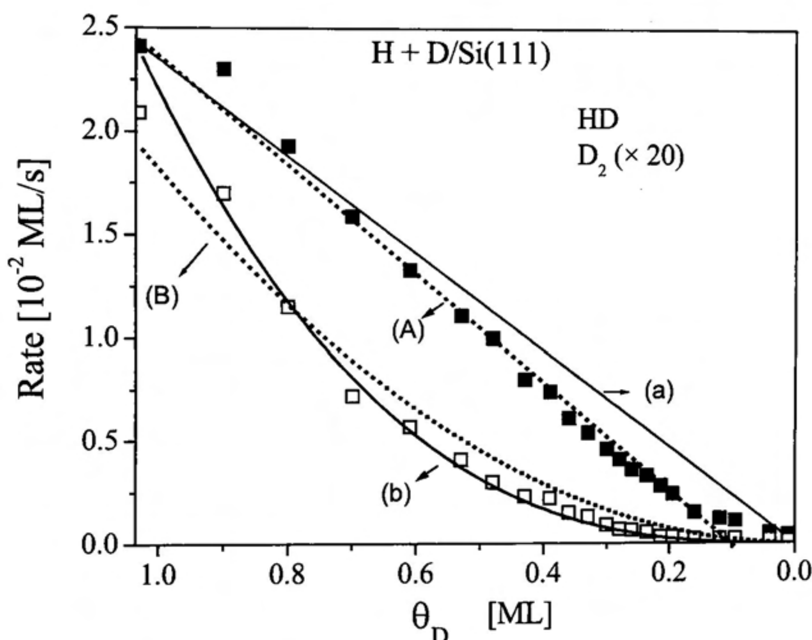

Fig. 5.1: Replots of DLK's results on HD and D_2 rate curves on the reaction system of H + D(1 ML)/ Si(111) at 630 K (Ref. [8]). Both dotted lines (A) and (B) are the curves fitted by DLK with the first- and second-order rate laws for the HD and D_2 rate data, respectively. One can notice that (A) does not tends to the (0,0) point. The true first-order rate curve (curve (a): $\propto \theta_D$) deviates seriously from the data points. Curve (b) is the best fit result with a rate equation $dN_{D_2}/dt \propto \theta_D^{2.8}$.

Apart from these deviations in kinetics, DLK finds that the D_2 rate curves measured for low θ_D^0 where AID competes with sticking to dangling bonds are difficult to be

reproduced with the same kinetic equations obtained on the basis of the HA picture as on the metal surfaces [9, 10]. Furthermore, DLK observes a somewhat strong surface temperature (T_s) dependence on the D_2 AID rates. Such T_s sensitive AID seems to be at variance with the HA picture since Harris and Kasemo consider that a hot-precursor-mediated process including a generalized ER pathway or the HA one is characterized with a less temperature effect [11].

In this chapter we repeat the same experiment as DLK did on the system H + D/Si(111) for various T_s and θ_D^0. We show that AID and ABS reaction orders are higher than the values expected in the HA mechanism. Both the ABS and AID kinetics are similar to those on the Si(100) surface except that the AID reaction order is a bit smaller than that on Si(100). Kinetic mechanisms of ABS as well as AID on Si(111) surfaces are discussed in terms of an immobile hot precursor (hot complex)-mediated scheme proposed on the Si(100) surface [4].

5.2 EXPERIMENT

The experimental details have been discussed in CHAPTER 2. Here, we describe only the essence of the experiments. Our hydrogen-surface reaction apparatus consists of a beam chamber and an ultra high vacuum chamber. The beam line consists of three differentially pumped chambers, which assure the surface reactions under a high vacuum in a pressure range of 10^{-10} Torr even when the H beam is applied. The H or D beam was generated by a radio frequency plasma of H_2 or D_2 mixed with Ar (1:1 pressure ratio), respectively. The H or D beam flux is about $3.5 \pm 1.5 \times 10^{12}$ $cm^{-2}s^{-1}$. We used an n-type (P doped) Si(111) surface with an electrical resistivity of 7.8 Ωcm. The reaction chamber is equipped with an Ar^+ ion gun, an Auger electron spectrometer (AES), a quadrupole mass spectrometer (QMS), and a sample manipulator. The desorbing species of D_2 and HD were detected simultaneously with the QMS in an angle-integrated mode. In order to obtain a clean surface, an Ar^+ ion beam-sputtered surface was thermally annealed in the 1×1 phase at 1173 K for 30 s and then in the 7 ×7 phase at 1083 K for 10 min. The sample was further cooled down to 620 K to prepare D-terminated surfaces with a mono-deuteride phase or to 420 K for a

di-deuteride phase. The cooling rate of the sample all through the experiment was 0.5 K/s, slow enough to ensure the reconstruction from 1×1 to 7×7 [12]. Temperature-programmed-desorption (TPD) spectra of deuterium were measured with the QMS under the condition of a 3.4 K/s heating rate.

5.3 RESULTS

5.3.1 β_2 TPD

As is the case of D_2 AID on the Si(100) surface [2-4], we anticipate that AID on the Si(111) surface is also associated with β_2 TPD arising from a di-deuteride phase.

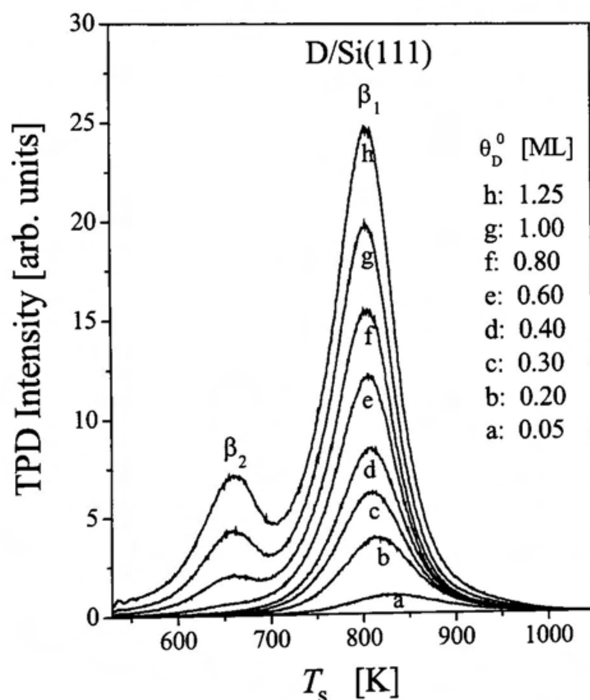

Fig. 5.2: D_2 TPD spectra from the D/Si(111) surfaces as a function of initial D coverages θ_D^0. β_1: TPD arising from the mono-deuteride phase, β_2: TPD arising from the di-deuteride phase.

While the reaction order of β_2 TPD on the Si(100) surface has been well established to be two with respect to di-deuteride (DSiD) coverage θ_{DSiD} [6, 13], little is known about β_2 TPD [14] on the Si(111) surfaces. Therefore, we first investigate the kinetics of β_2 TPD by means of an isothermal desorption method.

D_2 TPD spectra were measured for various θ_D^0. Results are shown in Fig. 5.2. For θ_D^0 < 0.7 ML, the measured TPD spectra show a single peak around 800-820 K, generally denoted as β_1 TPD arising from a mono-deuteride phase. The peak of the β_1 TPD spectra shifts to a lower temperature region with θ_D^0. From the isothermal desorption curves (not shown), we obtained the desorption reaction orders of 1.3-1.5 for the wide temperature range well overlapped with the β_1 TPD region. This is in good agreement with the results reported by Reider et al. [15], and thus the same method may be also applicable to β_2 TPD. The second peak around 660 K is attributed to β_2 TPD arising from a di-deuteride phase [14, 16, 17]. An isothermal desorption experiment for various di-deuteride phases was performed on the surfaces saturated at T_s = 420 K with 0.25 ML excess DSiD[18].

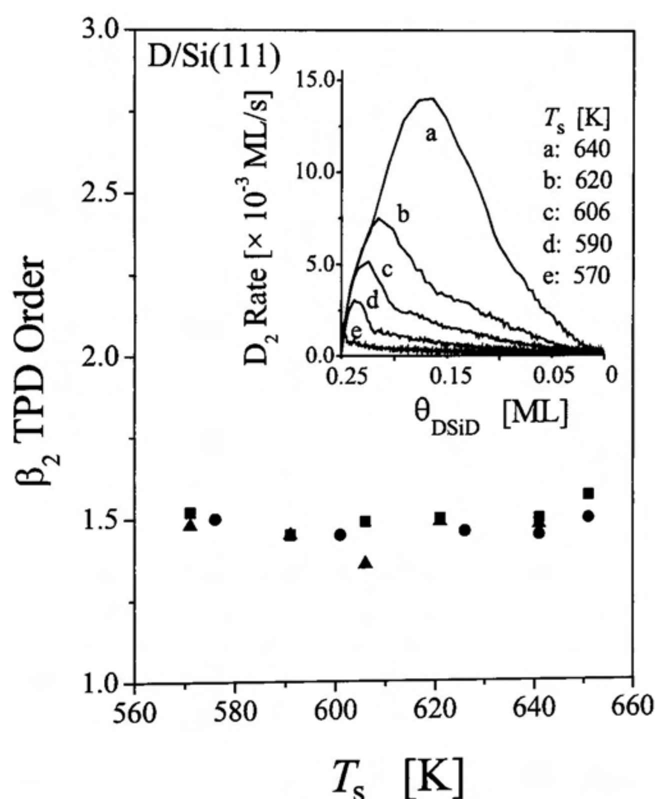

Fig. 5.3: Plots of β_2 TPD orders as a function of T_s. The temperatures for isothermal desorption (T_s) were reached by employing various heating rates as 3.4 K/s (solid circle), 20 K/s (solid squares), and 100 K/s (solid triangles). The inset shows D_2 isothermal decay curves as a function of di-deuteride coverage θ_{DSiD} for various T_s achieved with the 100 K/s heating rate.

The inset in Fig. 5.3 shows the decay profiles of the β_2 TPD rates as a function of momentary DSiD coverage θ_{DSiD}. Here, θ_{DSiD} was determined from time integration of the D_2 rate curves. Overshooting of the D_2 rates were always observed in the initial stages of desorption. It became stronger as the temperature for the isothermal desorption was set higher. After self-termination of this first sharp desorption, desorption order m was determined by using a least squares method to fit the data with the rate equation $dN_{D_2}/dt = k_{\beta_2}\theta_{DSiD}^m$. Here k_{β_2} is the rate constant. As a result, the reaction order of about 1.5 rather than 2 [14] was obtained with respect to θ_{DSiD}.

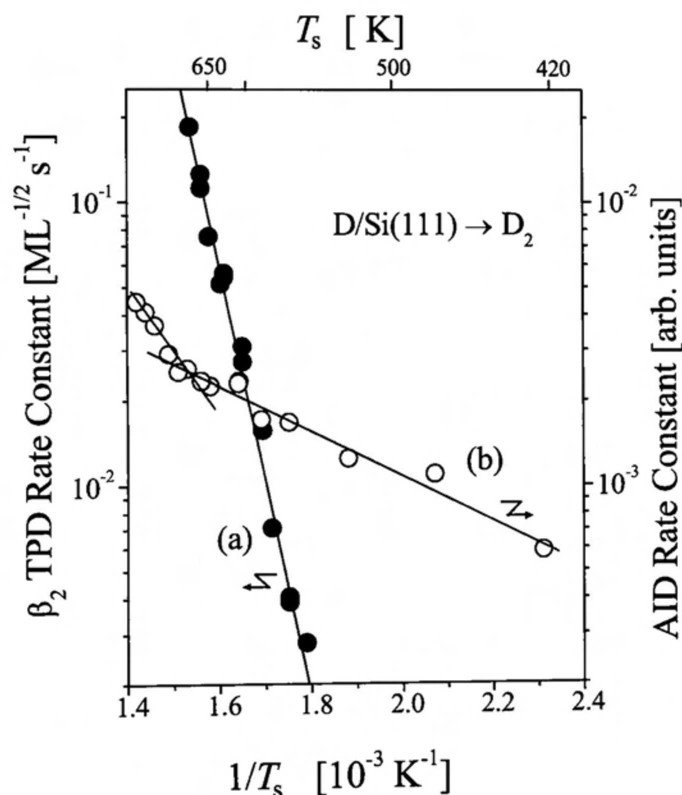

Fig. 5.4: Arrhenius plots of the D_2 desorption rate constants. (a): β_2 TPD, (b): D_2 AID. The solid lines are the best fitted Arrhenius equations (see text).

The reaction order was found to be independent of T_s as plotted in Fig. 5.3. It was not affected by the heating rate to the desired temperature, too. In case of Si(100) it has been proposed that β_2 TPD proceeds via a (1,1) elimination of two D atoms from a pair of adjacent di-deuteride units, leaving behind a doubly occupied Si dimer DSi-SiD

[6]. In contrast to this simple desorption picture on the Si(100) surface, the fractional order of 1.5 for the Si(111) surface is somewhat difficult to illustrate its mechanism in terms of the surface atomic configuration. If the order value of 1.5 with respect to θ_{DSiD} is taken literally, one can say that three D atoms among four from two di-deuteride species take part in one D_2 desorption for β_2 TPD. Thus a third-order kinetics in θ_D could be expected for β_2 TPD. From the Arrhenius plot of k_{β_2} in Fig. 5.4, we obtain the activation energy of 1.5±0.2 eV and the pre-exponential factor of 8.7×10^{10} $ML^{-1/2}$ s^{-1}. The evaluated values are considerably lower than the corresponding values for β_1 TPD, activation energy of 2.45±0.5 eV and pre-exponential factor of $1\sim2\times10^{15}$ s^{-1} [14].

5.3.2 AID and ABS

5.3.2.1 *T_s Dependence*

If AID is associated with an LH mechanism like β_2 TPD, strong temperature dependence can be anticipated for AID. In order to reveal the dependence of ABS and AID on T_s, HD and D_2 rates were measured by admitting H beams onto the D(1 ML)/Si(111) surface prepared at 620 K where no stable di-deuterides are present on the surface. The quick temperature rise from 620 K to desired temperatures was accomplished within a few seconds by means of a direct resistive heating of the sample. D_2 and HD rate curves measured as a function of H exposure time t for various T_s are shown in Fig. 5.5. While the HD desorption receives a little T_s effect, the D_2 rate curves are found to exhibit a strong T_s dependence. This strong T_s dependence of D_2 rates is in good agreement with the DLK's result [8] except for the T_s range above 630 K where rate data were not available. For T_s = 443 K, the size of the D_2 rate step around $t = 0$ is extremely low compared to that for T_s = 620 K. For T_s = 663 K, the D_2 rate sharply jumps up even prior to H exposure due to the occurrence of β_1 TPD. The admission of H onto this surface causes a further big rate jump due to AID. For T_s = with 733 K, on the other hand, no net D_2 rate step is present at $t = 0$, and therefore the observed D_2 desorption can be attributed solely to β_1 TPD, of which intensity is also plotted in Fig. 5.6 (d). Because considerable D adatoms are still present on the surface as confirmed in Fig. 5.5 (left panel), the observed decrease in D_2 rates with increasing T_s above 650 K

can never be explained by the HA mechanism.

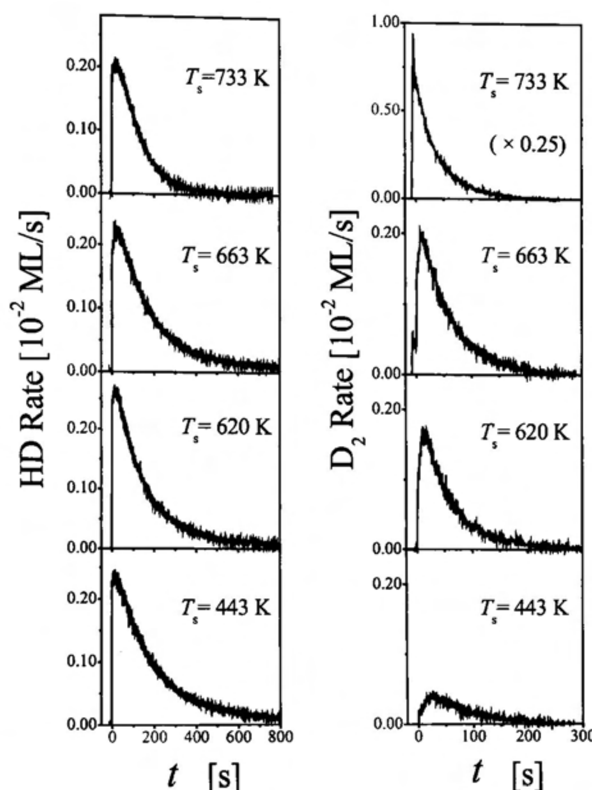

Fig. 5.5: Plots of HD and D_2 rate data as a function of H exposure time t on the reaction system of H + D(1 ML)/Si(111) at various T_s. One should note that the D_2 rate curve measured at T_s = 733 K is mainly due to β_1 TPD without D_2 AID for the entire exposure period.

The observed temperature effect on the rate of D_2 AID may be characterized with e.g., a size of rate step at $t = 0$, an apparent maximum rate at the peak, or total yield. We plot all these quantities as a function of T_s in Fig. 5.6. As defined in the inset, curve (a) stands for the initial rate step at t = 0, curve (b) the maximum rate at the peak, and curve (c) the integrated rates. In order to minimize the effect of fluctuation in D or H beam intensities the D_2 rates have been normalized with corresponding HD rates, which are actually not much affected by T_s as shown in Fig. 5.5 (left panel). For comparison, the decomposed β_2 and β_1 TPD spectra are also plotted in Fig. 5.6. The thermal desorption spectrum (d) is closely related to the β_1 TPD spectrum since it can

be superimposed to the β_1 TPD line with a certain normalization factor. It is quite clear that D_2 AID occurs efficiently at the temperature region corresponding to β_2 TPD. The shift of the D_2 AID peak is only 10 K to the lower temperature region from the β_2 TPD peak at 660 K. For $T_s \gtrsim 650$K, the D_2 AID rate decreases quite rapidly with increasing T_s. This is due to removal of D adatoms in competition with β_1 TPD. Curve (a) looks similar in shape to the β_2 TPD spectrum particularly around the peak. This spectral similarity suggests that D_2 AID is associated with β_2 TPD like the case of the Si(100) [4] and Ge(100) [19]. D_2 AID may be attributed to D_2 desorption arising from a di-deuteride phase transiently formed by H atoms.

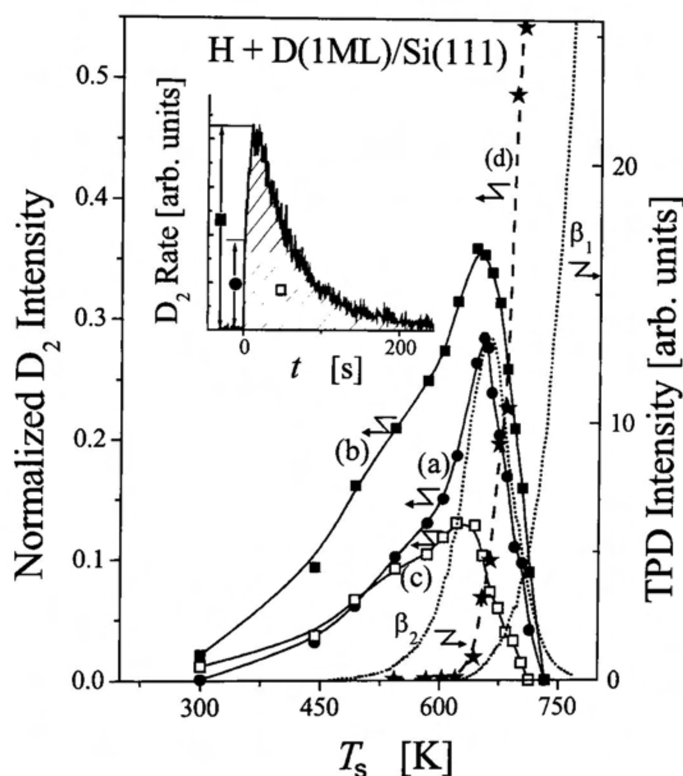

Fig. 5.6: Plots of D_2 rates as a function of T_s: (a): initial rate step at $t = 0$ (solid circles), (b): maximum rate at the peak (solid rectangles), and (c): integrated yield (open rectangles) as defined in the inset. Curve (d) is the plot of D_2 β_1 rates just before H exposure at $t = 0$. Each point was normalized with corresponding HD rate. The decomposed β_1 and β_2 TPD spectra are also plotted for comparison.

Figure 5.7 shows a plot of the reaction order for the D_2 desorption during H exposure

as a function of T_s. D_2 desorption orders were determined by fitting the experimental rate data to the single term rate equation $dN_{D_2}/dt = k\theta_D^m$. The inset in Fig. 5.7 shows the log-log plots of D_2 rates for T_s = 443, 620, and 713 K together with the corresponding best fit curves. Here, the momentary D adatom coverages θ_D during H exposure were evaluated by integrating the HD and D_2 rate curves [2]. D_2 desorption order was determined to be about three for 300 K $\le T_s \le$ 650 K where AID occupies the whole D_2 desorptions since the rate of β_1 TPD is quite low. The measured reaction order of about three is in good agreement with the refitted result of the DLK's data in Fig. 5.1(b). Thus, we know that D_2 AID proceeds along a third order kinetics in θ_D. This fact clearly rules out the HA mechanism.

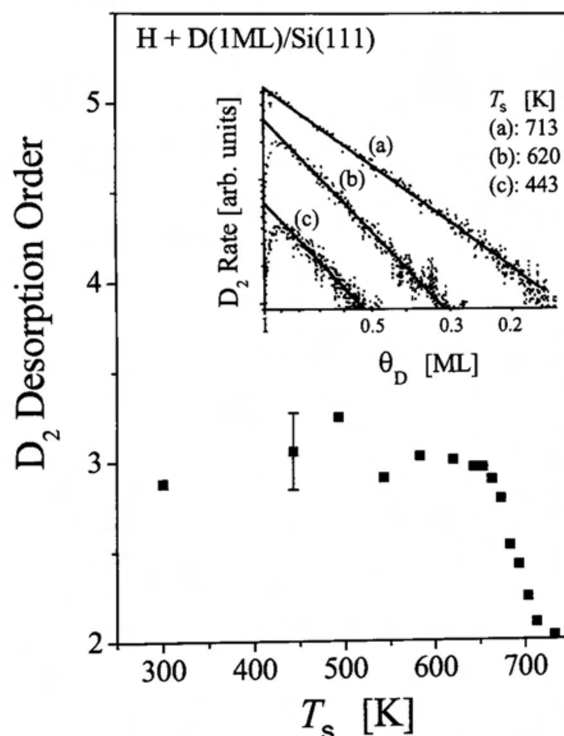

Fig. 5.7: Plots of D_2 desorption order as a function of T_s. The inset shows log-log plots of the D_2 rate curves and corresponding fits with the rate equation $dN_{D_2}/dt = k\theta_D^m$ to evaluate desorption order m.

With increasing T_s well above 650 K the D_2 desorption orders were found to be decreased systematically tending to two. As shown in Fig. 5. 5 (right panel), β_1

channel thermal desorption begins to occur as T_s exceeds 650 K. It completely replaces D_2 AID when T_s > 733 K. If D and H adatoms are spatially randomly sticked, probability of a configuration of two adjacent D adatoms may be proportional to θ_D^2. This leads to such an apparent second-order kinetics for β_1 TPD. The observed decrease in D_2 desorption order for $T_s \geq 650$ K is thus caused by β_1 TPD.

An Arrhenius plot of k is given in Fig. 5.4. It does not show a straight line but a curved one. For 400 K< T_s <650 K the activation energy is evaluated to be 0.16 ± 0.02 eV. For $T_s \geq 650$ K the rate constant increases and the activation energy can be evaluated to be 0.5 ± 0.1 eV. The activation energy of ~0.16 eV is considerably lower than the activation energy of 1.5±0.2 eV for β_2 TPD. Physical meaning of the apparently small activation energy for AID will be discussed in the discussion part.

5.3.2.1 θ_D^0 *dependence*

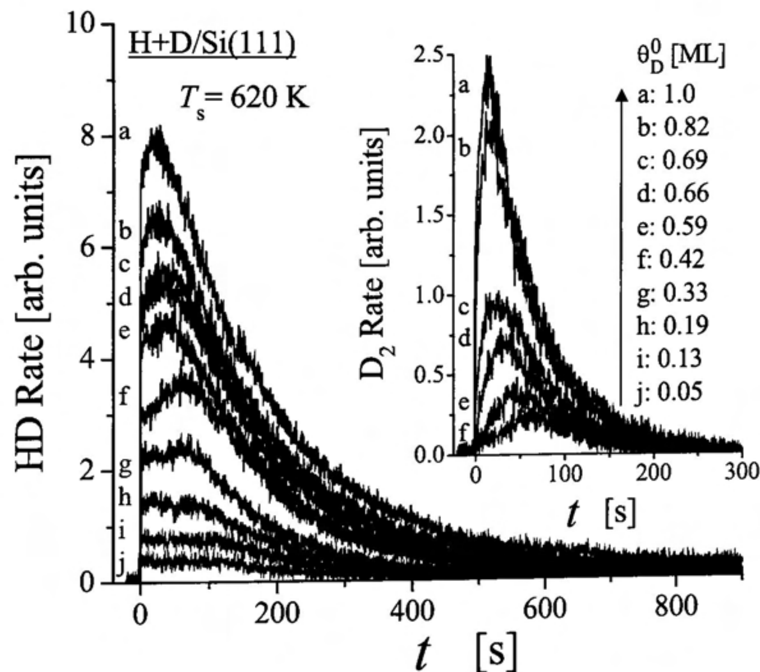

FIG. 5.8: Plots of HD and D_2 rate curves for various θ_D^0 at T_s =620 K.

It is important to know how H adsorption to dangling bonds competes with ABS or AID. HD and D_2 rate curves were measured at T_s = 620 K for various $\theta_D^0 \leq 1.0$ ML

where no any spontaneous thermal desorptions are included. HD and D_2 rate curves are plotted for various θ_D^0 in Fig. 5.8. D_2 AID is found to be quite nonlinear in θ_D^0 since D_2 molecules are hardly seen for $\theta_D^0 \leq 0.3$ ML. An induction time to the maximum rate can be recognized for any θ_D^0, but it becomes shorter with increasing θ_D^0. On the other hand, the HD rate curves exhibit more complex features: for low $\theta_D^0 \leq$ 0.5 ML, they exhibit a bimodal spectral line shape with a fast rate jump followed by the second peak. The second peak systematically shifts to the early time region with increasing θ_D^0. The trend is analogous to that of D_2 AID not only in coverage range but also in time range, suggesting that while the first peak is obviously attributed to ABS, the second peak is attributed to HD AID.

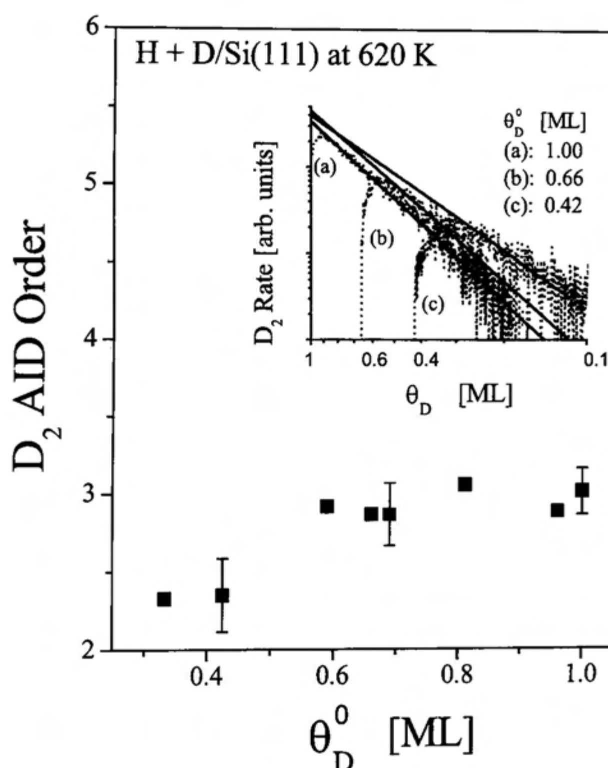

Fig. 5.9: Plots of D_2 AID order as a function of θ_D^0. Inset shows log-log plots of D_2 rate curves fitted with the rate equation $dN_{D_2}/dt = k\theta_D^m$.

Reaction orders of D_2 AID were then evaluated as a function of θ_D^0 by applying the rate data in Fig 5.8 to the single term rate equation as employed before. Results

are plotted in Fig. 5.9. The inset shows the least squares fit of the measured D_2 rate data. Notice that the evaluated reaction orders are nearly constant ~ 3 for 0.6 ML ≤ θ_D^0 ≤ 1.0 ML. On the other hand, for θ_D^0 ≤ 0.4 ML the reaction order tends to ~2.3. The value of ~2.3 is close to two, which might fulfill the criterion of the HA mechanism. However, this does not necessarily mean that the HA mechanism is the case, but manifests an isotope effect on AID. This will be cleared after analyzing the rate curves in the next section. Effect of stable di-deuterides DSiD on ABS and AID was examined at T_s = 420 K on the surface saturated with DSiD, i.e., θ_D^0 = 1.25 ML [18]. Figure 5.10 shows the plots of D_2 rates versus t for θ_D^0= 1.25 (curve (a)) and 1.0 ML (curve (b)). At such lower temperature of 420 K the yield of D_2 AID is low for θ_D^0 D ≤ 1.0 ML as already shown in Fig. 5.6.

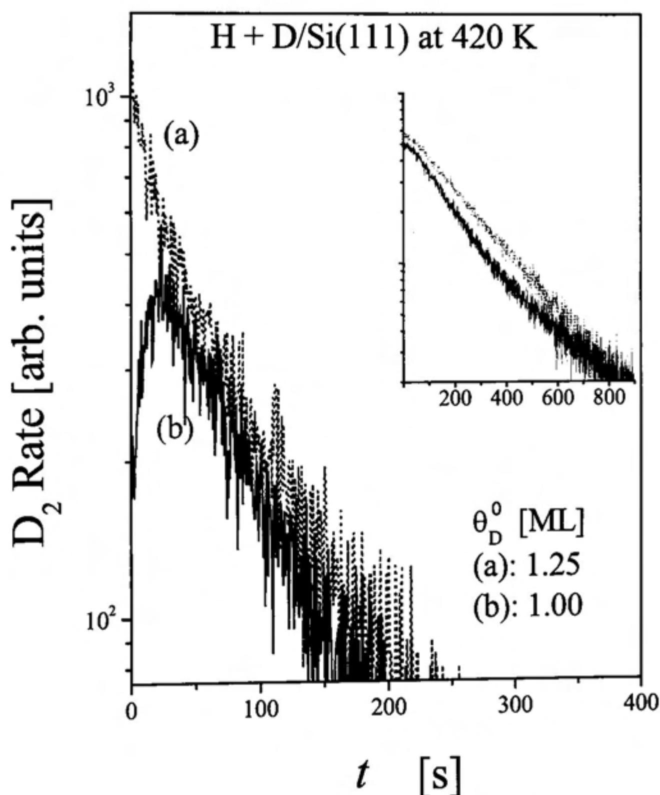

Fig. 5.10: Plots of D_2 rate for (a): 1.25 ML and (b): 1.00 ML as a function of H exposure time t. The inset shows the corresponding HD rates.

Contrary to this trend, for θ_D^0 = 1.25 ML we can admit an efficient occurrence of D_2

AID as demonstrated in Fig. 5.10 (a). Notice that for θ_D^0 = 1.25 ML the initial rate step, which is immediately followed by the exponential decay, is almost one order of magnitude larger than that for θ_D^0 = 1.0 ML. For θ_D^0 = 1.0 ML, the D_2 rate first increases to reach the peak and then decreases exponentially. After the peak, two rate curves are found to decay along the same kinetics.

5.4 DISCUSSION

So far, we have discovered that the HA mechanism cannot explain the D abstraction by H. As shown in Fig. 5.6, the AID rate spectra as a function of T_s look like the β_2 TPD spectrum arising from a di-deuteride phase at least for $T_s \geq 600$ K. This spectral similarity to β_2 TPD suggests that D_2 AID is associated with β_2 TPD. In addition to this spectral similarity, D_2 AID can be related to β_2 TPD via their reaction order since the 1.5th-order rate law in θ_{DSiD} can be converted to the third-order rate law in θ_D provided that $\theta_{DSiD} \propto \theta_D^2$. Therefore, we conclude that AID occurs from the di-deuteride phase transiently formed by H atoms. On the other hand, kinetics of ABS is not understood since its reaction order has not been obtained yet. The ABS mechanism may be understood by analyzing the measured HD rate curves after obtaining appropriate rate equations to describe HD as well as D_2 desorption processes. In this discussion, firstly, we propose rate equations for ABS and AID which can fit the observed kinetic data. We fit the rate equations to the rate data to extract characteristic features in AID and ABS. Secondly, we discuss the physical origin of the extremely low activation energy evaluated for AID as well as the implication of the third-order rate law for D_2 AID. Finally, we propose a hot complex model to comprehensively explain the observed rate law as well as isotope effects on ABS.

5.4.1 Rate Equations at T_s=600 K

a. D_2 Rate Equation: For the D_2 rate equation on the Si(111) surface, we modify the D_2 rate equation proposed on the Si(100) surface [3, 4] so that it may satisfy the observed third-order rate law in θ_D and θ_H. Hence the D_2 rate equation proposed here is comprised of two third-order AID terms in θ_D and θ_H,

$$\frac{dN_{D_2}(t)}{dt} = \eta(t)\{c_1\theta_D^3 + c_2\theta_D^2\theta_H\}. \tag{5-1}$$

Here, both c_1 and c_2 are the rate constants including the flux of H atoms, and η (t) for the AID efficiency is the function of t through total coverage θ_{D+H}. It is characterized with an S-shaped increase from zero at $\theta_{D+H}=0$ to unity when the AID reaction becomes steady at θ_{D+H} at about 1.0 ML. We express this with a sigmoid curve based on an error function [3],

$$\eta(t) = \frac{1}{2}\{1 + erf(\frac{\theta_{D+H}(t) - \theta_0(\theta_D^0)}{w(\theta_D^0)})\}. \tag{5-2}$$

Here, $\theta_0(\theta_D^0)$ is the threshold coverage when η (t) becomes 0.5, and w(θ_D^0) represents the width of the steeply increasing portion. Since the induction time is observed even for the surface saturated at θ_D^0 = 1 ML, η (t) is used for the whole D coverage region examined.

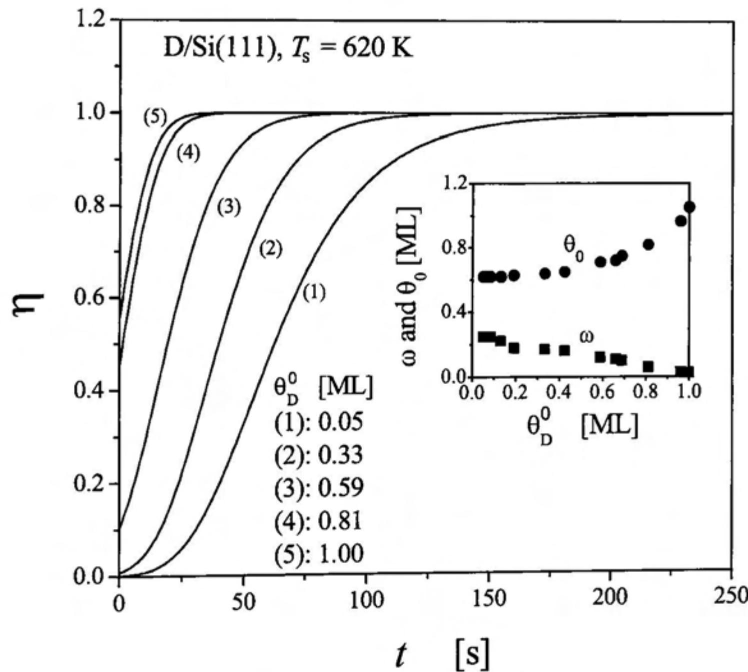

Fig. 5.11: Plots of η (eq.(5-2) in the text) versus t curves for various θ_D^0 at 620 K. The inset shows changes of two parameters w and θ_0 as a function of θ_D^0.

In practical curve fitting of the D_2 rate data obtained at T_s = 620 K, we first determined θ_D by integrating the HD and D_2 rate curves as a function of t [2], and

then evaluated θ_H by assuming that during H exposure increase along the same curve as for the D uptake (not shown). After the surface saturation, θ_{D+H}= 1.0 ML was taken for further H exposure since DSiD species are quite unstable at T_s = 620 K. The best fit curve was obtained self consistently for the two parameters in η (t) as well as for all the rate constants in eq.(5-1) as well as in eq.(5-3) for HD. In Fig. 5.11 we plot η (t) obtained in this way for various θ_D^0. The employed parameters w(θ_D^0) and $\theta_0(\theta_D^0)$ are plotted in the inset. The width parameter w(θ_D^0) decreases almost linearly with θ_D^0, tending to zero. On the other hand, the threshold coverages $\theta_0(\theta_D^0)$ increase slightly superlinearly, exceeding unity at θ_D^0= 1 ML.

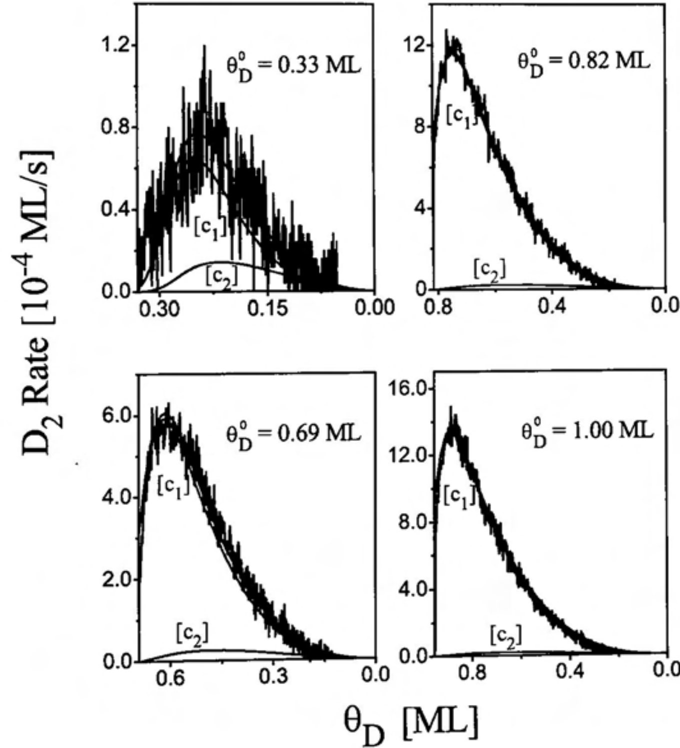

Fig. 5.12: Fits of D_2 rates equation (5-1) in the text to the D_2 data measured at T_s = 620 K. Solid lines represent each term of the rate equation (1); [c1]: $c_1\eta\theta_D^3$, [c2]: $c_2\eta\theta_D^2\theta_H$, and thick solid line: sum of [c1] and [c2].

The best fit D_2 rate curves for various θ_D^0 in plotted in Fig. 5.12. The $c_1\eta\theta_D^3$ term becomes predominant because of the isotope effect of c_1/c_2 =10 ~ 20. The $c_2\eta\theta_D^2\theta_H$ term

is important only for $\theta_D < 0.4$ ML. Thus the D_2 AID orders determined from the single term rate equation in Fig. 5.9 can be justified for $\theta_D^0 \leq 0.5$ ML is caused by the c_2 term of eq.(5-1).

b. HD Rate Equation: Since H adatoms accumulate on the surface through termination of dangling bonds as well as substitution of D adatoms, HD desorptions proceed not only along the ABS channel but also along the AID one. HD AID follows also a third-order kinetics in θ_D and θ_H like D_2 AID. For ABS we found that the first-order kinetics at low θ_D^0 switches to the second-order one at high θ_D^0. We first tried to assure this kinetics switching by employing η (t) likely to the case on Si(100) surfaces [3]. As a result, it turned out that no good fit was obtained because of a somewhat strong coupling between ABS and AID through η (t). After trial and error analysis, we came to the conclusion that the following rate equation for HD desorption is by far the best applicable to the measured HD rates;

$$\frac{dN_{HD}(t)}{dt} = a_1(\theta_D^0)\theta_D + a_2(\theta_D^0)\theta_D^2 + \eta(t)(C_1\theta_D^2\theta_H + C_2\theta_D\theta_H^2). \tag{5-3}$$

The two rate constants $a_1(\theta_D^0)$ and $a_2(\theta_D^0)$ for ABS were taken as a function of θ_D^0. Both C_1 and C_2 are the rate constants for AID, independent of θ_D^0. Using eq.(5-3) we fit the HD rate data obtained for various θ_D^0 at T_s = 620 K. The same θ_D and θ_H as well as η (t) used for the fit of the D_2 rate curves in Fig. 5.12 were employed. Figure 5.13 shows representative HD rate curves and the corresponding best fit results. For θ_D^0 = 0.07 ML, the HD desorption is found to occur via the first-order ABS reaction with a minor contribution of HD AID. With increasing θ_D^0 to 0.42 ML, the first-order ABS pathway is still the major desorption channel, prevailing the second-order ABS pathway. HD AID via the C_1 term becomes important as about one third of the initial D adatoms have been lost. With increasing θ_D^0 further to 0.82 ML, the situation becomes complicated since the second-order ABS channel prevails the first-order one. This is because the dangling bond density is already low from the beginning of H

exposure. Moreover, as H exposure proceeds, HD AID along the C_1 term in eq.(5-3) becomes a major desorption channel, prevailing ABS.

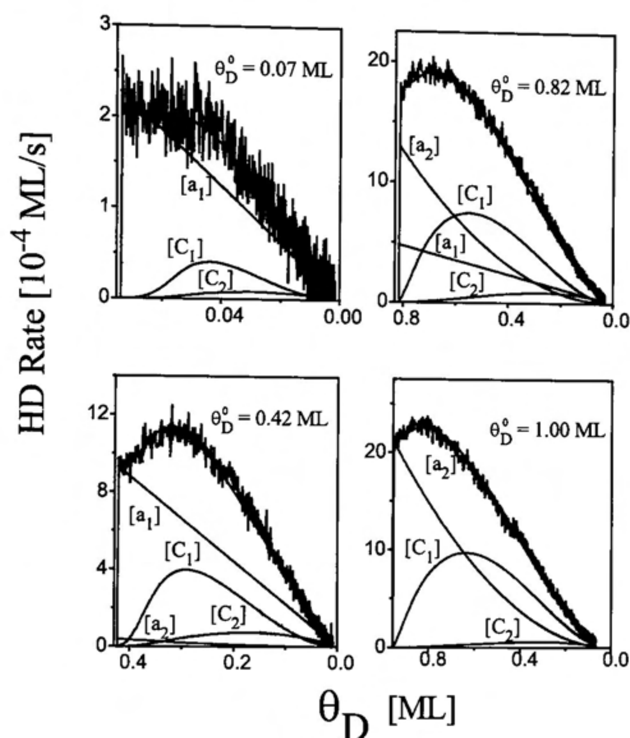

Fig. 5.13: Fits of the HD rate equation (5-3) in the text to the HD rate data measured at T_s = 620. Solid lines represent each component of the rate equation (5-3); [a1]: $a_1\theta_D$, [a2]: $a_2\theta_D^2$, [C1]: $C_1\eta\theta_D^2\theta_H$, and [C2]: $C_2\eta\theta_D\theta_H^2$. The thick solid lines represents their sum.

From comparison between C_1 in eq.(5-3) with c_2 in eq.(5-1) we can confirm possible isotope effects on AID for the same geometrical condition. Since $C_1 > c_2$, HD AID takes place more efficiently than D_2 AID. Similar isotope effects could be expected between HD and H_2 AID.

The initial HD rates and their decomposed components are plotted together with D_2 AID rate steps at $t = 0$ as a function of θ_D^0 in Fig. 5.14. The curves [a1] and [a2] are respectively the first and second terms in eq. (5-3) at t = 0, and the curve [a1+a2] represents their sum. As can be seen from Fig. 5.14 [a1], the first-order HD ABS along the a_1 term increases with θ_D^0 up to around 0.4 ML, peaking around θ_D^0 = 0.5 ML

followed by a decrease to zero at θ_D^0 = 1.0 ML. On the other hand, as shown in Fig. 5.14 [a2], the alternative second-order ABS along the a_2 term begins to emerge at about θ_D^0 = 0.4 ML and increases rapidly with θ_D^0, crossing over the first-order ABS around θ_D^0 = 0.7 ML.

The inset of Fig. 14 shows the removal of total D adatoms via ABS or AID for various θ_D^0. For low $\theta_D^0 \leq$ 0.5 ML, D adatoms removed from the surface mainly by the ABS channel. For $\theta_D^0 \approx$ 1.0 ML, on the other hand, only 35% of the total D adatoms removed along the same channel but 65% along the AID channel.

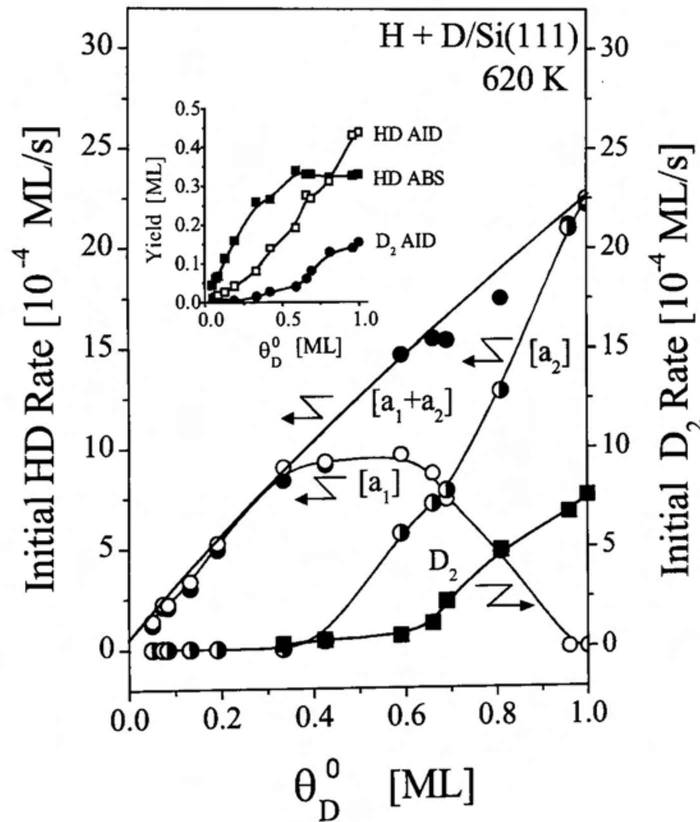

Fig. 5.14: Plots of initial HD rates decomposed by eq. (5-3) in the text as a function of θ_D. [a1]: $a_1\theta_D\,(t=0)$, [a2]: $a_2\theta_D^2\,(t=0)$, and [a1 + a2] : sum of [a1] and [a2]. For comparison the initial D2 rates determined from eq.(5-1) in the text are also plotted (solid rectangles). The inset shows the integrated yields of HD ABS, HD AID, and D2 AID as a function of θ_D^0.

5.4.2 AID in Steady State

In the above discussion we have seen that AID is associated with β_2 TPD. However, the D_2 AID rate spectra shown in Fig. 5.6 have a long tail down to 300 K far below the typical β_2 TPD region. Moreover, the Arrhenius plot of D_2 rate constants in Fig. 5.4 yields the very small activation energy of ~0.16 eV, much smaller than that for β_2 TPD by one order of magnitude. In this subsection we discuss this problem. The Arrhenius plot of the AID rate constants k in Fig. 5.4 was obtained after the induction time when both of the reactions ABS and AID become steady. If the surface has been already saturated with di-deuterides before H exposure, ABS and AID are both steady from the very beginning of H exposure. This effect on AID can clearly be seen in Fig. 5.10 for T_s=420 K. The surface saturated with 0.25 ML DSiD (Fig. 5.10 (a)) exhibits very strong D_2 AID at $t = 0$, while the surface without DSiD for θ_D^0=1.0 ML (Fig. 5.10 (b)) shows the induction time. However, after the induction time the D_2 AID reaction on the two surfaces proceeds along the same kinetics, indicating that the surface saturates with di-hydrides or di-deuterides after the induction time in order to reach the maximum rate. The saturation coverage of 0.25 ML at T_s = 420 K is not low as it refers to an average of one DSiD per 2×2 cell. If one DSiD unit locates at the center of every 2×2 unit cells, DSiD and SiD units are alternately arranged. In such a surface geometry, the di-hydrides HSiD are formed by H atoms exclusively at the neighboring sites of the stable DSiD. The spatially close configuration between DSiD and HSiD will result in prompt D_2 AID without long range migration and thus no induction time in the rate curves. The excess di-deuterides or di-hydrides formed beyond the saturation coverage have to be extinguished to reduce the increased free energy. The surface will do this by generating AID. This is a generalized β_2 TPD occurring under the steady state condition established during surface exposure to H atoms.

Therefore, the nascent desorption in the AID process is basically activationless as the adsorption and desorption reaction occurs in a steady state under exposure to H. Thus, the rate for D_2 AID (R_{AID}) is in principle equal to the rate of H sticking for AID ($R_{stick/AID}$), i.e., $R_{AID} = R_{stick/AID}$. AID occurs at sites where DSiD and SiD units are

arranged side by side. For the concentration of SiD units θ_{SiD} and for the D sticking rate constant k_s , sticking rate at AID sites is expressed as $R_{stick/AID} = k_s \theta_{SiD} \theta_{DSiD}$. Then R_{AID} can be expressed as,

$$R_{AID} = k_s \theta_{SiD} \theta_{DSiD} . \tag{5-4}$$

Taking the coverage relations $\theta_{DSiD} = \theta_D^2$ and $\theta_{SiD} = \theta_D$ for $\theta_D^0 \leq 1$ ML, eq. (5-4) results in a third-order kinetics for D_2 AID as observed in Fig. 5.7. Recalling that $R_{AID}(= dN_{D_2}(t)/dt) = k\theta_D^3$, one can obtain ,

$$k = k_s. \tag{5-5}$$

Therefore, we understand that the observed activation energy for AID arises from the sticking rate constant or sticking cross section of H atoms to SiD units. Since the H sticking reaction to SiD units is exothermic, k_s may be less sensitive to T_s, causing such a low activation energy of ~0.16 eV as obtained in Fig. 5.4.

Kubo et al. [7] also obtain quite low activation energy of about 0.2 eV for AID on the Si(100) surface. They consider that the origin of such low activation energy stems from the desorption process of adjacent di-hydrides by which the surface system is stressed. Thus this idea ignores the H sticking process to make di-deuterides.

5.4.3 Hot Complex-Mediated Reaction Model

The rate equation analysis exhibited that the reaction order for ABS is two with respect to θ_D for high θ_D^0. This is unexpected if the process proceeds along a direct ER pathway. Such a second-order ABS reaction was also found on Si(100) [3, 4, 7]. However, one should recall that the second-order kinetics observed there was nominal, but the first-order kinetics with respect to DSi-SiD species was essential [3]. Hayakawa et al. [4] proposed a new model based on a hot complex (HC)-mediated ABS and AID. From the phenomenological similarities as appeared in the ABS and AID

reactions on the two different surface planes, the HC model may again be invoked on the Si(111) surface. A direct ER reaction may not be the case on the Si surfaces since the observed ABS cross sections 3-6. Å^2 [4, 20, 21] is larger than to the theoretical values for the ER reaction σ <1 Å^2 [22]. According to Hansen and Vogel [23], H atoms incident to the D-terminated Si surfaces see an attractive, though corrugated, chemisorption potential at any impact site. It is laterally bound by the potential corrugations and hence immobile along the surface. We consider such a bound, hot precursor, presumably vibrationally excited, as a complex between the incident H and D/Si moiety. In case of Si(100) doubly occupied Si dimers DSi-SiD have been considered as a skeleton of such a hot complex since the reconstructed Si(100) surface has a 2×1 structure and it keeps the same dimer structure up to θ_D^0 = 1 ML. On the Si(111) surface, on the other hand, it has been reported that the adsorption structure of hydrogen varies with surface coverages. According to Takayanagi's DAS model [24, 25], there are 19 dangling bonds in each rhombohedral Si(111)- 7×7 unit cell; 12 of them are at Si adatoms, 6 at Si rest atoms, and one at a corner hole. For very low H or D coverages below 0.01 ML the 7×7 structure is found to be intact as observed experimentally [26] and theoretically [27]. With further H exposures, however, it is no longer stable since the Si adatoms tend to build up islands [28, 29]. The surface comes close to a nearly bulk truncated 1×1 structure at high coverages around 1 ML for $T_s \geq$ 620 K [30, 31]. Even at around room temperatures Si adatoms are removed by exposing them to H atoms [28]. For the present experimental conditions for $T_s \geq$ 300 K and $\theta_{D+H} \geq$ 0.05 ML, these STM observations strongly suggest that reactions of H atoms mainly take place on the rest atom layer. Therefore, we tentatively take a skeleton for the hot complex with a geometrical structure as illustrated in Fig. 5.15. A pair of Si rest atoms are bridged by a back bonding Si atom denoted as Si· · ·Si. If the two Si atoms are terminated with a D atom, the hot complex may be designated as (H+DSi · · · SiD)*. This is an analogy of the hot complex (H+DSi-SiD)* designated on the Si(100) surface.

Abstraction of adatoms are supposed to occur in energy relaxation process of the hot

complex, competing with breakage of the Si back bonds to form HSiD. At the low coverage regime, the hot complex may involve a dangling bond, and therefore ABS competes with sticking. This could lead to the first-order ABS as described in eq. (5-3). As H exposure proceeds, such dangling bonds will be fully terminated by H atoms, and then the incident H atoms have more chance to form a hot complex with DSi・ ・ ・SiH species.

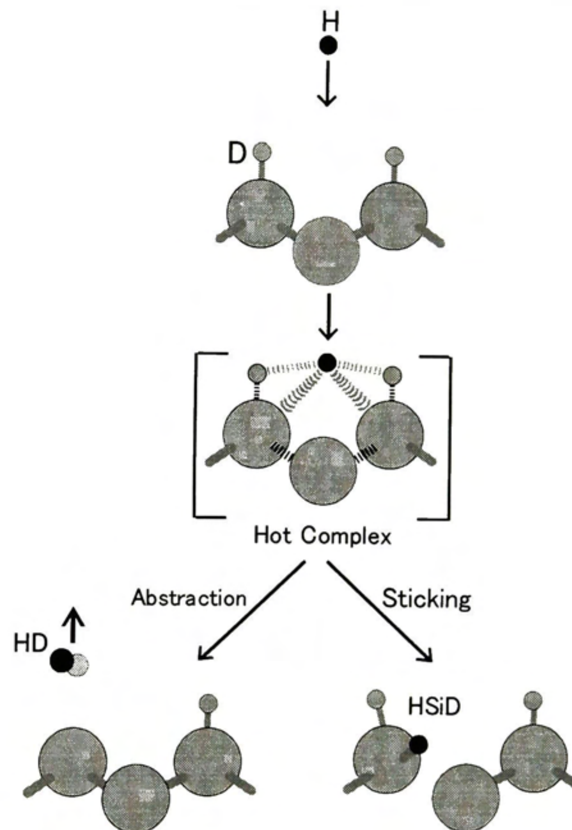

Fig. 5.15: Hot complex-mediated reaction model. Here, at first an H atom attacks the D-terminated Si(111)-1×1 surface. It is then chemisorbed in a chemisorption potential forming a hot complex. The bars between the H atom and two D atoms or two Si atoms schematically represent attractive interactions (not bonding between H-Si and H-D). From this situation, it can either abstract one of the two D atoms or stick to one of the two Si atoms to form a di-hydride.

During relaxation of (H+DSi・ ・ ・SiH), HD ABS competes with H_2 ABS. In this case

an isotope effect is expected. The isotope effect may lead to a preferred abstraction of a lighter H adatom to a heavier D adatom due to quantum effects such as a zero-point vibrational energy effect on potential barriers, tunneling through reaction barriers, or an attempting frequency factor for access to transition states. All these quantum effects on reactions accompanied by nuclear movement predict that the lighter atom can be superior to the heavier one in the transitions. Therefore, in order to generate HD desorption along the ABS pathway the skeleton of the hot complex should be exclusively DSi · · · SiD.

For a low D coverage case but at nearly H saturation, the probability to find DSi · · · SiD may be proportional to θ_D^2. This is associated with the second-order ABS term in eq. (5-5). For $\theta_D^0 \le 0.5$ ML, the first-order ABS channel prevails the second-order ABS one as shown in Fig. 5.13, and thus the total HD yield via the ABS pathway is mainly determined by the first-order ABS rate. As can be seen in the inset of Fig. 5.14 the HD yield along the ABS pathway monotonously increases with increasing θ_D^0 until it levels off at θ_D^0 = 0.5 ML.

For high D coverages $\theta_D^0 > 0.5$ ML, on the other hand, incident H atoms make a hot complex mainly with DSi · · · SiD at the early stages of exposure. As the dangling bond density is decreased with increasing θ_D^0, the first-order ABS channel is eventually replaced with the second-order ABS channel. Efficient ABS and AID result in a quick D substitution with H, and thence the incident H atoms will tend to make more hot complexes with DSi · · · SiH, which generates H_2 rather than HD due to the expected isotope effect in the ABS pathway. Thus the second-order ABS rates decrease rapidly with *t*. However, this decrease in ABS rate is partly compensated by the increase in HD AID rate. The HD AID channel prevails the D_2 AID channel owing to the isotope effect. Thus the total D_2 AID yield plotted in the inset of Fig. 5.14 are always smaller than that of HD AID.

From the inset of Fig. 5.14, we can know the loss of D adatoms under exposure to H atoms proceed mostly along the ABS pathway for $\theta_D^0 \le 0.5$ ML. For θ_D^0 about 1.0 ML, on the other hand, the AID channel is dominant, ~65% as AID and ~35% as ABS. The

simulations so far reported for ABS and AID on the Si(100) surfaces [22, 32, 33] have neglected the H sticking to terminated Si atoms. The result in the simulation on Si(100) by Hansen and Vogl [23] seems to be partly reasonable since it does not predict any HA pathways but admits efficient adsorption. However, the employed Tersoff's potential [34] does not allow H atoms to stick to the Si-Si bonds. Thus, the post adsorption reaction or AID associated with β_2 TPD is not considered. In order to perform dynamic simulation that can properly mimic the reaction kinetics observed here for ABS and AID, it is highly desirable to construct a new potential energy surface so as to allow sticking to the terminated surfaces.

5.5 SUMMARY

We have measured the desorption kinetics of D abstraction by H on the D/Si(111) surfaces. Reactions of D abstraction by H were categorized into the direct abstraction (ABS) and the adsorption-induced-desorption (AID) of surface adatoms. Effects of both the adatom coverage and surface temperature (T_s) on ABS and AID were studied. As a result, the hot atom (HA) mechanism was ruled out since the reaction orders of both ABS and AID were found to be larger than the values expected for the HA mechanism; the reaction order of AID is about three, independent of T_s, while the reaction order of ABS is about two for $\theta_D^0 \gtrsim 0.8$ ML. The AID reaction is associated with β_2 TPD through the reaction order as well as the rate spectra as a function of T_s.

AID could be observed even for the temperature region well below β_2 TPD. Particularly, when the surface was saturated with 0.25 ML di-deuterides, the D_2 rate was found to be high even at the early stages of exposure to H atoms. For such low temperatures the di-deuterides cannot be mobile on the surface. This fact infers that D_2 AID is possible when di-hydrides are formed by H atoms at the vicinity of the di-deuterides. The Arrhenius plot of the AID rate constants exhibits low activation energies ~0.16 eV for a wide temperature region below 650 K above which it increases to ~0.5 eV. The origin of such low activation energies for AID was explained in terms of a steady state reaction under H exposure, where the AID rates are determined by

the sticking process of H atoms to the terminated Si atoms to form di-hydrides rather than the desorption process.

The rate equations for both D_2 and HD desorptions for the high temperature regimes were precisely formulated to fit the ABS and AID rate data. It was evaluated that about 65% of the 1 ML D adatoms are abstracted through the AID channel, while about 35% are abstracted via the ABS pathway. A hot complex (HC)-mediated reaction model proposed to explain the second-order rate law confirmed for the ABS reaction.

REFERENCES

[1] A. Dinger, C. Lutterloh, and J. Küppers, Chem. Phys. Lett. 311 (1999) 202.

[2] S. Shimokawa, A. Namiki, T. Ando, Y. Sato, and J. Lee, J. Chem. Phys. 112 (2000) 356.

[3] F. Khanom, S. Shimokawa, S. Inanaga, A. Namiki, M. N. -Gamo, and T. Ando, J. Chem. Phys. 113 (2000) 3792.

[4] E. Hayakawa, F. Khanom, T. Yoshifuku, S. Shimokawa, A. Namiki, and T. Ando, Phys. Rev. B 65 (2001) 033405.

[5] M. C. Flowers, N. B. H. Jonathan, A. Morris, and S.Wright, Surf. Sci. 396 (1998) 227.

[6] M. C. Flowers, N. B. H. Jonathan, Y. Liu, and A. Morris, J. Chem. Phys. 99 (1993) 7038.

[7] A. Kubo, Y. Ishii, and M. Kitajima, J. Chem. Phys. 117 (2002) 11336.

[8] A. Dinger, C. Lutterloh, and J. Küppers, J. Chem. Phys. 114 (2001) 5338.

[9] Th. Kammler, S. Wehner, and J. Küppers, J. Chem. Phys. 109 (1998) 4071.

[10] Th. Kammler, D. Kolovos -Vellianitis, and J. Küppers, Surf. Sci. 460 (2000) 91.

[11] J. Harris and B. Kasemo, Surf. Sci. 105 (1981) L281.

[12] J. -L. Lin, D. Y. Petrovykh, J. Viernow, F. K. Men, D. J. Seo, and F. J. Himpsel, J. Appl. Phys. 84 (1998) 255.

[13] P. Gupta, V. L. Colvin, and S. M. George, Phys. Rev. B 37 (1988) 8234.

[14] M. C. Flowers, N. B. H. Jonathan, Y. Liu, and A. Morris, J. Chem. Phys. 102 (1995) 1034.

[15] G. A. Reider, U. Höfer, and T. F. Heinz, J. Chem. Phys. 94 (1991) 4080.

[16] G. Shulze and M. Henzler, Surf. Sci. 124 (1983) 336.

[17] B. G. Koehler, C. H. Mak, D. A. Arthur, P. A. Coon, and S. M. George, J. Chem. Phys. 89 (1988) 1709.

[18] R. J. Culbertson, L. C. Feldman, P. J. Silverman, and R. Haight, J. Vac. Sci. Tech. 20

(1982) 868.

[19] S. Shimokawa, A. Namiki, M. N. -Gamo and T. Ando, J. Chem. Phys. 113 (2000) 6916.

[20] D. D. Koleske, S. M. Gates, and J. A. Schultz, J. Chem. Phys. 99 (1993) 5619.

[21] S. A. Buntin, J. Chem. Phys. 105 (1996) 2066.

[22] B. Jackson and D. Lemoine, J. Chem. Phys. 114 (2001) 474.

[23] U. Hansen and P. Vogl, Phys. Rev. B 57 (1998) 13295.

[24] K. Takayanagi, Y. Tanishiro, M. Takahashi, and S. Takahashi, Surf. Sci. 164 (1985) 367.

[25] K. Takayanagi, Y. Tanishiro, and M, Takahashi, S. Takahashi, J. Vac. Sci. Technol. A 3 (1985) 1502.

[26] R. -L. Lo, I. -S. Hwang, M. -S. Ho, and T. T. Tsong, Phy. Rev. Lett. 80 (1998) 5584.

[27] A. Vittadini and A. Selloni, Phys. Rev. Lett. 75 (1995) 4756.

[28] J. J. Boland, Surf. Sci. 244 (1991) 1.

[29] J. J. Boland, Adv. Phys. 42 (1993) 129.

[30] F. Owman and P. Mårtensson, Surf. Sci. Lett. 303 (1994) L367.

[31] C. J. Karlsson, F. Owman, E. Landemark, Y. -C. Chao, P. Mårtensson, and R. I. G. Uhrberg, Phys. Rev. Lett. 72 (1994) 26.

[32] P. Kratzer, J. Chem. Phys. 106 (1997) 6752.

[33] P. Kratzer, Chem. Phys. Lett. 288 (1998) 396.

[34] J. Tersoff, Phys. Rev. B 38 (1988) 9902.

CHAPTER 6
Summary

The kinetic study on H-induced ABS and AID have been discussed on Si(100)-2×1 surface in Chapter 3, 4 and that on the Si(111) 1×1 surface in CHAPTER 5. Though the basic kinetic processes of AID and ABS on both the surfaces are quite similar, there exist some differences in the observed kinetics. This difference in the kinetics can be considered to arise from the geometrical difference of mono-hydrides and di-hydrides between the Si(100) and Si(111) surfaces. In the following sections, the common and different features are described briefly.

6.1 COMMON FEATURES

The common kinetic features observed for ABS and AID on Si(100) and Si(111) surfaces are as follow

(a) For both the surfaces, ABS and AID do not follow the hot atom mechanism.

(b) AID is associated with the β_2 TPD mechanism through the T_s dependence as well as the reaction order. Upon H exposure to the D/Si surfaces transient di-deuterides or di-hydrides are formed. These di-deuterides play an essential role in the AID process.

(c) ABS efficiency with respect to incident flux is about 0.4 and thus ABS cross section is very high ($\geq 5\,Å^2$). This value of cross section is higher than the expected value for the direct Eley-Rideal reaction since it theoretically yields extremely small cross sections $<1\,Å^2$.

(d) ABS reaction order is observed to change from 1st-order to 2nd-order with increasing initial D coverages θ_D^0.

(e) There exists an isotope effect on both ABS and AID processes.

(f) Both ABS and di-deuteride formation are explained by the hot –complex model.

The hydrogen related chemistry including ABS and AID as well as TPD the reactions occur rather locally. This suggests that the local electronic structure determines the

chemical character. The characteristic feature to determine the surface chemistry on Si surfaces is the covalent bonds formed by the sp^3 hybridized orbitals.

6.2 DIFFERENT FEATURES

The main difference in the ABS and AID reactions among two surfaces is recognized in the AID reaction orders,

(a) In case of Si(100), the D_2 AID order is 3.7, whereas on Si(111) surface it is 3. These reaction orders are related to the respective β_2 TPD order since the respective reaction orders are two and 1.5 with respect to di-deuteride coverages.

(b) In the low temperature regime where the dideuterides are stable on the surface, the value of three for the AID reaction order is found to come from the sticking process rather than the desorption process. In this condition, the local structure for AID is such the sites where SiD and DSiD units are arranged side by side (Fig. 6.1(a)). On the other hand, the AID reaction order on Si(100) at 420 K was found to be about 4 (CHAPTER 4). This can be explained similarly, but based on the prepairing mechanism as shown in Fig. 6.1(b). Namely, the local structure is such that one doubly occupied Si dimer is adjacent to the existing di-deuteride.

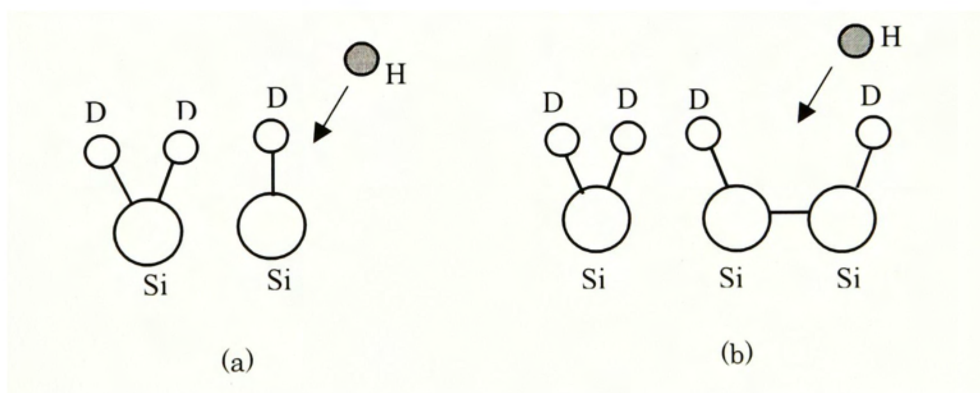

Fig. 6.1: Low temperature AID: (a) Case for Si(111)) and (b) for Si(100) surface

It was found that the reaction order increases upto 5~6 with decreasing temperatures down to room temperature. It is known that at such low temperatures the Si(100) surface takes a trend to be patched with a di-deuteride 1×1 structure [1]. Therefore, two neighboring di-deuterides are locally allowed to exist stably, which requires more dense di-deuterides for the D_2 AID reaction at lower temperatures.

6.3 FUTURE PLAN

There are some unsolved problems in the H-induced processes on the Si(100) and Si(111) surfaces, which can be itemized as future works,

(a) low temperature regime experiment on the saturated Si(100) surface,

(b) dynamics such as angular dependence and time-of-flight measurement on ABS and AID processes,

(c) experimental evidence for the hot-complex which initiates all the H reactions on the terminated Si surfaces.

REFERENCES

[1] J. J. Boland, Surf. Sci. 261 (1992) 17.

ACKNOWLEDGEMENTS

Words will be funny to try to express my gratitude to my Ph.D. supervisor **Professor Akira Namiki**. I have received exclusive and intensive hands on experience on the experimental apparatus and innovative taughtful guidance on the research techniques from him throughout my graduate study period. Without his support, I am sure this thesis might not have been produced in this extent.

Among the teaching staffs, sincere appreciation goes to **Mr. S. Inanaga** for his earlier and successful effort to make me understand the potential energy surface of Si surface and to developing C++ program. I am really thankful to him as I received his cordial support in many cases in this period. Thanks to **Mr. T. Fujimoto** for his help in troubleshooting of the circuits and the electrical device problem of the experimental setup. I also want to thank to **Dr. H. Tsurumaki**.

Dr. S. Shimokawa has a great contribution in my study period. To me he was not just a senior, but was a kind of teacher at the earlier times in Namiki laboratory. I wish to thank him from the deepest of my heart. Additionally, I also thank every present and past group members of the Namiki laboratory for the unique and stimulating environment they have provided. Particularly, I want to thank **Mr. Faridur Rahman,** who was directly involved in performing the Si(111) experiment and who also helped me in writing this thesis.

There are few persons, who have direct or indirect contributions in writing this thesis. Among them, suggestions from **Mr. Bhupendra Bimal Chhetri** (KIT, Japan) and **Dr. Samina Azad** (Washington, USA) were quite helpful in writing this thesis. Thanks to both of them.

My family members, who are not directly related (except my husband) to this thesis but indeed related me greatly, always provided me with inspirations and made sacrifice in great extent. Namely, my daughter **S. Helen Junko Rahman** sacrificed a lot, as I couldn't pay much attention to her while I was really busy. My parent's inspiration helped me to become strong enough to finish this thesis, though they are residing far away in Bangladesh.

Finally, I want to express my thanks to Japanese Government as it provided the scholarship during this tenure to make possible my living and study in Japan.

Fouzia Khanom
March 2003

Appendix

Symbols and Abbreviations

A. SYMBOLS

Symbols (in the order of their first appearance)

Symbol	Description	First in
Å	Angstrom, unit of length	Section 1.1
Si	Silicon	Section 1.1
H_2	Hydrogen molecule	Section 1.1
H	Hydrogen atom	Section 1.2
3D	Three dimensional	Section 1.2
σ	Sigma (bond)	Section 1.2
π	Pi (bond)	Section 1.2
θ_H	H coverage	Section 1.2
θ_D	D coverage	Section 1.2
T_s	Surface temperature	Section 1.2
β_1	Beta one (TPD peak)	Section 1.3
β_2	Beta two (TPD peak)	Section 1.3
D	Deuterium atom	Section 1.3
H_{ad}	H adatom (adsorbed H atom)	Section 1.3
θ_{HSiH}	Coverage of dihydride	Section 1.3
k_{LH}	Rate constant in the LH rate law	Section 1.4
ν	Pre-exponential factor	Section 1.4
exp()	The exponential function	Section 1.4
E_A	Activation energy	Section 1.4
$Å^2$	Unit of area	Section 1.4
σ	Cross-section	Section 1.4
D_{ad}	D adatom (adsorbed D atom)	Section 1.4
ϕ	Flux	Section 1.4
H^*	Hot H atom	Section 1.4
D^*	Hot D atom	Section 1.4
D/Si	D terminated Si surface	Section 1.5
H(g)	Gaseous H atom	Section 1.5

Symbol	Description	First in
Sp^3	s-and p-orbital derived hybridized orbital	Section 1.5
Ar^+	Argon ion	Section 2.1
l/s	Liter per second	Section 2.1
Hz	Hertz, unit of frequency	Section 2.2
S/N	Signal noise ratio	Section 2.3
M/e	Ratio of mass and electron	Section 2.3
Mo	Molybdenum	Section 2.4
B	Boron	Section 2.4
P	Phosphorus	Section 2.4
n	Negative	Section 2.4
p	Positive	Section 2.4
C	Carbon	Section 2.4
O	Oxygen	Section 2.4
R	Resistance	Section 2.5
V	Voltage	Section 2.5
I	Current	Section 2.5
θ_D^0	Initial D coverage	Section 3.1
K_{ER}	Rate constant for the direct ER abstraction	Section 3.2
J_{in}	Incident flux (cm^2/s)	Section 3.2
N_{abst}	Number of abstracting particles (cm^2/s)	Section 3.2
N_{stick}	Number of sticking particles (cm^2/s)	Section 3.2
N_{ref}	Number of reflecting particles (cm^2/s)	Section 3.2
N_{dihyd}	Number of dihydride particles (cm^2/s)	Section 3.2
s	Sticking probability	Section 3.2
$I(D_2)$	Intensity of D_2	Section 3.2
$I(HD)$	Intensity of HD	Section 3.2
N_0	Si density per unit area	Section 3.2
θ_{DD}	Coverage of doubly occupied Si dimers with the same D atoms	Section 3.2
θ_{HD}	Coverage of doubly occupied Si dimers with the H and D atoms	Section 3.2
θ_{HH}	Coverage of doubly occupied Si dimers with the same H atoms	Section 3.2

Symbol	Description	First in
η	Escaping probability from sticking to dangling bonds (eta)	Section 3.2
t	Time	Section 3.4
c_j, k_j	Fitting parameter	Section 3.4
erf(x)	Error function	Section 3.4
θ_0	Position of the maximum slope of η function	Section 3.4
w	Width of the η function changing from low to high coverage	Section 3.4
C_j	Fitting parameters	Section 3.4
k_{ABS}	Rate constant for ER type abstraction	Section 4.1
C_n	Rate constants	Section 4.1
$I_0(D_2)$	Initial D_2 rate (intensity)	Section 4.3
$I_0(HD)$	Initial HD rate (intensity)	Section 4.3
m	Reaction order	Section 4.3
k	Rate constant	Section 4.3
ξ	Abstraction probability	Section 4.3
I_{ref}	Reflected H flux	Section 4.3
E_B	H-substrate binding energy	Section 4.3
θ_{DSiD}	Coverage of di-deuteride	Section 5.3
k_{β_2}	Rate constant for β_2 TPD	Section 5.3
c_1, c_2	Rate constants for D_2 AID	Section 5.4
a_1, a_2	Rate constants for HD ABS	Section 5.4
C_1, C_2	Rate constants for HD AID	Section 5.4
R_{stick}	Rate of sticking of H atoms	Section 5.4
R_{AID}	Rate of loss of surface adatoms via AID	Section 5.4
R_{ABS}	Rate of loss of surface adatoms via ABS	Section 5.4
k_s	Sticking rate constant	Section 5.4

B. ABBREVIATIONS

Abbreviations (in alphabetical order)

Abbreviation	Full form
ABS	Abstraction
AC	Alternating current
AES	Auger electron spectrometer
AID	Adsorption-induced-desorption
CID	Collision-induced-desorption
CMOS	Complementary metal oxide semiconductor
CVD	Chemical Vapor desposition
DAS	Dimer-adatom-stacking fault
DC	Direct current
DF	Density functional
DLK	Dinger, Lutterloh, and Küppers
ER	Eley-Rideal
eV	Electron-volt
HA	Hot atom
HC	Hot-complex
LEED	Low energy electron diffraction
LH	Langmuir-Hinshelwood
LITD	Laser-induced thermal desorption
ML	Mono-layer
RF	Radio-frequency
SHG	Second harmonic generation
STD	Spontaneous thermal desorption
STM	Scanning-tunneling microscope
TMP	Turbo molecular pump
TOF	Time-of-flight
TPD	Temperature-programmed-desorption
TSP	Titanium sublimation pump
QMS	Quadrupole mass spectrometer